Progress in the application of surface engineering methods in immobilizing TiO_2 and ZnO coatings for environmental photocatalysis

Amir H. Navidpour, Ahmad Hosseinzadeh, John L. Zhou*, Zhenguo Huang

Centre for Green Technology, School of Civil and Environmental Engineering, University of Technology Sydney, 15 Broadway, Ultimo, NSW 2007, Australia

Corresponding author:

Prof John Zhou, junliang.zhou@uts.edu.au

ABSTRACT

Photocatalysis is widely used for the degradation of organic pollutants, with TiO_2 and ZnO as the best candidates with unique properties. However, agglomeration and recycling are major challenges in practical photocatalysis applications. Advanced deposition processes can provide nanotubular or hierarchical structures which are more promising than suspended particles. More importantly, higher efficiency of photoelectrocatalysis than photocatalysis for the degradation of persistent organic pollutants including perfluorooctanoic acid (PFOA) necessitates catalyst immobilization. Photoelectrocatalysis exhibited remarkably higher efficiency (56.1%) than direct photolysis (15.1%), electrocatalysis (5.0%) and photocatalysis (18.1%) for PFOA degradation. This paper aims to review the progress in the application of anodizing and thermal spraying as two major industrial surface engineering processes to bridge the gap between laboratorial and practical photocatalysis technology. Overall, thermal spraying is considered as one of the most efficient methods for the deposition of TiO_2 and ZnO photocatalytic films.

Keywords: Anodizing; Perfluorooctanoic acid; Photocatalysis; Photoelectrocatalysis; Thermal spraying

Graphical Abstract

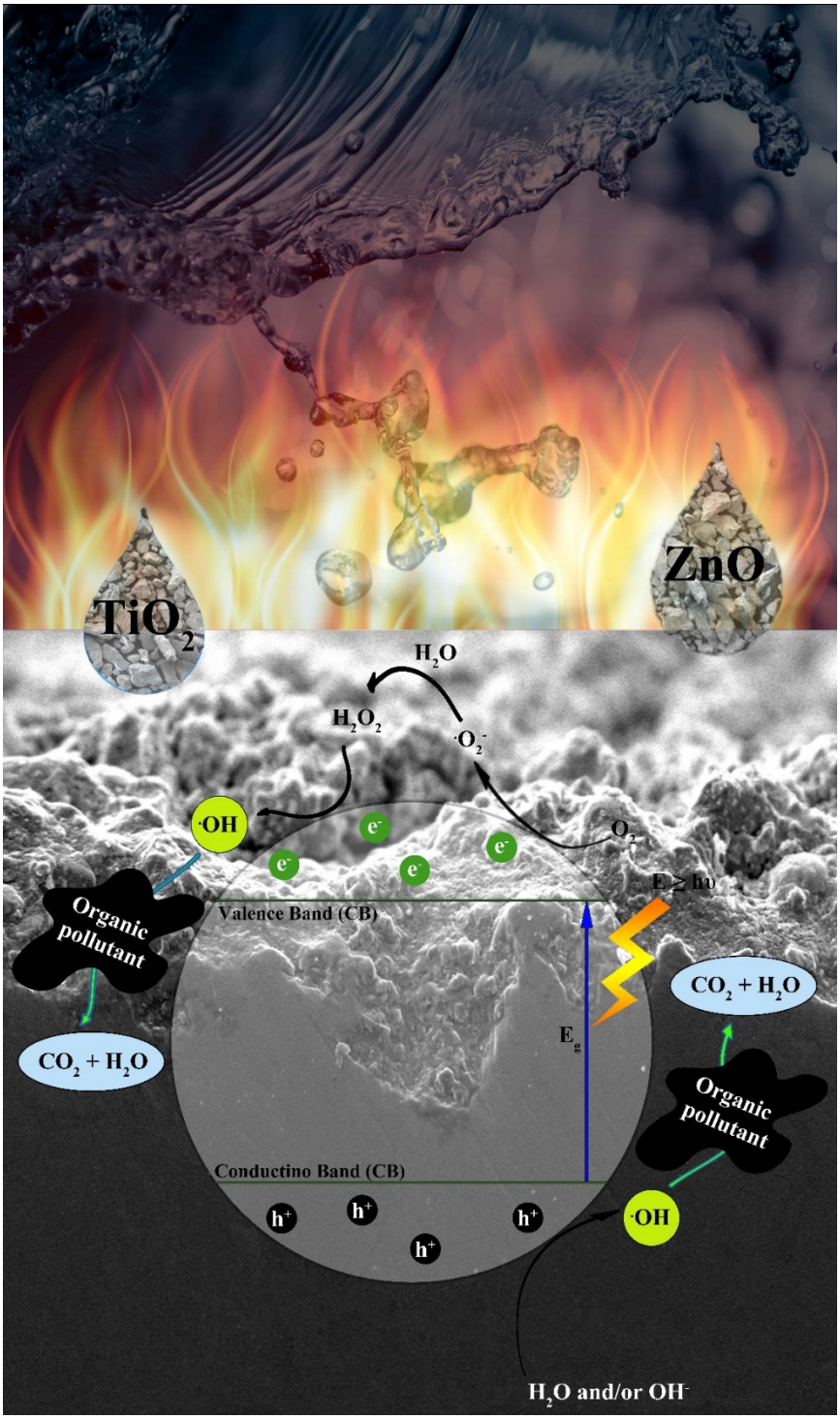

1. Introduction

Environmental photocatalysis occurs via the absorption of photons with energy equal to or greater than the band gap energy of semiconductor, resulting in photogeneration of charge carriers, separation of charge carriers, transfer of charge carriers to the surface of photocatalyst, and redox reactions.[1-3] Since the recombination of photogenerated e^-/h^+ pairs could quench the redox potential of semiconducting material, its rate should be minimized to achieve the highest photocatalytic activity. Several strategies have been used to lower the recombination rate of e^-/h^+ pairs including heterojunction formation, metal deposition, creation of oxygen vacancies, and non-metal/metal ion doping.[4,5] Surface reactions could happen only if the oxidation and reduction potentials are more negative and positive than valence band and conduction band levels, respectively.[6] The probable events which could occur during a photocatalytic reaction, though at varying degrees based on the photocatalytic system, are illustrated in Fig. S1.

TiO_2 is the most common photocatalyst due to its high oxidizing potential, nontoxicity, and easy immobilization on different surfaces.[5] Among all TiO_2 polymorphs, anatase and rutile phases are used in photocatalytic applications.[7] However, brookite TiO_2 has shown higher photocatalytic activity than that of rutile TiO_2 in some cases.[8] Among these phases, macrocrystalline rutile TiO_2 is thermodynamically stable under ambient conditions.[9] Anatase is a meta-stable phase and its band gap energy, which is approximately 3.2 eV, is higher than rutile phase.[10] Overall, when it comes to the pure phases, anatase TiO_2 shows a higher photocatalytic activity than rutile TiO_2. Improved surface hydroxyl density and higher mobility of e^-/h^+ pairs could be responsible for superior photocatalytic activity of anatase TiO_2 than its other polymorphs.[11] Discrepancy with the recombination kinetics of charge carries might be considered as another major reason for the higher photocatalytic efficiency of anatase TiO_2. Photoluminescence measurements have confirmed that a higher recombination rate of charge carriers is observed for rutile TiO_2 than anatase TiO_2.[12]

Compared to TiO_2, ZnO has great advantages including easy crystallization, fast transport of charge carriers, and the presence of intrinsic impurities which leads to its higher electron mobility.[4] Zinc oxide crystallizes in three different crystal structures including Wurtzite (hexagonal), zinc blende (cubic), and rocksalt (cubic).[13,14] Wurtzite ZnO is known as the most stable phase of ZnO thermodynamically at ambient temperature and pressure.[14] The preparation method could highly affect zinc oxide crystal structure and its morphology.[15] Nanoflowers are a novel class of small particles with a similar structure to plant flower in a nanometer scale which include numerous layers of petals to introduce a large surface area in a small structure. High surface to volume ratio and good charge transfer of nanoflowers could result in the high efficiency of surface reactions in 3D structure of nanoflowers.[16] Besides, a lower aggregation of nanoparticles could be observed during photocatalysis.[17] Moreover, ZnO nanoflowers showed improved light-scattering properties compared with other morphologies such as 1D nanorods.[18] Therefore, 3D ZnO nanoflowers could be more beneficial than other nanostructures for photocatalytic applications.[17] A similar conclusion has been made by Liao et al. who suggest much higher photocatalytic activity of 3D nanotube arrays of TiO_2 than its one-dimensional arrays.[19] ZnO has a lower price than TiO_2 and a similar photodegradation mechanism to TiO_2 and therefore is considered as an alternative to it.[20,21] As the most stable phase of zinc oxide, wurtzite is the most common polymorph of ZnO used for photocatalytic applications, which also takes advantage of its ease of synthesis compared with pristine zinc blende and rocksalt ZnO phases. Wurtzite zinc oxide has shown a higher photocatalytic activity than that of TiO_2 in some cases, as tabulated in Table S1. However, unpredictable physical and chemical properties of metastable phases of ZnO are more exciting than its stable counterpart.[22] Razavi-Khosroshahi et al. used high-pressure (6 GPa) torsion (HPT) technique to develop nanostructured rocksalt ZnO with a large fraction of oxygen vacancies, which could be stable at ambient conditions. The use of HPT method could not only induce rocksalt phase, but also creates oxygen vacancies as confirmed by Raman spectra. The sample processed under

the pressure of 6 GPa, which takes advantage of its high concentration of oxygen vacancies, has shown higher photo-absorption ability than other samples due to the minimum band gap energy. Owing to the high potential of light harvest, formation of rocksalt ZnO phase and creation of oxygen vacancies, Rocksalt ZnO has shown higher photocatalytic activity than both wurtzite ZnO and anatase TiO_2 phases.[23]

In this paper, the applications of TiO_2 and ZnO in the photocatalytic degradation of per- and polyfluoroalkyl substances (PFAS) as representative of persistent organic pollutants are discussed. Then, the application of two industrial surface engineering methods including anodizing and thermal spraying in the immobilization of TiO_2 and ZnO for photocatalytic purposes is reviewed.

2. PFAS as emerging and persistent organic pollutants

PFAS are among 3000 anthropogenic compounds which are very stable due to their strong carbon-fluorine (C-F) bonds with a bond energy of 544 kJ/mol.[24] Therefore, PFAS are highly persistent and widely detected in the environment. [25] Perfluorooctane sulfonic acid (PFOS) and perfluorooctanoic acid (PFOA) constitute high proportion of PFAS detected in the aquatic environment. Chemical and physical properties of PFOA and PFOS are summarized in Table S2. PFOA and PFOS can be mainly originated from their use and wastewater treatment plants directly, or indirectly from the degradation of some precursor compounds such as perfluorooctane sulfonyl fluoride and fluorotelomer alcohols.[26] In general, PFAS have high thermal stability and low friction coefficient, and are capable of repelling both oil and water. Therefore, they have found widespread applications in firefighting foams. They are also used for manufacturing many industrial, commercial and household products including coatings for textiles, carpets, nonstick surfaces, and paper coatings.[27]

PFAS are extensively distributed in drinking, marine, surface and ground water, with concentrations generally ranging from pg/L to μg/L.[28] For example, 16 PFAS were detected

in the influent (0.04-91 ng/L) and effluent (0.01-107 ng/L) samples from wastewater treatment plants in China.[29] Notably, higher concentrations (mg/L level) have been reported in ground and surface water after firefighting activities.[30] Surprisingly, the highest levels of PFAS (g/L range) were observed in some wastewater.[28] For instance, extremely high concentration of PFOS (1650 mg/L) was reported in wastewater from electronics industries, which is much higher than its solubility in pure water.[31] The concentration of PFAS in drinking water has been widely monitored in different countries, with concentration up to 84 ng/L of PFOA in Japan, as shown in Table S3. In comparison, significantly higher concentrations of some PFAS compounds have been reported in landfill leachate from different case studies, with the highest concentration of 4400 ng/L for PFOS (Table S4).

In addition, it has been shown that PFOX (X = S or A) could have toxic effects.[25,26] The exposure pathways of PFAS, chemical structures of PFOA and PFOS, and recent methods used for their control are illustrated in Fig. 1. Physical adsorption processes transport PFAS from one phase (e.g. water) to the sorbent. Notably, in case of PFOA and PFOS, the adsorption capacity of anion exchange resin (AIX) is superior than that of granular activated carbon (GAC) and powdered activated carbon (PAC).[32] In comparison, redox processes such as photocatalysis can be used for the efficient degradation of PFAS.

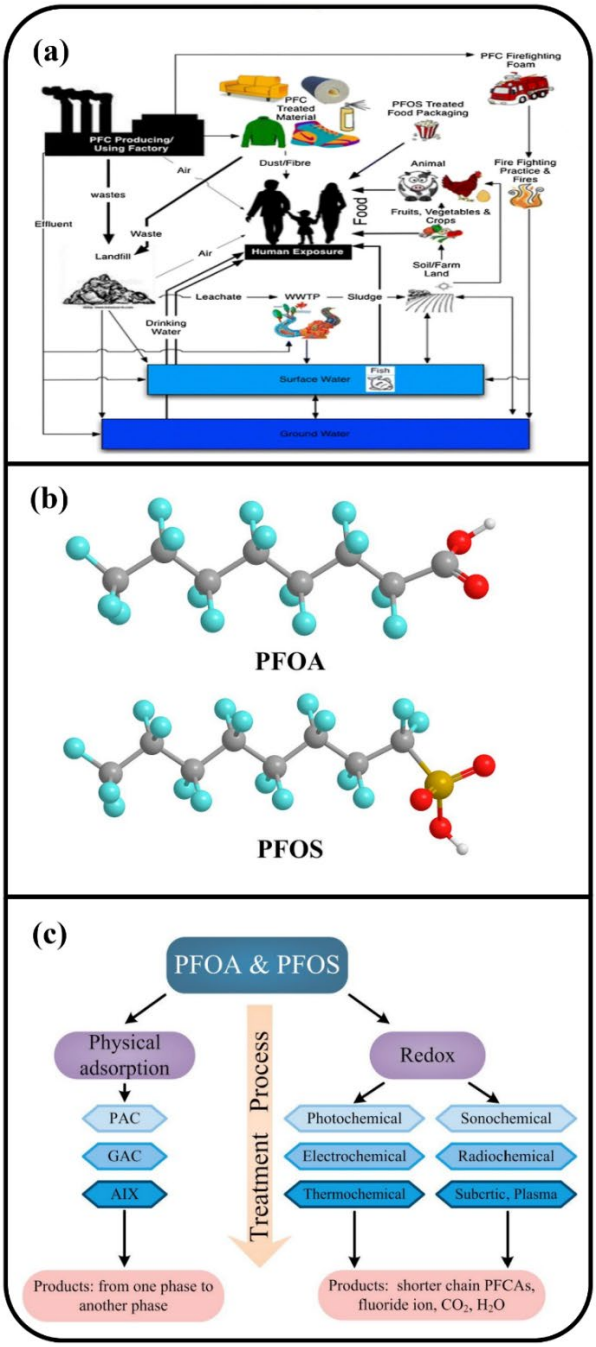

Fig. 1. (a) Exposure pathways of PFAS. Reproduced with permission from [33]. Copyright © 2012 Fardin Oliaei et al., Springer Nature. (b) chemical structures of PFOA and PFOS (C: gray, F: blue, O: red, S: yellow, and H: white). Reproduced with permission from [32]. Copyright © 2017 Shana Wang et al., Elsevier. (c) recent methods used for removal of PFOA and PFOS. Reproduced with permission from [32]. Copyright © 2017 Shana Wang et al., Elsevier.

2.1. Degradation intermediates and mechanism of PFOA

Various methods including adsorption, ion exchange, filtration, biodegradation and membrane bioreactor have been used for decomposition of PFAS with different efficiencies. Since most microorganisms are unable to degrade PFAS in water,[26] some methods that can cleave C-F bonds are preferable for degradation of PFAS. Thus, UV photolysis and photocatalysis have received major attention for PFAS degradation. Giri et al. have shown that the removal rate and efficiency of UV photolysis could decrease remarkably when treating very low initial concentrations of PFOA, which might be attributed to its strong C-F bonds.[34] In general, direct photolysis of PFOA can be improved when VUV light (185 nm) is used as the source of irradiation. The C-C bonds of PFOA with the bond energy of 347 kJ/mol could be cleaved by both UV sources of 185 nm (photon energy = 646.8 kJ/mol) and 254 nm (photon energy = 471.1 kJ/mol). In comparison, the C-F bonds of PFOA could be cleaved only by UV of 185 nm (with photon energy of 646.8 kJ/mol).[35] It has been shown that the photodegradation of PFOX results in the formation of lower perfluorinated compounds (PFCs), perfluoroheptanoic acid (PFHpA), perfluorohexanoic acid (PFHxA), perfluoropentanoic acid (PFPeA), perfluorobutanoic acid (PFBA), perfluoropropanoic acid (PFPrA), and trifluoroacetic acid (TFA), by sequential defluorination.[36,37] It is worth mentioning that shorter carbon chains of PFASs are less toxic than PFOA.[38] Various methods have been used for the degradation of PFOA, which are generally divided into two main categories of photo-reduction and photo-oxidation processes. Photo-reduction is known as a workable mechanism for the degradation of PFOX which is usually recalcitrant towards oxidation.[32] However, some strong oxidants including persulfate ($SO_4^{\bullet -}$) have been effectively used for the degradation of PFOX.[39] Photo-oxidation of PFOX is initiated by the cleavage of C-C bonds between –COOH and $–C_7F_{15}$ groups. The schematic common pathway for the photo-oxidation of PFOA is illustrated in Fig. 2, and explained as follows:[26,32,40]

i. Formation of perfluorinated alkyl radicals ($C_7F_{15}COO^{\bullet}$) by the transfer of an electron from the carboxylate terminal group to photocatalyst, phosphotungstic acid, persulfate or some other species including Fe^{3+}/Fe^{2+},

ii. Kolbe decarboxylation reaction of $C_7F_{15}COO^{\bullet}$ radicals that leads to the production of perfluoroalkyl radicals ($C_7F_{15}^{\bullet}$) by the cleavage of C-C bonds between $-COO^{\bullet}$ and $C_7F_{15}^{-}$. Photo-electrons can also break C-C bond that results in the formation of CO_2 and $C_7F_{15}^{\bullet}$ from perfluorinated carboxylate anions, $C_7F_{15}COO^{-}$, as it occurs in direct photolysis,

iii. Formation of $C_7F_{15}OH$ (unstable alcohol) by the reaction of molecular oxygen, molecular water, or $^{\bullet}OH$ with the terminal carbon atom of $C_7F_{15}^{\bullet}$ due to its higher density of electrons,

iv. Formation of $C_6F_{13}COF$ by the elimination of HF from $C_7F_{15}OH$,

v. Production of PFHpA with one less CF_2 unit compared to initial PFOA (through hydrolysis of acid fluoride),

vi. Production of PFHxA, PFPeA, PFBA, PFPrA, and TFA in a stepwise manner, and

vii. Continuation of photolysis until the complete mineralization of PFOX.

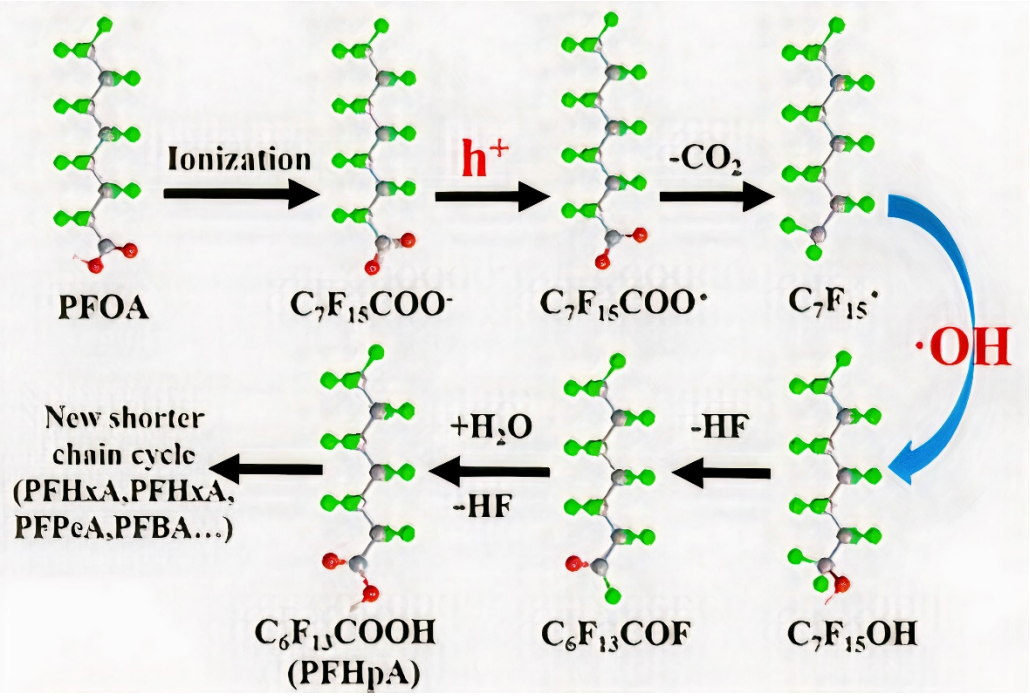

Fig. 2. Schematic common pathway for photo-oxidation of PFOA. Reproduced with permission from [40]. Copyright © 2019 Yaoyao Wu et al., John Wiley and Sons.

2.2. Application of TiO_2 and ZnO in photocatalytic degradation of PFOA

The kinetics of PFOA photocatalysis have been studied to analyze the specific reaction process under UV irradiation.[26] For instance, photocatalytic degradation of PFOA by TiO_2 is shown in Fig. S2. As evident, the concentration of PFOA has continuously deceased with time. PFHpA was the first intermediate produced during photocatalysis, with its concentration reaching a peak within 6 h. PFHxA and PFPeA were the second and third intermediates produced during the process. Unlike PFHpA, the concentrations of PFHxA and PFPeA have continuously increased during 8 h. Notably, shorter chain compounds of PFOA might have been produced but have not been detected due to their low concentration.[41] Some reports on the application of TiO_2 and ZnO for photocatalytic degradation of PFOA are compiled in Table S5.

It can be concluded that metal doping can improve the photocatalytic degradation of PFOA whereas co-doping of Fe and Nb has increased the efficacy from 1% to 14%.[42] The same trend was observed by Li et al. for the degradation of PFOA using dielectric barrier discharge (DBD)

with La/Ce-doped TiO_2.[43] In general, metal ion doping can significantly reduce the recombination rate of photo-generated electron-hole pairs which is the main reason for the improved photocatalytic activity of metal-doped TiO_2.[42-44] Loading of metallic nanoparticles is another major strategy to significantly lower the recombination rate of e^-/h^+ pairs. For instance, Fe- and Cu-loaded TiO_2 have improved the efficiency from 14% (unloaded TiO_2) to 69% (Fe-loaded TiO_2) and 91% (Cu-loaded TiO_2).[44] In another research, similar amount of Pt, Pd, and Ag, 1.0 at.%, has been loaded on TiO_2. FE-SEM elemental mapping and TEM images of TiO_2 nanoparticles (20-40 nm) modified by Pt, Pd, and Ag nanoparticles (~5 nm) are shown in Fig. 3(a-f). The UV-vis DRS spectra of TiO_2 samples are compared in Fig. 3(g). Notably, in order to improve the surface properties of titania before loading metallic nanoparticles, commercial TiO_2-P25 has been annealed at 400 ˚C for 1 h (400-TiO_2). Although the loading metallic nanoparticles have not changed the band gap energy, they have significantly affected the light harvest especially in the visible-light region (Fig. 3(g)).

The effect of the initial PFOA concentration on its degradation using these catalysts is shown in Fig. 3(h). It is clear that the apparent rate constants of photocatalytic degradation of PFOA have decreased gradually by increasing the initial PFOA concentration from 20 to 80 mg/L for pure TiO_2. On the other hand, the apparent rate constants of photodegradation of PFOA have been enhanced by increasing the initial concentration of PFOA (up to 60 mg/L) for TiO_2 loaded by Pt, Pd, and Ag nanoclusters at varying degrees. During PFOA photodegradation process, the ratios of apparent rate constants between doped TiO_2 (loaded by Pt, Pd and Ag nanoclusters) and pure TiO_2 are 3.1, 2.9 and 1.4, respectively. Compared to pure TiO_2, Pt loading can significantly improve the photocatalytic degradation of PFOA at relatively high PFOA concentration of 60 mg/L. The result is very promising since PFOA concentration is very high in some wastewater as reported previously.[28]

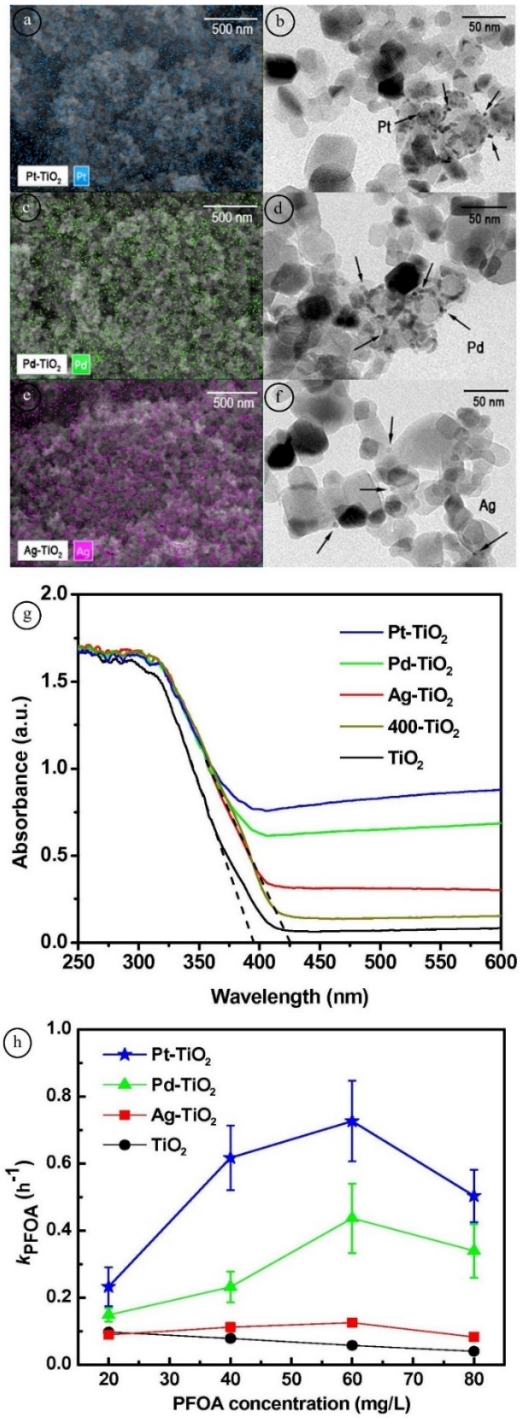

Fig. 3. (a-f) FE-SEM elemental mapping and TEM images of TiO_2 nanoparticle modified by Pt, Pd, and Ag nanoparticles, (g) UV-vis DRS spectrum of TiO_2 modified by Pt, Pd, and Ag nanoparticles; and (h) effect of initial concentration of PFOA on the efficiency of degradation. Reproduced with permission from [45]. Copyright © 2016 Mingjie Li et al., Elsevier.

By far, Pt was the most efficient metallic nanoparticle treating different initial concentrations of PFOA. The larger the work function, the higher is the efficiency of modification by metallic nanoparticles (φPt = 5.65 eV, φPd = 5.55 eV, and φAg = 4.26 eV).[45] The larger the work function, the larger is the potential difference between the conduction band of TiO_2 and the Fermi level of metallic nanoparticles which increases the driving force to transfer electrons from the conduction band of TiO_2 to metallic nanoparticles. It is notable that the larger work functions of Pt, Pd and Ag than that of TiO_2 (4.2 eV) leads to formation of a Schottky barrier at the metal-TiO_2 interface which is responsible for the increased driving force.[46] Although ZnO has not been widely used for photocatalytic degradation of PFOA, it has shown promising photocatalytic activity even higher than that of TiO_2 in some cases (Table S5). TiO_2 and ZnO are well-known due to their strong oxidizing power for the degradation of numerous organic pollutants. However, it can be seen (Table S5) that undoped/unmodified TiO_2 and ZnO are not highly efficient for degradation of PFOA. The main reason is that unlike most refractory pollutants which can be degraded by hydroxyl radicals via hydrogen abstraction, PFOX could not be attacked by hydroxyl radicals due to the lack of hydrogen atoms to be abstracted.[32,47] However, the mechanism is not fully understood since some researchers have concluded that $^{\bullet}OH$ contributes to PFOA degradation.[48] Huang et al. have concluded that both photo-generated holes and $^{\bullet}OH$ could be responsible for PFOA degradation, although photo-generated holes could play a more important role.[49] The more dominant role of photo-generated holes than $^{\bullet}OH$ in photocatalytic degradation of PFOA using TiO_2 has also been confirmed by Xu et al.[41] Overall, the photo-recombination rate of charge carriers should be minimized to achieve high efficiency. Pure TiO_2 and ZnO could suffer from the high recombination rate of charge carriers which limits their efficacy, compared to doped/modified TiO_2 and ZnO.

2.3. Key factors in photocatalytic degradation of PFOA

Solution pH, wavelength of irradiation source, temperature, and peroxymonosulfate (PMS) are among the key factors affecting the photodegradation of PFOA. It has been suggested that compared to basic solutions, acidic solutions promote higher degradation efficiencies when using TiO_2 as the catalyst[26] , mainly due to the Colombian attraction between PFOA and the catalyst. The surface of TiO_2 is positively charged in acidic pH, while PFOA becomes negatively charged (pK_a = 2.8). Thus, electrostatic interaction between TiO_2 and PFOA is greatly enhanced in acidic solutions. Notably, a similar trend has also been observed by using ZnO as the catalyst. The effect of pH on the photocatalytic degradation of PFOA using TiO_2 and ZnO is shown in Fig. S3(a, b) where increasing solution pH from 3 to 5, 7 and 9 has gradually decreased the efficiency of PFOA degradation.[41,50]

The wavelength of light source is another major factor affecting the efficiency of photodegradation. In general, the effect of wavelength irradiation is largely dependent on the photo-adsorption ability of the catalyst. Xu et al. have evaluated the effect of different wavelengths (185 nm, 254 nm, 400-770 nm) on the degradation of PFOA using TiO_2 as the catalyst (Fig. S3(c)).[41] Firstly, it can be seen that UV irradiation is more efficient than visible-light irradiation which is mainly attributed to the higher photo-adsorption of TiO_2 in wavelengths under 400 nm (UV region) than above 400 nm (visible region).[41,42] Secondly, both wavelengths of 185 nm and 254 nm had presented similar efficiencies.

The effect of temperature on the photocatalytic degradation of PFOA using ZnO is shown in Fig. S3(d). It is clear that temperature should be optimized to achieve the highest efficiency of degradation. Although increasing temperature from 278 K to 288 K and 298 K has improved the efficacy, due to reduction of the activation energy of reaction and increase of the probability of intermolecular collision, further temperature increase has suppressed the degradation of PFOA. Notably, the adsorption capacity of ZnO decreases at high temperatures.[50]

Recently, it has been shown that incorporation of PMS could significantly affect the degradation efficacy of PFOA using TiO_2 as the photocatalyst. Notably, TiO_2/PMS has resulted

in degradation of PFOA under visible-light irradiation which is of high importance (Fig. S3(c)). Moreover, PMS has significantly improved the degradation efficiency of PFOA compared to pure TiO_2. The most striking point is that such a system can be easily provided by physical mixing PMS and TiO_2 which has introduced TiO_2/PMS as a potential catalyst for photocatalytic degradation of PFOA under either visible or UV irradiation.[41] The schematic pathway for the degradation of PFOA using PMS is illustrated in Fig. S3(e). To bridge the gap between laboratorial and practical photocatalysis, the immobilization of TiO_2 and ZnO using industrial surface engineering methods is of high importance, which is discussed in detail below.

3. Role of surface engineering in improving photocatalysis

Although TiO_2 and ZnO nanoparticles possess high specific surface area, there are major drawbacks such as agglomeration and weak magnetic properties, which have limited their photocatalytic applications. Surface engineering might be considered as a potential solution and is generally divided into compositional modification and microstructural modification methods. Based on the thickness, compositional modification methods are divided into thin films and thick films approaches.[51] Compositional modification methods could be divided into solution state, gaseous state, solid state and molten/semi-molten state, as classified in Fig. S4. In general, the more is the surface roughness, the higher photocatalytic efficiency is expected due to the higher specific surface area.[52] The development of nanostructured materials and extension of porosity are popular approaches for improving the photocatalytic activity,[53] by increasing the depth of light penetration into the photocatalytic material[54,55] which could enable sublayers to participate in photo-generation of electron-hole pairs. Increasing film thickness remarkably improves the photocatalytic efficiency,[56-58] as Xianyu et al. reported 3.7 times higher photocatalytic activity of TiO_2 films (670 nm thickness) compared to that of 70 nm thickness.[58] The improved photocatalytic activity of semiconductor films with increasing thickness is

generally related to the higher surface roughness,[57,59] which results in the higher specific surface area.

4. Anodizing

Self-organized nanotube layers are perhaps the most surprising and spectacular 1D structures[60] which can be formed by easily automated electrochemical anodic oxidation as a relatively simple and cost effective method.[61,62] Due to its capability in the production of self-organized structures at room temperature and development of highly uniform morphologies, electrochemical anodic oxidation has attracted the greatest interest among various methods used for the production of TiO_2 nanotubes.[63] The schematic illustration of the anodization set-up and the resulting nanotube structure are shown in Fig. 4(a). This method has the advantages of being reproducible, and capable of tuning the dimension, wall thickness and pore size of the vertically oriented titania nanotubes by controlling the anodization parameters.[64,65] Anodic oxide films may have porous or compact structures depending on the metal substrate and functional parameters.[61] The morphological characteristics including pore size, wall thickness/roughness, aspect ratio, and tube-to-tube spacing of nanotubes, are mainly dependent on the composition, temperature and pH of the electrolyte, postgrowth treatment, and conditions of electrochemical process (e.g. applied voltage, current density, time and temperature of anodization and electrodes).[65,66] An extremely higher photodegradation efficiency (82%) has been observed by using annealed TiO_2 nanotubes compared to commercial TiO_2 nanoparticles (30%) under the same experimental conditions.[67] Notably, anodizing can yield highly oriented TiO_2 nanotubes which offer enhanced photodegradation performances[68,69] and better adherent strength.[65]

4.1. Advantages of porous oriented nanotubes

Compared with common TiO_2 nanoparticles, oriented direction and increased velocity of electron transport will reduce the recombination rate of photogenerated electron/hole pairs.[70,71] Besides, nanotube structures possess higher photo-absorption ability owing to their high ratio of length to tube diameter, and have larger pore volume and specific surface area.[72] An important advantage of ordered nanotube arrays is the possibility of modification of nanotubes using doping species, cocatalysts and junctions, at desired locations, or with desired regular patterns and geometries, along the tube wall. It provides engineering of reaction sites for photocatalytic reactions which target both the selectivity of reactions and higher efficiencies.[73] Moreover, highly ordered infrastructures are favorable for their high transfer of charge carriers.[74] The defined geometry offers special diffusion paths for transportation of ions, electrons and holes through the tube wall, and transfer of the reactants into the tube through tubular depth.[75] In photocatalysts, the hollow structures could significantly increase their light conversion, electron percolation, and ion diffusion at the interface of semiconductor-electrolyte.[76] The size of the pores should be $\leq$ 100 nm in the nanoporous materials.[77] An ideal porous structure of highly ordered TiO_2 is composed of pores within the closed packed arrays of hexagonal cells, as shown in Figs 4(b) and 4(c). The wall thickness (W), interpore distance (D_c), and pore diameter (D_p) are among characteristic parameters of porous anodic TiO_2. In general, the depth of pores (thickness of the oxide layer) is dependent on the type of electrolyte, anodization time, and anodization potential.[78] The purity of the substrate is among factors that could significantly affect the degree of order of nanotube arrays. Figure 4(d-g) shows the effects of both the purity of Ti substrates (99.6% and 99.99%) and a second anodization step on the order domains of TiO_2 nanotubes. Although both substrates have resulted in the development of relatively ordered nanotube arrays though at varying degrees, irregular and round shaped nanotubes have been formed after first anodization step. The degree of order is increased by using a second anodization step (for both substrates), and a closed-packed hexagonal has been achieved as a result of pre-textured surfaces.[79]

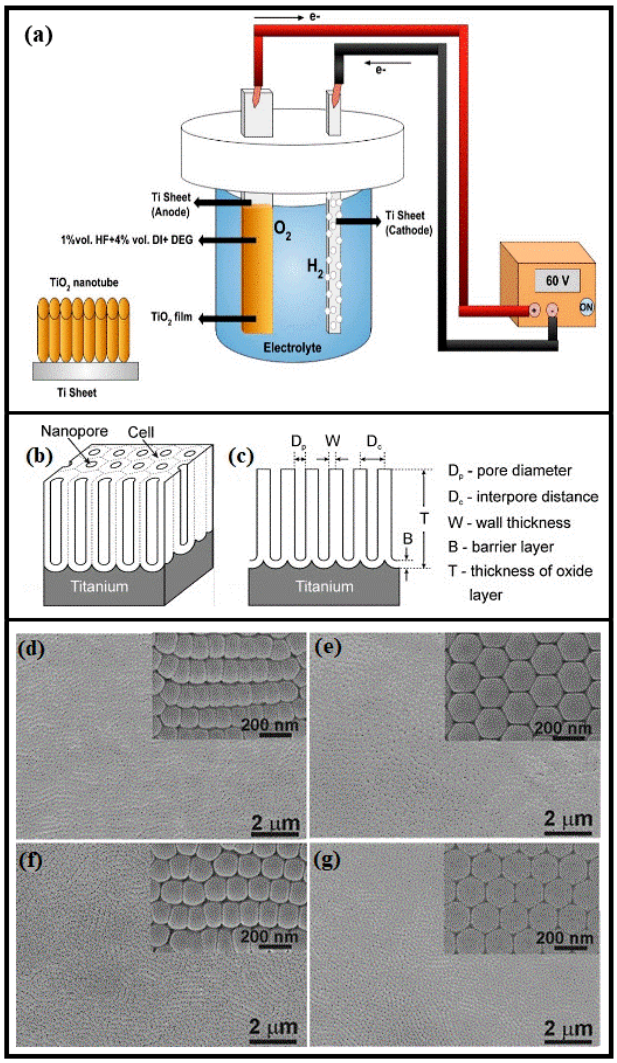

Fig. 4. (a) Schematic illustration of the anodization setup and the structure of resultant titania nanotubes. Reproduced with permission from [80]. Copyright © 2019 Najia Mahdi et al., MDPI. (b) ideal structure of porous anodic TiO_2 (ATO). Reproduced with permission from [78]. Copyright © 2010 Grzegorz D. Sulka et al., Elsevier. (c) cross section of the anodized layer with structural features of anodic TiO_2. Reproduced with permission from [78]. Copyright © 2010 Grzegorz D. Sulka et al., Elsevier. SEM micrographs of ordered TiO_2 nanotubes grown on pure Ti (99.6%) after 1st (d) and 2nd anodization (e); (f) and (g) micrographs for TiO_2 nanotubes grown on Ti with 99.99% purity, with insets showing magnifications. Reproduced with permission from [79]. Copyright © 2007 Jan M. Macak et al., John Wiley and Sons.

Some strategies could be used for the development of open-ended nanotubes. For example, immersing the anodized TiO_2 in HF acid solution could break the adhesion of nanotubes to the underlying substrate (first step). In the second step, the separated nanotube film could be exposed to a saturated HF or H_2SO_4 acid solution which leads to the nanotube opening.[81] Raising the anodization voltage at the end of process (for a short time) is another method which could break the adhesion of nanotube layer to the substrate and open the tube bottoms simultaneously.[82] Enhancement of the roughness factor and light absorption, originated from increase of the length to diameter ratio of nanotubes, could result in higher photocatalytic activities.[83] Zhang et al. synthesized highly ordered nanoporous TiO_2 to evaluate the effect of porosity on the photocatalytic degradation of methyl orange. The apparent rate constant of photocatalytic degradation of methyl orange has been remarkably increased by using nanoporous titania nanotubes ($r_{app} = 0.0574\ h^{-1}$) compared with titania nanotubes ($r_{app} = 0.0412\ h^{-1}$) which signifies the crucial importance of nanoporous structures.[84] Dikici et al. synthesized both microporous and nanoporous TiO_2 structures for the photocatalytic degradation of methylene blue. They concluded that although nanoporous titania layers could show higher photocatalytic activity than that of microporous layers, the production of microporous structures could be more preferable due to their reproducibility and low cost. Besides, microporous titania layers could take advantage of scattered micropore distribution, rough surfaces, and mixed phase structure (rutile and anatase) which could all enhance the photocatalytic performance.[85] Liao et al. concluded that TiO_2 nanotubes with 3D structures were more effective (38%) than planar nanotube arrays (22%) formed on titanium foil in the photocatalytic degradation of methyl orange. First, these 3D structures are more efficient in the absorption of scattered radiation than nanotubes that are vertically grown in two-dimensional arrays. Since these nanotubes are capable of absorption of refracted and/or reflected light, the loss of photons, originated from scattering effects, could be potentially minimized in the liquid. The schematic illustration of the improvement in the photoactivity of 3D nanotube arrays is

shown in Fig. S5. In addition, dye molecules possess easier access to the surface of photocatalyst (through interstitial fissures between the nanotubes) which could play an important role in photocatalysis. Notably, 3D nanotube arrays showed a higher photocurrent which signifies their higher efficiency of photoelectron transfer, more photo-absorption ability, and lower recombination rate of photo-induced electrons and holes. Since photocatalysis is a series of oxidative and reductive reactions on photo-activated surface, higher photocurrent should improve redox properties and photocatalytic activity. Thus, 3D nanotube arrays showed a much higher photocatalytic activity than 1D arrays.[19] It is notable that TiO_2 photospheres need a separation step after treatment which has limited their potential applications under ambient environments.[86]

Recently, TiO_2 nanotubes have been used for the photocatalytic degradation of PFOA (Table S6). Although there is a consensus that suspended catalysts are more efficient than immobilized ones,[87] photocatalytic activity of TiO_2 nanotubes is comparable to or even more efficient than that of TiO_2 particles (Table S5). Notably, TiO_2 nanotubes have shown higher photocatalytic activity than TiO_2 P25 layer, with similar thickness, for the degradation of Acid orange 7 and methylene blue[88] which could signify the crucial effect of these nanostructures on the photocatalytic activity as discussed previously. Extremely higher efficacy of TiO_2 nanotubes than TiO_2 nanoparticles has also been reported by other researchers.[67] Park et al. have evaluated the effect of pH on the photocatalytic degradation of PFOA using TiO_2 nanotubes. Increasing pH from 3 to 5, 7, 9 and 11 has reduced the degradation efficiency[89] which is consistent with the results by Xu et al. in the case of TiO_2 particles.[41] Unfortunately, anodizing has not yet been used to produce ZnO nanotubes for PFOA degradation, to the best of our knowledge.

4.2. Application of anodizing in improved separation of charge carriers in photoelectrocatalysis (PEC)

PEC in which a voltage bias is applied, is considered as an efficient approach for the separation of the photo-generated electron-hole pairs. Thus, the production of titania photoelectrodes has attracted the attention of researchers for several purposes including photocatalysis. Overall, applying an electrical field provides a pathway for the transfer of photogenerated electrons to the electrically conductive substrate. Under these circumstances, the separation of the photogenerated electron-hole pairs is improved and an enhanced photocatalytic activity is expected.[71,90] In the case of n-type semiconductors such as TiO_2, applying a positive potential could lead to the formation of a reverse biased interface which drives the photogenerated electrons and holes to the back contact and to the interface, respectively.[90] Overall, a reduction in the recombination rate of photo-generated e^-/h^+ pairs and improved quantum efficiencies are the main benefits of using PEC approach over photocatalytic processes. The PEC activity of titania photoelectrodes is generally related to the photocurrent density under the same conditions.[71] Huang et al. produced free standing TiO_2 nanotubes via anodization for improvement of photovoltaic and PEC properties. The PEC, photocatalytic, and electrocatalytic activities of their optimum samples over the degradation of methylene blue are shown in Fig. S6(a).

The PEC degradation rate of methylene blue (0.04022 min^{-1}) is considerably higher than both photocatalytic (0.01129 min^{-1}) and electrocatalytic degradation rates (0.00009 min^{-1}), which is explained by the intensified separation of photo-excited electron-hole pairs using externally applied voltage.[91] Liu et al. fabricated various anodized titania photoanodes for PEC degradation of methyl orange, and studied the effects of open-ended nanotube structure and deposition of Pt nanoparticles on their PEC activity. Notably, Pt-anodized-TiO_2 film has shown the highest photoactivity reaching 80% photodegradation after 5 min. The schematic of effect of Pt nanoparticles on the separation of charge carriers at TiO_2 surface is shown in Fig. S6(b). It is also noteworthy that a higher photodegradation rate was observed for open-ended TiO_2 nanotubes (0.27 min^{-1}) than common TiO_2 nanotubes (0.16 min^{-1}) which might be attributed to

the easier access of methyl orange to the inner surface of titania nanotubes.[92] It is notable that smooth and flat surfaces are not advantageous for light harvesting. In general, hierarchical macro/mesoporous structures could allow scattering of light within the interiors of their cavities and inside their pore channels which both lead to the improvement of light harvest and offer more photo-generation of e^-/h^+ pairs.[93] Photocatalytic fuel cells (PFC) are a new concept of PEC which has been recently used for wastewater treatment.[94] PFC was firstly reported by Kaneko et al. where NH_3, Pt and nanoporous titania film were used as the fuel, cathode, and anode materials, respectively.[95] A PFC system is composed of an electrolyte, a cathode electrode (carrying an electrocatalyst), and a photoanode electrode (carrying a mesoporous nanocrystalline semiconducting film). The electrocatalyst material is generally made of dispersion of Pt nanoparticles in nanoparticulate carbon.[96] The properties of functional materials highly depend on their structure. Therefore, the microstructure of electrode materials is of great importance, as an easily controllable parameter in a PFC system. PFC systems have advantages as they can potentially use solar light as an energy source, enable fast/direct production and transfer of photogenerated electrons, provide high degradation proficiency of pollutants, operate under moderate reaction conditions, and provide high-performance electrode materials.[94]

Ye et al. developed a TNA-Cu PFC system (a titania nanotube array photoanode and a Cu cathode) for the photodegradation of 4-chloro-2-methylphenoxyacetic acid (MCPA). Compared to the conventional photocatalytic process, a higher MCPA degradation was observed using a TNA-Cu PFC system which has been attributed to better separation of photo-excited e^-/h^+ pairs and generation of highly reactive oxygen species including H_2O_2, $^{\bullet}O_2^-$ and $^{\bullet}HO_2$. The contributions of different oxidants to the photodegradation of MCPA by PC and PFC methods are shown in Fig. S6(c).[70] The application of PEC in the degradation of various organic pollutants, and the comparison of its efficiency with photocatalysis in some case studies

are summarized in Table 1. As evident, PEC is more efficient than photocatalysis for pollutant degradation in all cases.

Table 1. Application of PEC and photocatalysis in the degradation of organic pollutants and their efficiency comparison.

Photoelectrode	**Pollutant (concentration)**	**Source of light**	**PEC activity**	**Photocatalytic activity**	**Reference**
$BiFeO_3/TiO_2$	Rhodamine B (20 mg/L)	500 W Xe lamp with a UV filter	100% (150 min)	16% (150 min)	[97]
Pt-TNTs/RGO	Methylene blue (5 mg/L)	150 W Xe lamp with a UV filter	80.9% (120 min)	20.7% (120 min)	[98]
F-doped TiO_2	Methylene blue (10 mg/L)	450 W metal halide lamp with a UV filter	92.9% (240 min)	30.2% (240 min)	[99]
$TiO_2/SrTiO_3$	Methylene blue (10 mg/L)	300 W Xe lamp - filtered light (λ=365 nm)	~100% (15 min)	~100% (105 min)	[100]
TNT	Real textile wastewater	100 W UV-B lamp	~7.0% (60 min)	~6.6% (60 min)	[101]
TNT	Real textile wastewater	100 W UV-B lamp	54.8% (60 min)	41.3% (60 min)	[101]
CeO_2 QDs/Ag_2Se	Tetracycline (20 mg/L)	8 W halogen lamp	95.8% (75 min)	92.3% (90 min)	[102]
Cu_2O/TiO_2	Rhodamine B (5 mg/L)	500 W tungsten-halogen lamp with a UV cut-off filter	84.3% (20 min)	5.0% (20 min)	[103]
TNT	Salicylic acid (20 mg/L)	500 W Xe lamp (full wavelength range)	~100% (120 min)	74.3% (120 min)	[104]
RGO-CeO_2-TNT	Bisphenol A (10 mg/L)	500 W Xe lamp with a UV filter	k_{app} (min^{-1}) = 0.0146 (with Fenton reaction)	k_{app} (min^{-1}) = 0.0114 (with Fenton reaction)	[105]
RGO-CeO_2-TNT	Tetrabromobisphenol A (10 mg/L)	500 W Xe lamp with a UV filter	k_{app} (min^{-1}) = 0.0003	k_{app} (min^{-1}) = 0.0002	[106]

TiO_2	Rhodamine B (4.2 mg/L)	4 W medium pressure mercury lamp	k_{app} (min^{-1}) = 0.0053	k_{app} (min^{-1}) = 0.0029	[107]
CeO_2@Fe_2O_3	Tetracycline (30 mg/L)	300 W Xe lamp with a UV filter	68.5% (60 min)	58.8% (60 min)	[108]
TiO_2	Gaseous isopropanol (17 ppmv)	10 W UV LED	~57% (10% relative humidity)	~39% (10% relative humidity)	[109]
TiO_2	Gaseous isopropanol (17 ppmv)	10 W UV LED	~51% (20% relative humidity)	~31% 20% (relative humidity)	[109]
TiO_2	Gaseous isopropanol (17 ppmv)	10 W UV LED	~38% (30% relative humidity)	~22% (30% relative humidity)	[109]
TiO_2	Gaseous isopropanol (17 ppmv)	10 W UV LED	~35% (40% relative humidity)	~19% (40% relative humidity)	[109]
TNT	Methyl orange (5 mg/L)	350 W Xe lamp	78.0% (60 min)	39.4% (60 min)	[110]
CeO_2-TNT	Methyl orange (5 mg/L)	350 W Xe lamp	98.1% (60 min)	56.5% (60 min)	[110]
TiO_2/SnO_2	Methylene blue (20 mg/L)	500 W Xe lamp	95.8% (120 min)	84.2% (120 min)	[111]

Note: TNT (TiO_2 nanotube arrays), RGO (reduced graphene oxide), QD (quantum dot), EG (exfoliated graphite)

PEC has been used for the degradation of PFOA recently. Surprisingly, an external voltage of 2.0 V has remarkably increased the degradation efficiency of PFOA from approximately 70% (without externally voltage) to 99.5% which has been mainly attributed to the reduced recombination rate of e^-/h^+ pairs. Notably, acidic environment was more effective than alkaline condition, mainly due to the fact that the adsorption of OH^- on the anodic surface of titania nanotubes hinders the decarboxylation reaction of $CF_3(CF_2)_6COO^-$ on the surface of anodic TiO_2.[89] Peng et al. synthesized carbon and nitrogen co-doped TiO_2 nanotubes for photocatalytic degradation of PFOA.[112] C-N co-doped TiO_2 photoanode, surface topography, and surface morphology of C-N co-doped TiO_2 nanotubes are shown in Fig. 5(a-c). The degradation efficiency of PFOA in direct photolysis, electrocatalysis, photocatalysis and PEC over the nanotubes is compared in Fig. 5(d). In terms of removal percentage, PEC was the most effective process in PFOA degradation with 56.1%, compared with direct photolysis (15.1%), electrocatalysis (5.0%) and photocatalysis (18.1%). Moreover, increasing the applied voltage up to 1.0 V has improved the removal rate which has been mainly attributed to the efficient separation of photogenerated electron–hole pairs. Time dependency of short-chain intermediates in PEC degradation of PFOA is shown in Fig. 5(e). It is notable that $^{\bullet}OH$ and $CH_3^{\bullet}$ have been suggested as the main active species for PEC degradation of PFOA. The main mechanism for PEC degradation of PFOA is illustrated in Fig. 5(f).

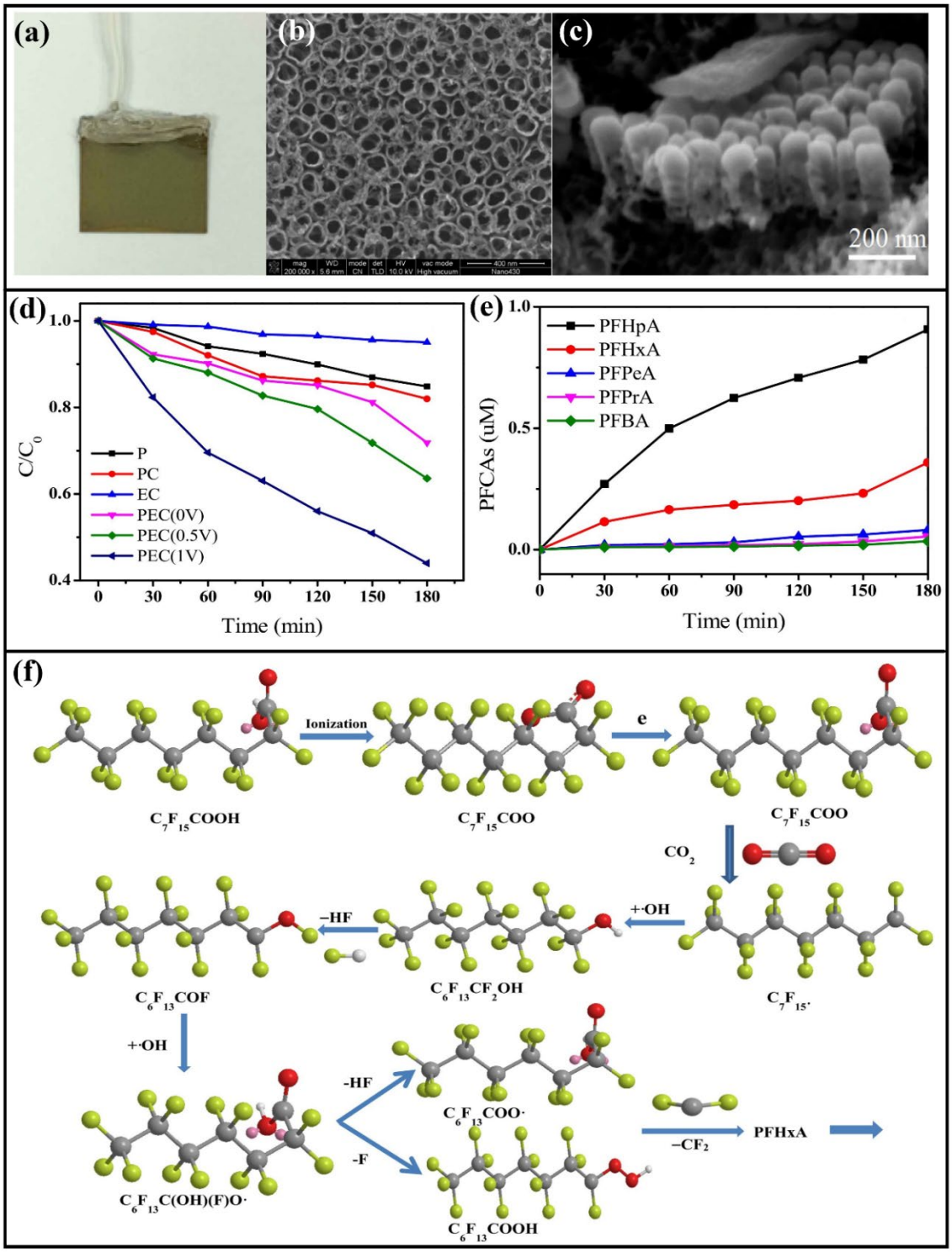

Fig. 5. (a) C-N co-doped TiO_2 photoanode, (b) surface topography of C-N co-doped TiO_2 nanotubes, (c) surface morphology of C-N co-doped TiO_2 nanotubes, (d) comparison of direct photolysis (P), electrocatalysis (EC), photocatalysis (PC) and PEC for PFOA degradation, (e) time dependency of short-chain intermediates (PFCAs) in PEC, and (f) main mechanism for degradation of PFOA in PEC. Reproduced with permission from [112]. Copyright © 2017 Yen-Ping Peng et al., Elsevier.

Compared with TiO_2, anodized ZnO nanotube arrays have not been widely studied for photocatalytic applications which might be attributed to their weak stability in solutions. It has been stated that the lowest solubility of zinc oxide could be observed at pH 9.3. Besides, the type of anions in solution could affect its rate of dissolution.[113] However, various ZnO nanostructures such as nanoneedle arrays, nanoflakes, nanoporous structures and stripe-like arrays have been synthesized by anodizing Zn. He et al. synthesized different morphologies of ZnO, including nanowires, nanodots, and nanoflowers, by electrochemical anodization of Zn foil using different concentration of electrolyte and reaction time.[114] Farrukh et al. used NaOH and $(NH_4)_2SO_4$ electrolytes to synthesize ZnO nanoflakes for the photocatalytic degradation of methylene blue under UV illumination. They concluded that ZnO produced in NaOH solution might have a higher photocatalytic activity than that produced in $(NH_4)_2SO_4$ solution which was attributed to the inhibitive effect of SO_4^{2-} ions and competitive absorption between methylene blue and SO_4^{2-} ions.[115] Ramirez-Canon et al. synthesized different morphologies of ZnO such as flake-like nanostructures, nano flower-like, nanorods and nanowires, using different electrolytes including H_3PO_4, HCl, NaOH, $H_2C_2O_4$, HNO_3 and $KHCO_3$. They concluded that the shape of the nanostructures was mainly determined by the type of electrolyte and its concentration. The largest size (100 nm) of nanostructures was obtained using 0.1 M of $KHCO_3$ and HNO_3, while the smallest size was obtained using 0.1 M of NaOH and H_3PO_4. In general, higher concentrations of electrolyte could provide higher concentrations of Zn^{2+} and OH^- needed for ZnO production, which results in denser ZnO nanostructures and thicker ZnO layers.[116] In addition, increasing the anodization time could increase the concentrations of Zn^{2+} and OH^-.[114] Molar concentration of the electrolyte and using pulsed UV irradiation during growth can significantly affect the nanoporosity of ZnO films. Using pulsed UV irradiation might increase both the etching rate and the growth rate of ZnO.[117] In the case of TiO_2, nanoporous structures provide a much higher specific surface area which results in a higher photocatalytic activity consequently.

Overall, it can be concluded that TiO_2 and ZnO nanotube structures could not only improve the photocatalytic efficiency compared to suspended catalysts, but also enable the application of PEC (with higher efficacy than photocatalysis) in the degradation of organic pollutants.

4.3. Limitations of anodizing

The as-anodized TiO_2 nanotube arrays are usually amorphous which necessitates a post heat treatment at high temperature. The conversion of amorphous structure to crystalline structure is required to improve properties of TiO_2 nanotubes such as mechanical strength, catalytic activity, and electrical conductivity.[118] Water, water-vapor treatment, and highly reactive oxygen plasma are among potential methods which have been used to synthesize crystalline TiO_2 nanotubes at room temperature. The crystalline or amorphous structure of as-anodized TiO_2 nanotube arrays depends on the anodization parameters such as time of anodization, applied potential and type of electrolyte.[118,119] Although there is no distinct temperature for the crystallization of amorphous titania nanotubes, annealing process above 300 ˚C leads to the formation of anatase phase while a mixture of anatase and rutile phases are formed at annealing temperature above 550 ˚C.[120] It is also noted that increasing the anodization voltage could increase the anatase phase content.[121]

5. Application of thermal spraying processes in deposition of thick TiO_2 and ZnO films

Thermal spraying consists of projection of molten or semi-molten particles (ceramics, metals or cermets) from powder, wire, or suspension/solution feedstock.[122] Then, fully or partially melted droplets are flattened, and rapidly cooled and solidified to form the coating. The occurrence of some chemical reactions including oxidation (in the case of deposition of metals) or phase transformations (in the case of deposition of ceramics/metals) is expected during heating the feedstock material.[123] All types of materials with stable molten phases could be deposited using thermal spraying processes. In comparison to PVD, CVD and sol-gel processes,

thermal spraying could provide a wider range of and often higher thickness of coatings.[124] Typical thicknesses of some major immobilization processes are compared in Fig. 6. Thermal spraying is therefore a promising method for photocatalytic applications. It is worth mentioning that thermal spraying, like other immobilization methods, can cause the formation of textured films as reported for TiO_2 in some cases.[125,126]

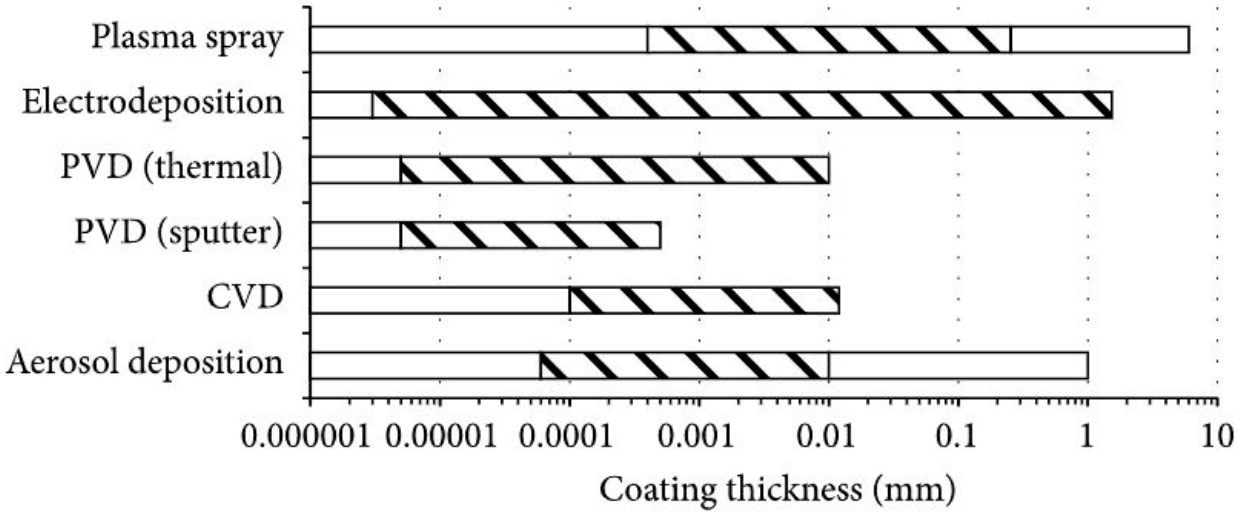

Fig. 6. Comparison of typical thicknesses of major immobilization processes. Reproduced with permission from [127]. Copyright © 2017 Bailey Moore et al., Hindawi.

5.1. Various techniques of thermal spraying

Particle velocity and flame temperature are two major characteristics used for the classification of different methods of thermal spraying.[122] General thermal spraying processes are shown in Fig. S7. The schematic illustration of thermal spraying process is shown in Fig. 7(a). Flame temperature against particle velocity for general thermal spraying processes is compared in Fig. 7(b).

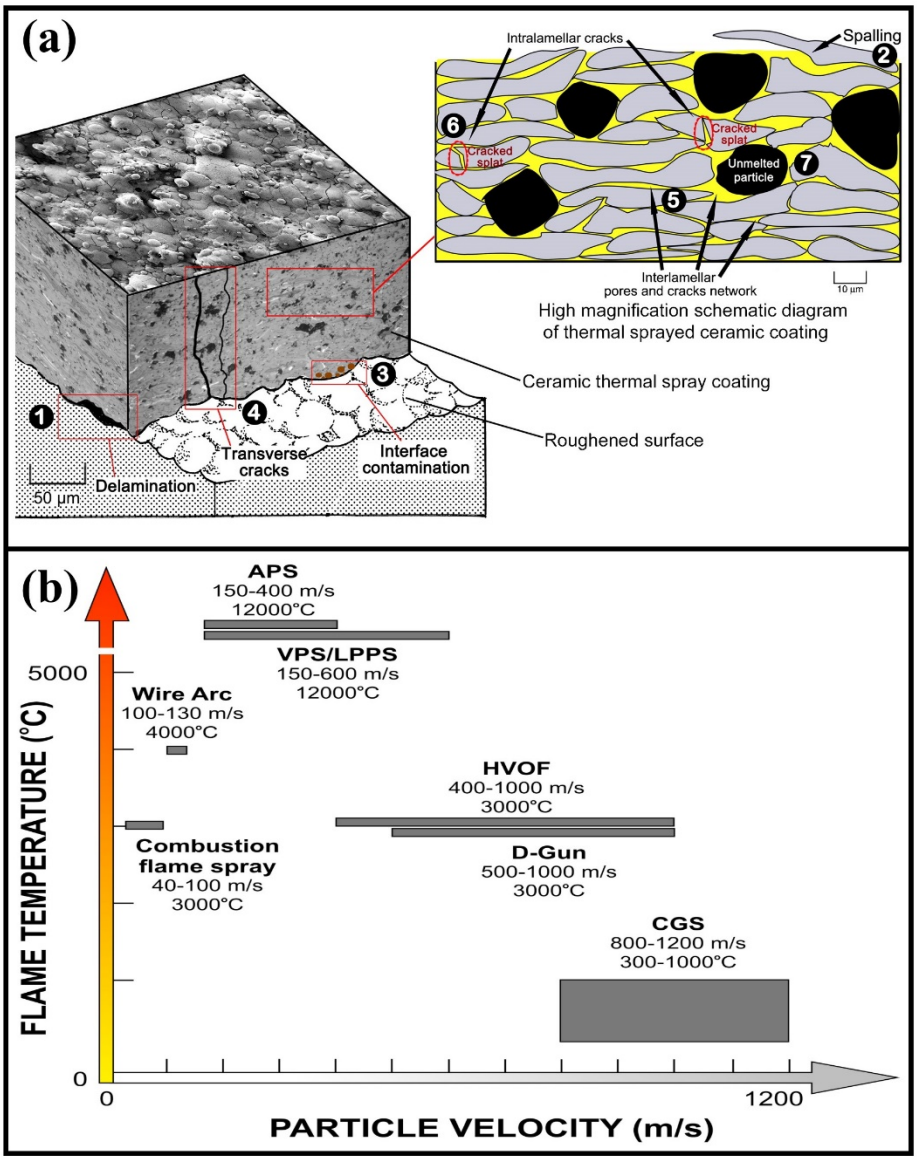

Fig. 7. (a) Schematic illustration of thermal spraying process. Reproduced with permission from [128]. Copyright © 2014 Andrew Siao Ming Ang et al., Taylor & Francis. (b) flame temperature against particle velocity for some general thermal spraying processes. Reproduced with permission from [129]. Copyright © 2011 Maria Oksa et al., MDPI.

The development of thermal spraying processes has a direct relationship with improvement of the temperature-velocity as a major characteristic of spray devices.[130] Process variables for typical thermal spraying processes are summarized in Table S7. Thermal spraying is known as the most versatile modern method of surface engineering in terms of scope of applications, range of materials, and economics.[122] Flame spraying (FS), as the simplest method of thermal

spraying, has been widely used for the deposition of TiO_2 coatings. Although cold spraying (CS), FS, atmospheric plasma spraying (APS) and high velocity oxy-fuel (HVOF) could all be used for the deposition of ceramic materials, plasma spraying is the most versatile method of thermal spraying processes due to the high temperature of plasma flame that is needed for full or partial melting of high melting point materials.[131] Notably, high velocity air-fuel (HVAF) and suspension plasma spraying (SPS) are among novel thermal spraying methods which have received remarkable attention due to their unique properties. HVAF could take advantage of providing highly adherent films with insignificant porosity. Besides, its low processing temperature could minimize thermal damage (such as oxidation or phase transformation) to the feedstock material.[132] Compared with HVOF, HVAF has lower flame temperatures and operating costs (by using air instead of oxygen).[133] On the other hand, SPS is considered as an advancement in APS (with its smaller splat size and fine scale porosity) that enables spraying of fine particles (100 nm-5 μm). Besides, it is capable of depositing various specific architectures and novel microstructures.[132,134] For instance, it can be easily used for the deposition of N-doped TiO_2 coatings to improve the photocatalytic efficiency under visible-light irradiation.[135] Schematic relationship between the microstructure and feedstock of SPS and APS processes; and schematic of the formation of droplets in SPS is shown in Fig. 8(a, b). Although thermal spraying has been mainly used for the improvement of wear resistance, corrosion resistance and thermal resistance of surfaces,[123] it has recently received remarkable attention for photocatalytic applications.

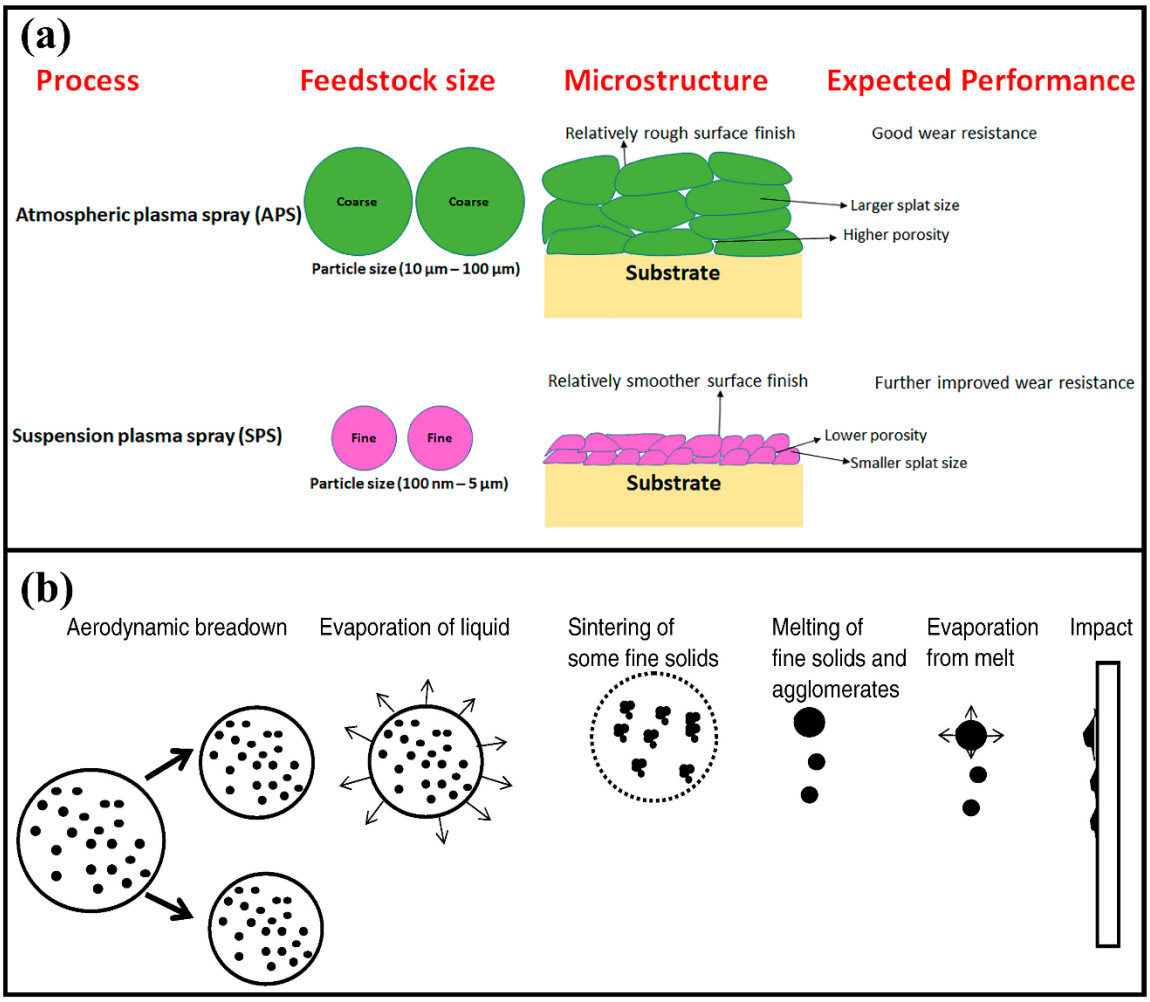

Fig. 8. (a) Schematic comparison of microstructure and feedstock relationship in SPS and APS films. Reproduced with permission from [134]. Copyright © 2019 Satyapal Mahade et al., MDPI. (b) schematic of the formation of droplets in SPS. Reproduced with permission from [136]. Copyright © 2009 Lech Pawlowski, Elsevier.

5.2. Cost-effectiveness of thermal spraying

Thermally-sprayed coatings have been widely used to protect devices against corrosion and wear.[137] Considering several criteria such as environment friendliness, reliability and process adaptability, thermal spraying is more widely used than other methods of surface engineering in many industries including paper, biomedical, metal processing and electronics.[138,139] Plasma spraying of large-scale devices including mill rolls is another example of commercial application of thermal spraying in which cost and processing time are of crucial importance.[140]

Due to its unique features such as reliability, thermal spraying has been widely used for the deposition of functional coatings, e.g. antimicrobial films, membranes for water filtration, and anti-fouling coatings.[141] Compared with other alternatives, thermal spraying can reduce chemical usage which, in turn, minimize chemical emissions and environmental pollution. The deposition of protective materials against wear and corrosion on machines can significantly increase their life by 2-8 times.

In terms of cost, the coating typically represents 20-40% of the total cost of products. The cost of deposition materials used in thermal spraying represents 50-80% of the cost of coating. Apart from deposition materials, the overall cost of deposition remarkably varies for different thermal spraying processes due to their different deposition rates and outputs.[139] In case of practical applications, cold spraying has been developed from a laboratory technique to a reliable method of commercial deposition in the last 20 years. For instance, is has found practical applications in the production of electronics devices including central processing unit (CPU).[142] Among different methods of thermal spraying, plasma spraying has made the highest contribution (around 45%) due to its capability in deposition of ceramics with high melting temperatures.[139] Typical pore size and relative total cost (including consumables, processing, and initial capital investment) of some major deposition processes are compared in Figs 9(a) and 9(b), respectively. Compared to other methods, plasma spraying could produce dense coatings, and is among the most cost-effective methods for the deposition of nanostructured films.[127] To support high deposition rate, uniformity of particle distribution, productivity and cost-efficiency of industrial processes, it is suggested to use plasma torches with high power throughputs. Notably, hybrid water stabilized plasma system with its high plasma temperature and enthalpy is known as an economical tool that meets all requirements for large-scale plasma spraying applications.[140] In addition, to enable cost effective and practical applications of thermal spraying in photocatalysis technology, it is essential to develop catalyst materials with excellent photocatalytic activities at low costs.

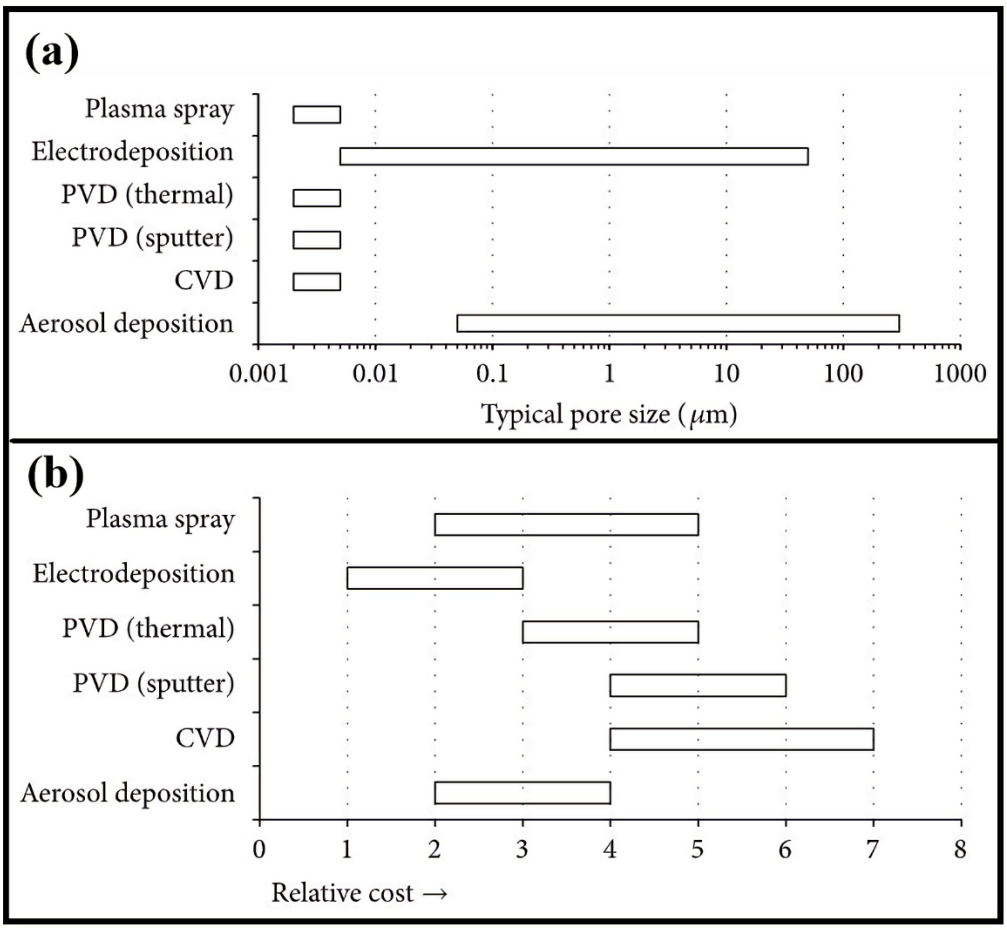

Fig. 9. Comparison of (a) typical pore size, and (b) relative cost of some major deposition processes. Reproduced with permission from [127]. Copyright © 2017 Bailey Moore et al., Hindawi.

5.3. Comparison between conventional plasma spraying, FS and HVOF

Ctibor et al. deposited agglomerated TiO_2 nanoparticles using different spraying methods i.e. gas-stabilized plasma (GSP), water-stabilized plasma (WSP), FS, and HVOF with different thicknesses for the photocatalytic degradation of gaseous acetone (Table S8). Although similar feedstock powders were used in GSP and FS processes, their phase composition and particle size differed from those used in HVOF and WSP processes. The remarkably higher surface roughness and porosity of TiO_2 films deposited by WSP than those deposited by HVOF have been attributed to the higher particle impact velocity of HVOF than plasma spraying. Similarly, higher particle impact velocity of plasma spraying than FS (Table S7) might be responsible for

the significantly lower surface roughness and porosity of TiO_2 films deposited by GSP than those deposited by FS. Notably, phase transformation from anatase to rutile has been observed in all cases.[143] Although FS and WSP processes have fabricated TiO_2 films with higher surface roughness and porosity, those deposited by HVOF and GSP have shown higher photocatalytic activity which clearly signifies the high importance of phase composition on the photocatalytic activity of thermally-sprayed TiO_2 films.

Bozorgtabar et al. deposited nanostructured TiO_2 films using methods of HVOF,[144] APS,[145] and FS[146] with similar feedstock (Degussa P25/P20 TiO_2) in all processes. The minimum anatase phase content was observed for TiO_2 film deposited by APS, which resulted in the highest crystallite size. Although FS resulted in similar crystallite size to APS, much higher anatase phase content was achieved using this method. In comparison, HVOF not only enhanced the formation of TiO_2 coatings with very high anatase phase content (even higher than that of the feedstock), but also minimized the average crystallite size (even lower than that of the feedstock).[144-146]

APS has generally resulted in the appearance of magneli phases (titanium suboxides with the general formula of Ti_nO_{2n-1}) which were mainly attributed to the reduction of titania when exposed to the high temperature of plasma jet.[145,147] Bordes et al. used APS for the fabrication of nanostructured TiO_2 coatings with different TiO_2 feedstock nanoparticles, with magneli phases being observed in all coatings. In addition, a low anatase phase content up to 20% was observed in the plasma-sprayed TiO_2 nanoparticles. Finally, it was concluded that the higher the anatase phase, the higher photocatalytic activity was expected[148] which has also been reported by other researchers for plasma-sprayed TiO_2.[149] To clarify the potential advantage of thermal spraying, a TiO_2 thin film (350 ± 10 nm thickness) was fabricated by sol-gel process, which was composed of pure anatase nanocrystals. Compared with APS, using sol-gel process has significantly reduced the surface roughness ($Ra = 1.0 \pm 0.1$ μm) which could play an important role in its lower photocatalytic activity.[148] Although photocatalytic activity of

magneli phases has been rarely investigated, a mixture of anatase/rutile and magneli phases showed promising photocatalytic activity which was superior than that of pure anatase phase. As an example, TiO_2 nanoparticles with mixed phases of anatase (32%), rutile (11%) and magneli phases (57%) showed 50-100 times higher photocatalytic H_2 evolution than that of plain anatase TiO_2, with similar loading of Pt.[150]

Overall, due to the highest content of anatase phase and the lowest crystallite size, HVOF has been introduced as the most efficient method of thermal spraying for TiO_2 deposition.[146] The deposition parameters could significantly affect the anatase content of TiO_2 coatings, as increasing the fuel flow rate from 120 to 240 mL/min remarkably decreased the anatase content from 80% to 8% while crystallite size only increased from 20.7 to 25.9 nm.[144] The same trend has also been reported for plasma-sprayed TiO_2 where increasing the argon flow rate from 28.5 to 36 L/min decreased the anatase content from 4% to 1.7%, while average anatase crystallite size remained stable (34.5 nm).[145] Overall, the higher the anatase phase content and the lower the crystallite size, the higher photocatalytic efficiency has been observed.[144]

5.3.1. Suspension plasma spraying

Toma et al. deposited nanostructured TiO_2 films using APS, SPS and HVOF for the photodegradation of nitrogen oxide pollutants, and SPS resulted in the production of a porous non-lamellar structure constituted by partially-melted/unmelted fine particles. In SPS, unlike APS, part of the plasma energy is devoted to evaporate the solvent, hence preventing the complete melting of the in-flight particles.[151] Besides, SPS takes advantage of using sub-micron or nano-sized particles that result in the formation of much smaller splats[132,134,152] which might be responsible for the formation of non-lamellar structure (Fig. 8(b)). Notably, both HVOF and plasma processes can be used to spray suspensions.[152] The solvent material is among the factors that can significantly affect the morphology of films deposited by SPS. For instance, compared with aqueous suspensions, using alcoholic suspensions could fabricate TiO_2

films with more porosity.[151] Unlike SPS, HVOF generally results in the formation of lamellar TiO_2 structures. Anatase phase content and its crystallite average size created by different methods of APS, SPS, FS, and HVOF are compared in Table 2.

Although Bozorgtabar et al.[144] and Toma et al.[151] used similar process of HVOF for TiO_2 deposition, anatase phase content and crystallite size of the deposited films were significantly different. The results suggested that both feedstock material and process parameters significantly affect the anatase phase content and its crystallite size. Remarkable effect of process parameters on the crystal structure could also be observed in the case of titania films deposited by SPS whereas a wide range of anatase phase content from 32% to 72% and from below 10% to above 90% have been reported by Bannier et al.[153] and Mauer et al.,[135] respectively. Notably, Bozorgtabar et al.[144] and Toma et al.[151] reported the appearance of magneli phases using APS for the deposition of TiO_2 despite of using different feedstock materials and process parameters. The striking point is the much higher anatase phase content of titania coatings deposited by SPS (> 96.0%) than that deposited by APS (10.9-12.2%) which could be mainly attributed to the lower heat input to the feedstock material using SPS.

Table 2. Anatase phase content and its crystallite average size created by different methods of APS, SPS, FS, and HVOF (SPS-W: SPS using aqueous suspension, SPS-A: SPS using alcoholic suspension).

Process	Properties of feedstock material	Anatase phase content (Vol%)	Average crystallite size of anatase (nm)	Other phases	Reference
HVOF	Anatase (Vol%) = 75%, agglomerated nanoparticles	80	20.7	Rutile	[144]
HVOF	Anatase (Vol%) = 100%, agglomerated nanoparticles	12.6	80.0	Rutile	[151]
APS	Anatase (Vol%) = 75%, agglomerated nanoparticles	5.1	83	Rutile and traces of magneli phases (Ti_3O_5 and Ti_6O_{11})	[144]
APS	Anatase (Vol%) = 100%, agglomerated nanoparticles	10.9 - 12.2	19.2 - 34.8	Rutile and traces of magneli phases (Ti_3O_5 and Ti_6O_{11})	[151]
SPS-W	Anatase (Vol%) = 100%, agglomerated nanoparticles	> 96.0	7.0 - 7.3	Rutile	[151]
SPS-W	Anatase (Vol%) = 80%, nanoparticles	91.9 - 95.1	34.9-38.7	Rutile	[151]
SPS-A	Anatase (Vol%) = 80%, nanoparticles	36.2	151.1	Rutile	[151]

SPS	Commercial suspension of TiO_2, anatase (Vol%) = 90%, nanoparticles	32 - 72	-	Rutile	[153]
SPS-W	Anatase (Vol%) = 99.9%, submicron	< 10 to > 90	-	Rutile	[135]
FS	Anatase (Vol%) = 75%, agglomerated nanoparticles	29	83	Rutile	[144]

5.3.2. Comparison between aqueous and alcoholic suspension

Using plasma spraying of aqueous suspension instead of alcoholic suspension has remarkably increased the anatase phase content from 36.2% to 91.9-95.1% and from 23.0% to 77.6-81.4%. In general, due to the risk of combustion associated with alcohols, water is more favorable than alcohols as a solvent in SPS.[151] Besides, water-based suspensions could increase the velocity of in-flight particles, and reduce the heat-input to the feedstock material by decreasing the jet temperature due to the higher vaporization temperature of water than alcohol.[154,155] Such a difference is related to the difficulties associated with atomization of aqueous suspensions.[154] Water-based suspensions could provide larger droplets with higher momentum which could facilitate the penetration of droplets to the center of plasma plume enabling greater acceleration.[154,155] The same trend has been observed in other research where higher anatase phase content had been developed using water-based SPS than with alcohol-based SPS.[156] However, switching from alcohol to water reduced the columnar characteristics of coatings deposited by SPS.[155] Although Bozorgtabar et al. introduced HVOF as the most efficient method for deposition of titania compared with APS and FS,[146] Toma et al. suggested SPS to be more promising than either APS or HVOF[151] and water-based SPS could be more efficient than alcohol-based SPS.[151,156]

5.3.3. Development of anatase TiO_2 phase during thermal spraying

High anatase phase content and reduced crystallite size have been introduced as the key parameters affecting the photocatalytic efficiency of titania films deposited by thermal spraying.[151] Bannier et al. sprayed the suspension feedstock in water to collect the particles and evaluate the phase transformation of TiO_2 during spraying (for in-flight particles) and after deposition (for immobilized TiO_2). The higher anatase phase content of in-flight particles than the coatings obviously signifies the occurrence of phase transformation of deposited TiO_2 nanoparticles on the substrate. Notably, cooling the substrate significantly enhanced the anatase

phase content.[153] Mauer et al. also evaluated the effect of substrate temperature on anatase fraction of TiO_2 coatings fabricated by SPS. Similar to Bannier et al., it has been shown that decreasing the substrate temperature could significantly increase the anatase phase content.[135] On the other hand, the substrate material has not notably affected the crystallite structure of TiO_2 coatings. In fact, anatase phase originates from either non-melted TiO_2 particles (which might have a high content of anatase phase) or its nucleation from melted TiO_2 particles.[135,153] In general, both rutile and anatase phases are observed in TiO_2 coatings deposited by thermal spraying even by using either pure rutile or pure anatase TiO_2 as the feedstock materials.[125,126,135,151] Solidification temperature or degree of undercooling could affect the nucleation of anatase/rutile from melted particles. It has been shown that high cooling rates (> $1.0*10^6$ K/s) could favor the nucleation of anatase phase.[146] Overall, two main strategies have been suggested to achieve high anatase phase contents: (i) reducing the heat-input to in-flight particles to prevent phase transformation of anatase (as a meta-stable phase) to rutile (as a stable phase) during spraying; and (ii) increasing the cooling rate of deposited particles to prevent phase transformation of anatase to rutile after spraying.[153]

These are both responsible for the much higher anatase phase content of TiO_2 coatings fabricated by HVOF compared with those fabricated by APS and FS.[146] The higher anatase phase content of TiO_2 coatings using longer stand-off distances could also be mainly attributed to the increase of cooling rate. It is notable that TiO_2 films deposited by SPS have shown a much higher photocatalytic activity than that deposited by sol-gel method. However, no linear correlation was found between the photocatalytic activity and anatase phase content (unlike other research).[153] Although the anatase phase content can highly affect the photocatalytic activity, the effect of surface properties (such as microstructure, crystallite size, surface roughness, band gap energy, porosity, and hydroxyl groups) should not be disregarded.[125,157] To compare photocatalytic performance of TiO_2 coatings deposited by suspension thermal spraying and by conventional thermal spraying, Toma et al. immobilized agglomerated TiO_2

P25 nanoparticles by methods of aqueous suspension plasma spraying, aqueous suspension HVOF and HVOF processes. Unlike titania films deposited by SHVOF with a low anatase phase content (26.8-41.5 vol%), a high anatase phase content was observed for those films deposited by SPS (67-80 vol%). The dependency of the photocatalytic activity on the anatase phase content of the deposited films is shown in Fig. 10(a).

In terms of the microstructure, despite the appearance of humps, the columnar morphology has not been observed for TiO_2 films deposited by SHVOF.[125,126] Decreasing average particle size/droplet might favor the formation of columnar microstructures in SPS (Fig. 10(b)). Using smaller particles in SPS, unlike APS, does not necessarily lead to the formation of finer microstructures.[155] The schematic of phonon scattering for coatings fabricated by different methods of SPS, APS and EB-PVD is shown in Fig. 10(c) where the highest scattering is attributed to SPS owing to the effective dispersion of porosity created along the coating thickness.[158] Apart from its several advantages, SPS is a cheaper process than EB-PVD in terms of running costs and initial investment.[159]

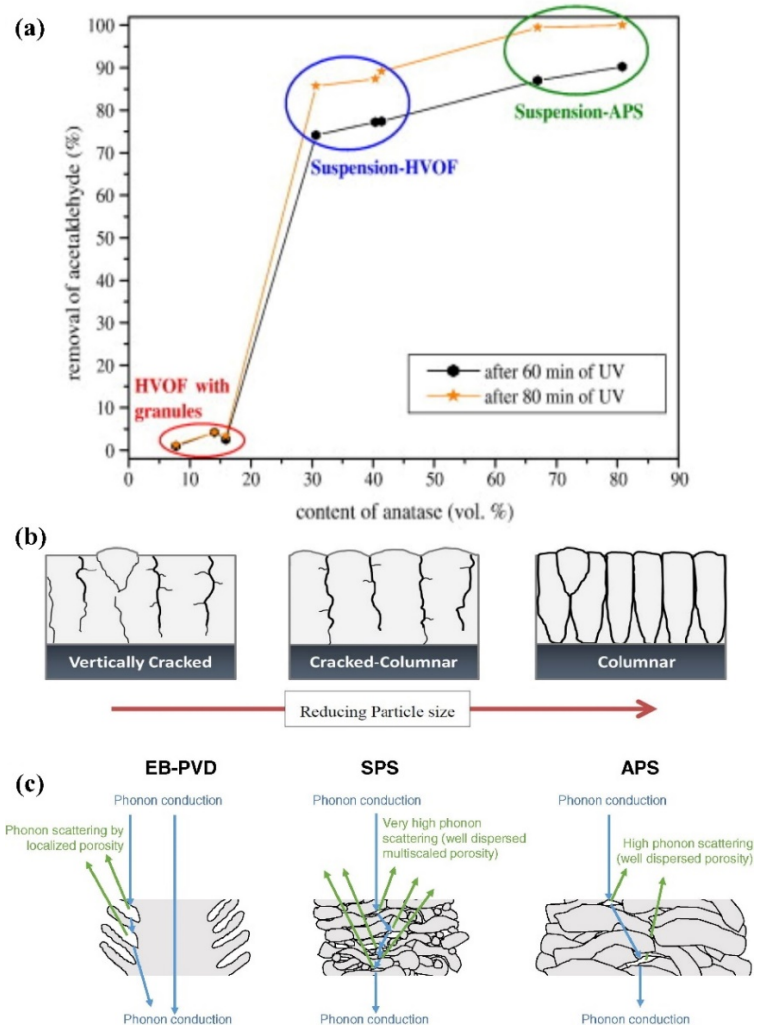

Fig. 10. (a) Dependency of photocatalytic activity on anatase content of TiO_2 films deposited by HVOF, suspension HVOF and SPS. Reproduced with permission from [149]. Copyright © 2009 F.-L. Toma et al., Elsevier. (b) schematic of effect of average particle size on the microstructure of coatings fabricated by SPS. Reproduced with permission from [155]. Copyright © 2015 F.-L. Nicholas Curry et al., MDPI. (c) schematic of phonon scattering for coatings fabricated by SPS, APS and EB-PVD. Reproduced with permission from [158]. Copyright © 2017 Benjamin Bernard et al., Elsevier.

The photocatalytic activity of TiO_2 films deposited by SHVOF and SPS processes is comparable to that deposited by conventional HVOF which has been mainly attributed to their higher anatase phase content. Although the increase of the anatase phase content from ~15% to ~30% significantly improved the photocatalytic efficiency from ~5% to ~75%, its further

increase to ~70% marginally increased the efficiency to ~85%.[149] It is nevertheless noteworthy that there are a few cases in which higher photocatalytic activity has been observed for titania films with lower anatase phase content. For example, Khammas et al. reported that nanostructured TiO_2 films with the lowest anatase phase content showed the highest photocatalytic activity, which was attributed to their increased specific surface area owing to their bimodal microstructure including fully melted splats and non-melted nanoparticles developed at lower flame heat power.[125]

5.4. Cold spraying

Although it is a major challenge to deposit coatings with pure anatase phase content using conventional thermal spraying processes, CS can be easily used for such a purpose.[160-164] It might be introduced as one of the most appropriate methods for immobilization of TiO_2 owing to its simplicity, low temperature of processing, and efficiency for deposition of large areas.[165] The low temperature (< melting point) of CS prevents phase transformation and provides the possibility of deposition of TiO_2 coatings with similar crystallite structure and grain size to the feedstock material.[163] Unlike conventional thermal spraying processes, plastic deformation of particles on the substrate results in the formation of coatings by CS.[166] Thus, the deposition of brittle materials including ceramics using CS process could be a challenge, e.g. there are reports in which the thickness of ceramic coatings deposited by CS has been limited to monolayers.[167] Chemical bonding between the substrate and TiO_2 particles (or among particles) might play an important role in the formation of TiO_2 coatings using CS.[161] Notably, the deformation of spherical agglomerated TiO_2 nanoparticles might occur upon high transient impact pressure on the substrate.[168] Both pressure and temperature of the working gas affect the kinetic energy of TiO_2 particles and their deformation upon impact.[162] Although TiO_2 films deposited by CS could suffer from lower adhesion strength than those deposited by conventional thermal spraying processes such as HVOF, APS and FS, appropriate bond coats might be used to

improve their adhesion strength. For instance, Gardon et al. used plasma-sprayed titanium sub-oxide (TiO_{2-x}) as the bond coat to increase the adhesion strength of cold-sprayed nanostructured anatase film. This new coated surface could facilitate the formation of chemical bonds due to its chemical composition, and provides easier deformation and breakdown of TiO_2 nanoparticles.[164]

Yamada et al. deposited thick TiO_2 films (up to 100 μm) using CS, by using helium as the working gas to improve the deposition rate. Increasing the working gas temperature from 25 ˚C to 400 ˚C could improve either the deposition rate or the thickness of coatings, by increasing the gas velocity and kinetic energy of the particles. It is worth mentioning that pure anatase TiO_2 has been fabricated at all temperatures. Notably, the maximum deposition efficiency was around 8% at 400 ˚C.[163] Using helium instead of nitrogen as the carrier gas also caused a greater adhesion which was attributed to the higher particle velocities.[169] Although helium can accelerate the particles faster than nitrogen, its high price could limit its industrial applications. Yamada et al. evaluated the effect of gases (helium and nitrogen) on the deposition of anatase TiO_2 coatings by CS, and concluded that the nature of gas might not be considered as a major factor affecting the quality of TiO_2 films. Enhancing the temperature increased the thickness of TiO_2 coatings in both cases. Surprisingly, cold-sprayed TiO_2 films showed a higher photocatalytic activity than the feedstock material, which was attributed to the increased specific surface area due to the breakdown or deformation of particles on the substrate. Due to the approximately similar surface area and crystallite structure, change of working gas and increasing the temperature (i.e. process gas conditions) have not significantly affected the photocatalytic activity of TiO_2 films.[160] Whereas Yamada et al. evaluated the effect of working gas temperature up to 400 ˚C,[160,163] Freitag et al. tested its effect in the range of 400-800 ˚C. Unlike TiO_2 films deposited at low pressures and temperatures, yellow coloration of TiO_2 layers was observed for those deposited at 600 ˚C (P = 35 bar) or 800 ˚C (P = 40 bar). The yellowish cold-sprayed TiO_2 could be originated from either nitrogen doping, reversible deformation

(expansion of crystal structure) of TiO_2 particles, or creation of oxygen vacancies during the deposition process. However, the creation of oxygen vacancies might have played the most important role since a yellow coloration was observed by heating white cold-sprayed TiO_2 coatings at 600 ˚C. Unlike white TiO_2 films, the yellowish ones showed photocatalytic activity under visible-light irradiation.[162]

Shen et al.[170] deposited (P, N, Mo)-doped TiO_2 particles using CS for the photocatalytic degradation of methylene blue, with TiO_2 film from 500 ˚C showing the highest photocatalytic activity under visible-light irradiation. Oxygen vacancies and color centers that could result in the red shift of absorption edge of TiO_2[170,171] might have originated from doping[170] or heating at elevated temperatures as suggested by Freitag et al.,[162] and could play an important role in the development of visible-light activated cold-sprayed (P, N, Mo)-doped TiO_2 films. Apart from its low temperature, CS could fabricate rough surfaces and porous structures[168,172] that are favored for photocatalytic applications. For instance, as reported by Toibah et al., CS resulted in the formation of TiO_2 films with the volume porosity of 45.1%. It has been shown that using porous feedstock materials could lead to the formation of TiO_2 coatings with higher porosity.[161] Overall, the plastic deformation of the feedstock material depends on its morphology, its chemical composition, and temperature of the spray jet.[173] Tang et al. showed the superior effect of powder morphology than gas temperature on the quality of Ta films deposited by CS,[174] also suggested by Nakano et al.[165] Using powders with a high volume of porosity could yield thicker coatings.[173] Using HVOF and CS processes for the deposition of anatase titania, Yang et al. reported that TiO_2 film deposited by CS showed a much higher photocatalytic activity than that deposited by HVOF, which was attributed to its higher anatase phase content and larger specific surface area. Unfortunately, rutile and anatase phase contents of TiO_2 film deposited by HVOF was not reported.[168] Thus, the deposition of TiO_2 films with high anatase phase contents by optimization of process parameters of HVOF, and comparing

their photocatalytic activity with that of pure anatase TiO_2 coating deposited by CS is worth studying.

5.5. Solution precursor plasma spraying

Unlike general methods of thermal spraying processes discussed above, solution precursor plasma spraying (SPPS) is a novel approach that uses solution precursors instead of suspensions/powders, hence could provide thinner nanostructured coatings with more homogenous structures.[175] Besides, it can take advantage of better control over the chemistry of films.[176] Overall, SPPS is more efficient than SPS as a single step method of nanostructured films deposition that can take advantage of using mixed liquid precursors as the feedstock.[177] Solvent vaporization, pyrolysis of precursor and its crystallization are three major processes that might happen during SPPS.[178] It has been shown that solvent could noticeably affect the quality of films in this method. For instance, both porous[176] and dense[179] TiO_2 coatings have been fabricated using titanium isopropoxide as the precursor, while using water as the solvent has resulted in the formation of TiO_2 films with more porosity than provided by alcohol. Increasing the plasma power did not significantly affect the microstructure whereas increasing the substrate temperature up to 450 ˚C resulted in the formation of sponge-like splats and increased porosity due to in situ evaporation of solvent and completion of pyrolysis process which can leave the pores on the fabricated film.[176] The formation of porous/spongy deposits by increasing the substrate temperature to 450 ˚C has also been reported in other studies.[178] Increasing the plasma power significantly decreased the anatase phase content, due to increase of the length and temperature of plasma jet, where TiO_2 film deposited at 45.5 kW has been composed of pure rutile phase.[176]

Similar to SPS, SPPS could also lead to the fabrication of TiO_2 columnar films.[179] Compared to SPS and APS processes, SPPS could deposit more porous coatings.[180,181] Besides, unlike SPS, using water or alcohol as the solvent could not significantly affect the

porosity of coatings deposited by SPPS.[180] On the downside, TiO_2 films deposited by SPPS suffer from low anatase phase content due to the high temperature of plasma jet.[176,179] Besides, using solution precursor might lead to the formation of TiO_2 coatings with some amorphous content (as observed by solution precursor HVOF).[182]

Like TiO_2 though at varying degrees, ZnO has also been deposited using thermal spraying processes for photocatalytic applications. Su et al. fabricated nanostructured pure ZnO and Al-doped ZnO coatings (with the average thickness of 15 and 55 μm, respectively) using APS for photocatalytic degradation of methylene blue. Al-doped ZnO film showed a higher photocatalytic activity than pure ZnO film which was attributed to its higher photo-adsorption ability and formation of p-n junctions.[183] It is notable that, in addition to the solid solution of Zn and Al, $ZnAl_2O_4$ spinel structure could be formed at high amounts of Al_2O_3 as reported by Tului et al. using 22wt% Al_2O_3.[184] The effect of stand-off distance on the quality of plasma-sprayed ZnO coatings has been investigated, with increasing distance from 6 cm to 8 cm reducing both porosity and surface roughness of the deposited films. ZnO film with the highest porosity and surface roughness has shown the highest photocatalytic activity. Notably, plasma-sprayed ZnO coatings showed higher photo-adsorption ability than the feedstock powder.[52] Unlike TiO_2, no phase transformation was observed in the case ZnO coatings fabricated by thermal spraying processes.[52,183] The yellowish plasma-sprayed ZnO films[52] might be originated from the creation of oxygen vacancies[185] at high temperatures, as reported for cold-sprayed TiO_2 coatings at high temperatures.[162,170] Although ZnO films deposited by APS have been efficient for the degradation of methylene blue under UV or UV-vis illumination,[52,183] further attempts are needed to drive visible-light activated ZnO coatings deposited by thermal spraying. In general, thermal spraying processes are not dependent on the substrate material which can facilitate their use for practical photocatalytic applications. For instance, Wallenhorst et al. deposited Zn/ZnO particles on wood using APS for development of UV-blocking properties.[186]

Unlike difficulties associated with deposition of TiO_2 coatings with high anatase phase content using solution precursor-based methods in both plasma spraying[176,179] and HVOF,[182] thermal stability of wurtzite ZnO phase at elevated temperatures has recently attracted the attention of researchers for deposition of ZnO by SPPS.[181,187,188] Yu et al. used two different solution precursors, 0.2 M zinc acetate water solutions and ethanol/water mixture, for deposition of ZnO films using SPPS. Both solution precursors resulted in the formation of ZnO coatings with narrowed band gap energies, compared with theoretical band gap energy of pure ZnO, which was attributed to creation of oxygen vacancies during thermal spraying.[181] The higher the heating/cooling gradient, the more is the concentration of oxygen vacancies and the lower is the band gap energy.[188] Notably, using a mixture of water/ethanol could be more efficient in the reduction of the band gap energy (due to the combustion heat of ethanol liberated in the plasma region). Moreover, its lower surface tension could break the solution droplets into smaller ones, during the injection, which can be more accelerated. A coral-like microstructure, composed of ZnO nanorods was formed using a water/ethanol mixture which provided higher specific surface area and higher photocatalytic activity than cauliflower-like morphology fabricated by using only water as the solvent. It has been stated that ethanol to water volume ratio affect the morphology of fabricated films.[181] However, Zhang et al. deposited ZnO_{1-x} coatings with the band gap energy of 2.15 eV[189] which is much lower than that reported by Yu et al. (i.e. 3.02 eV) where water/ethanol mixture was used as the solvent.[181] Thus, process parameters could play a more important role than type of solvent in creation of oxygen vacancies.

Although SPPS usually results in the formation of films with irregular particles and molten/flatten splats,[177,190-192] using appropriate solvents and deposition parameters could lead to the formation of hierarchical structures which are favored for photocatalytic applications.[181,188] Yu et al. evaluated the effect of solvent concentration and process parameters on the quality of ZnO films deposited by SPPS. Apart from cauliflower-like

microstructures composed of irregular particles, formation of various hierarchical structures (including nanorods, nanowires, and nanoflakes) has been reported in different conditions.[188] In addition to the formation of hierarchical structures, SPPS could provide textured films with preferential orientation along plane[181,188,193] which can be considered as the most favorable orientation of ZnO films owing to its superior photocatalytic activity than other crystal ZnO planes.[181] It has been concluded that formation and preservation of appropriate clusters are prerequisites for synthesis of nanostructured hierarchical films using SPPS.

An appropriate solvent, short stand-off distance, and high flow rate of solution followed by substrate preheating favor the formation of desired ZnO clusters.[188] Although oxygen-defective ZnO films with nanorod and nanowire morphologies have shown photocatalytic activity under visible-light irradiation, the fabrication of efficient visible-light activated ZnO films deposited by SPPS needs further attempts. In addition to several advantages of SPPS, combining well-dispersed suspensions of either Zn or ZnO nanoparticles with the solution precursor could provide nanoporous ZnO coatings as reported by Chen et al.[187] Overall, the development of efficient morphologies for photocatalytic applications including columnar cauliflower-like,[193-196] nanorods [181,191,197] and nanowires,[197] as observed for various materials, could offer SPPS as a promising method for the deposition of both TiO_2 and ZnO based photocatalysts. The final morphology of films deposited by SPPS could be easily controlled by adjusting composition of precursor solutions.[197] The main advantages and disadvantages of thermal spraying processes and general aspects of some surface engineering methods are summarized in Tables S9 and S10, respectively. Different types of surface topographies and morphologies of TiO_2 and ZnO coatings deposited by thermal spraying processes are depicted in Fig. 11.

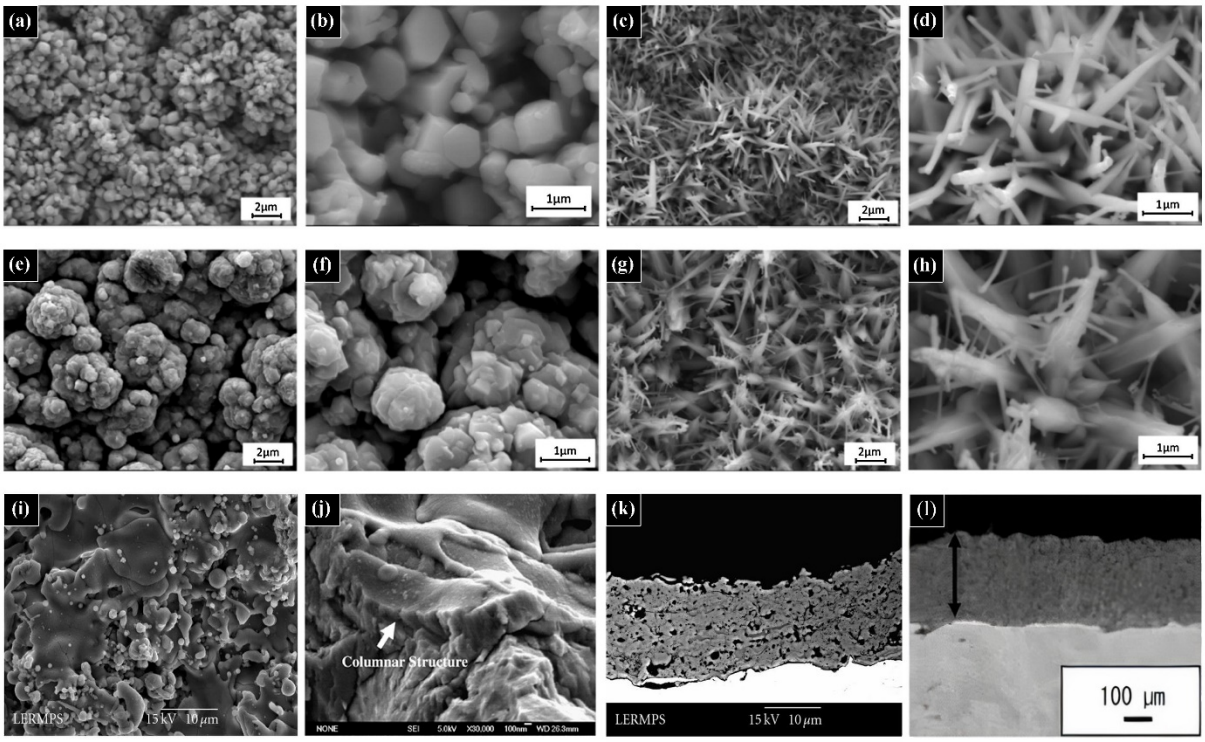

Fig. 11. (a-h) Surface topographies of ZnO coatings deposited by SPPS. Reproduced with permission from [188]. Copyright © 2019 Zexin Yu et al., Elsevier. (i) surface topography of TiO_2 film deposited by APS. Reproduced with permission from [151]. Copyright © 2008 Filofteia-Laura Toma et al., Hindawi. (j) surface morphology of TiO_2 film deposited by SPPS. Reproduced with permission from [179]. Copyright © 2008 Dianying Chen et al., John Wiley and Sons. (k) surface morphology of TiO_2 film deposited by HVOF. Reproduced with permission from [151]. Copyright © 2008 Filofteia-Laura Toma et al., Hindawi. (l) surface morphology of TiO_2 film deposited by CS. Reproduced with permission from [198]. Copyright © 2020 Noor Irinah Omar et al., MDPI.

By far, typical thickness and roughness of coatings fabricated by thermal spraying are higher than those provided by other methods which can offer this method as one of the most attractive processes for deposition of photocatalytic TiO_2 and ZnO coatings. Besides, it can take advantage of high adhesion strength of coatings to the substrate (Table S7). Moreover, the creation of in situ oxygen vacancies, due to the high rates of heating/cooling, can narrow the band gap energy of TiO_2 and ZnO films. Notably, unlike other methods of immobilization, it

can provide the possibility of on-sight repairs.[199] It is worth mentioning that fabrication of rough/porous surfaces using this method could improve the light-harvest (unlike smooth surfaces fabricated by general methods of surface engineering in gaseous and vapor states).[93] CS also can be effectively used for the deposition of TiO_2 and ZnO coatings with desired chemical composition or meta-stable phases such as rocksalt ZnO, with higher photocatalytic activity than wurtzite ZnO[23] and anatase TiO_2. Despite of its potential application in the immobilization of TiO_2 and ZnO, thermal spraying has not been used for the degradation of persistent organic pollutants including PFOA which is worth studying.

6. Future perspectives

Although SPPS is an ideal method for the deposition of wurtzite ZnO, further research is needed to fabricate either meta-stable rocksalt ZnO films or TiO_2 coatings with high anatase phase contents. Since PEC is generally more effective than photocatalysis for the degradation of pollutants, the deposition of ZnO and TiO_2 photoanodes using efficient thermal spraying processes for photocatalytic degradation of persistent organic pollutants, where effective separation of charge carriers is required, is worth studying. Notably, both TiO_2 and ZnO could suffer from their large band gap energies.[200,201] Using advanced surface engineering methods to deposit visible-light activated TiO_2 and ZnO coatings should provide pathways for practical applications of environmental photocatalysis in the future.

7. Conclusions

The industrial methods of anodizing and thermal spraying for depositing TiO_2 and ZnO that could facilitate their use in practical applications of photocatalysis have been reviewed. Although nanotubular structures suffer from low specific surface area than nanoparticulate structures, they are considered as the most desirable morphology for photocatalytic purposes owing to their unique properties including high adherent strength to the substrate, short carrier-

diffusion paths, and low recombination of e^-/h^+ pairs. More importantly, the application of anodizing in the production of nanotubes has initiated PEC with higher efficacy than photocatalysis for the degradation of persistent pollutants including PFOA. Overall, thermal spraying processes that facilitate the fabrication of thick and rough TiO_2 and ZnO films with in situ developed oxygen vacancies (providing narrow band gap energy) and various hierarchical structures on different substrates could be considered as one of the most promising methods for the deposition of photocatalytic coatings. Novel thermal spraying processes including CS and SPPS which can provide coatings with desirable chemical composition and nanoporous/columnar structures, respectively, are highly recommended for the deposition of TiO_2 and ZnO coatings for the degradation of persistent organic pollutants. Finally, PEC is shown to be more powerful than photocatalysis in the photodegradation performance.

Conflict of Interest

The authors declare that there is no conflict of interest.

References

[1] Parrino, F.; Loddo, V.; Augugliaro, V.; Camera-Roda, G.; Palmisano, G.; Palmisano, L.; Yurdakal, S. Heterogeneous Photocatalysis: Guidelines on Experimental Setup, Catalyst Characterization, Interpretation, and Assessment of Reactivity. *Catal. Rev.* 2019, 61 (2), 163-213.

[2] Zhu, S.; Wang, D. Photocatalysis: Basic Principles, Diverse Forms of Implementations and Emerging Scientific Opportunities. *Adv. Energy Mater.* 2017, 7 (23), 1700841.

[3] Laxma Reddy, P. V.; Kavitha, B.; Kumar Reddy, P. A.; Kim, K.-H. TiO_2-Based Photocatalytic Disinfection of Microbes in Aqueous Media: A Review. *Environ. Res.* 2017, 154, 296-303.

[4] Kumar, S.; Kumar, A.; Kumar, A.; Krishnan, V. Nanoscale Zinc Oxide Based Heterojunctions as Visible Light Active Photocatalysts for Hydrogen Energy and Environmental Remediation. *Catal. Rev.* 2020, 62 (3), 346-405.

[5] Kanan, S.; Moyet, M. A.; Arthur, R. B.; Patterson, H. H. Recent Advances on TiO_2-Based Photocatalysts Toward the Degradation of Pesticides and Major Organic Pollutants from Water Bodies. *Catal. Rev.* 2020, 62 (1), 1-65.

[6] Wen, J.; Xie, J.; Chen, X.; Li, X. A Review on G-C_3N_4-Based Photocatalysts. *Appl. Surf. Sci.* 2017, 391, 72-123.

[7] Ding, Z.; Lu, G. Q.; Greenfield, P. F. Role of the Crystallite Phase of TiO_2 in Heterogeneous Photocatalysis for Phenol Oxidation in Water. *J. Phys. Chem. B* 2000, 104 (19), 4815-4820.

[8] Tran, T. T. H.; Kosslick, H.; Schulz, A.; Nguyen, Q. L. Photocatalytic Performance of Crystalline Titania Polymorphs in the Degradation of Hazardous Pharmaceuticals and Dyes. *Adv. Nat. Sci. Nanosci.* 2017, 8 (1), 015011.

[9] Kandiel, T. A.; Robben, L.; Alkaim, A.; Bahnemann, D. Brookite versus Anatase TiO_2 Photocatalysts: Phase Transformations and Photocatalytic Activities. *Photochem. Photobiol. Sci.* 2013, 12 (4), 602-609.

[10] Farhadian Azizi, K.; Bagheri-Mohagheghi, M. M. Transition from Anatase to Rutile Phase in Titanium Dioxide (TiO_2) Nanoparticles Synthesized by Complexing Sol–Gel Process: Effect of Kind of Complexing Agent and Calcinating Temperature. *J. Sol-Gel Sci. Technol.* 2013, 65 (3), 329-335.

[11] Etacheri, V.; Di Valentin, C.; Schneider, J.; Bahnemann, D.; Pillai, S. C. Visible-Light Activation of TiO_2 Photocatalysts: Advances in Theory and Experiments. *J. Photochem. Photobiol. C* 2015, 25, 1-29.

[12] Qian, R.; Zong, H.; Schneider, J.; Zhou, G.; Zhao, T.; Li, Y.; Yang, J.; Bahnemann, D. W.; Pan, J. H. Charge Carrier Trapping, Recombination and Transfer During TiO_2 Photocatalysis: An Overview. *Catal. Today* 2019, 335, 78-90.

[13] Lee, K. M.; Lai, C. W.; Ngai, K. S.; Juan, J. C. Recent Developments of Zinc Oxide Based Photocatalyst in Water Treatment Technology: A Review. *Water Res.* 2016, 88, 428-448.

[14] Espitia, P.; Soares, N.; Coimbra, J.; Andrade, N.; Cruz, R.; Medeiros, E. Zinc Oxide Nanoparticles: Synthesis, Antimicrobial Activity and Food Packaging Applications. *Food Bioproc. Tech.* 2012, 5, 1447-1464.

[15] Alves, T. E. P.; Kolodziej, C.; Burda, C.; Franco, A. Effect of Particle Shape and Size on the Morphology and Optical Properties of Zinc Oxide Synthesized by the Polyol Method. *Mater. Des.* 2018, 146, 125-133.

[16] Shende, P.; Kasture, P.; Gaud, R. S. Nanoflowers: The Future Trend of Nanotechnology for Multi-Applications. *Artif. Cells Nanomed. Biotechnol.* 2018, 46, 413-422.

[17] Qu, Y.; Huang, R.; Qi, W.; Shi, M.; Su, R.; He, Z. Controllable Synthesis of ZnO Nanoflowers with Structure-Dependent Photocatalytic Activity. *Catal. Today* 2019, 355, 397-407

[18] Ong, C. B.; Ng, L. Y.; Mohammad, A. W. A Review of ZnO Nanoparticles as Solar Photocatalysts: Synthesis, Mechanisms and Applications. *Renew. Sust. Energy Rev.* 2018, 81, 536-551.

[19] Liao, J.; Lin, S.; Zhang, L.; Pan, N.; Cao, X.; Li, J. Photocatalytic Degradation of Methyl Orange Using a TiO_2/Ti Mesh Electrode with 3D Nanotube Arrays. *ACS Appl. Mater. Interfaces* 2012, 4 (1), 171-177.

[20] Daneshvar, N.; Salari, D.; Khataee, A. R. Photocatalytic Degradation of Azo Dye Acid Red 14 in Water on ZnO as an Alternative Catalyst to TiO_2. *J. Photochem. Photobiol. A* 2004, 162 (2), 317-322.

[21] Wang, H.; Wang, J.; Xiang, X.; Zhou, Y.; Li, Q.; Tang, A.; Liao, D.; Liu, Y.; Liu, H.-b. Preparation of PVDF/CdS/Bi_2WO_6/ZnO Hybrid Membrane with Enhanced Visible-Light Photocatalytic Activity for Degrading Nitrite in Water. *Environ. Res.* 2020, 191, 110036.

[22] Rajbongshi, B. M.; Samdarshi, S. K. Cobalt-Doped Zincblende–Wurtzite Mixed-Phase ZnO Photocatalyst Nanoparticles with High Activity in Visible Spectrum. *Appl. Catal. B* 2014, 144, 435-441.

[23] Razavi-Khosroshahi, H.; Edalati, K.; Wu, J.; Nakashima, Y.; Arita, M.; Ikoma, Y.; Sadakiyo, M.; Inagaki, Y.; Staykov, A.; Yamauchi, M.; et al. High-Pressure Zinc Oxide Phase as Visible-Light-Active Photocatalyst with Narrow Band Gap. *J. Mater. Chem. A* 2017, 5 (38), 20298-20303.

[24] Saleh, N. B.; Khalid, A.; Tian, Y.; Ayres, C.; Sabaraya, I. V.; Pietari, J.; Hanigan, D.; Chowdhury, I.; Apul, O. G. Removal of Poly- and Per-Fluoroalkyl Substances from Aqueous Systems by Nano-Enabled Water Treatment Strategies. *Environ. Sci. Water Res. Technol.* 2019, 5 (2), 198-208.

[25] Xu, B.; Liu, S.; Zhou, J. L.; Zheng, C.; Jin, W.; Zhang, T.; Qiu, W. PFAS and Their Substitutes in Groundwater: Occurrence, Transformation and Remediation. *J. Hazard. Mater.* 2021, 412, 125159.

[26] Xu, B.; Ahmed, M. B.; Zhou, J. L.; Altaee, A.; Wu, M.; Xu, G. Photocatalytic Removal of Perfluoroalkyl Substances from Water and Wastewater: Mechanism, Kinetics and Controlling Factors. *Chemosphere* 2017, 189, 717-729.

[27] Ross, I.; McDonough, J.; Miles, J.; Storch, P.; Thelakkat Kochunarayanan, P.; Kalve, E.; Hurst, J.; S. Dasgupta, S.; Burdick, J. A Review of Emerging Technologies for Remediation of PFASs. *Remediat. J.* 2018, 28 (2), 101-126.

[28] Olatunde, O. C.; Kuvarega, A. T.; Onwudiwe, D. C. Photo Enhanced Degradation of Polyfluoroalkyl and Perfluoroalkyl Substances. *Heliyon* 2020, 6 (12), e05614.

[29] Zhang, W.; Zhang, Y.; Taniyasu, S.; Yeung, L. W. Y.; Lam, P. K. S.; Wang, J.; Li, X.; Yamashita, N.; Dai, J. Distribution and Fate of Perfluoroalkyl Substances in Municipal Wastewater Treatment Plants in Economically Developed Areas of China. *Environ. Pollut.* 2013, 176, 10-17.

[30] Abunada, Z.; Alazaiza, M. Y. D.; Bashir, M. J. K. An Overview of Per- and Polyfluoroalkyl Substances (PFAS) in the Environment: Source, Fate, Risk and Regulations. *Water* 2020, 12 (12), 3590.

[31] Tang, C. Y.; Fu, Q. S.; Robertson, A. P.; Criddle, C. S.; Leckie, J. O. Use of Reverse Osmosis Membranes to Remove Perfluorooctane Sulfonate (PFOS) from Semiconductor Wastewater. *Environ. Sci. Technol.* 2006, 40 (23), 7343-7349.

[32] Wang, S.; Yang, Q.; Chen, F.; Sun, J.; Luo, K.; Yao, F.; Wang, X.; Wang, D.; Li, X.; Zeng, G. Photocatalytic Degradation of Perfluorooctanoic Acid and Perfluorooctane Sulfonate in Water: A Critical Review. *Chem. Eng. J.* 2017, 328, 927-942.

[33] Oliaei, F.; Kriens, D.; Weber, R.; Watson, A. PFOS and PFC Releases and Associated Pollution from a PFC Production Plant in Minnesota (USA). *Environ. Sci. Pollut. Res.* 2013, 20 (4), 1977-1992.

[34] Giri, R. R.; Ozaki, H.; Morigaki, T.; Taniguchi, S.; Takanami, R. UV Photolysis of Perfluorooctanoic acid (PFOA) in Dilute Aqueous Solution. *Water Sci. Technol.* 2011, 63 (2), 276-282.

[35] Merino, N.; Qu, Y.; Deeb, R. A.; Hawley, E. L.; Hoffmann, M. R.; Mahendra, S. Degradation and Removal Methods for Perfluoroalkyl and Polyfluoroalkyl Substances in Water. *Environ. Eng. Sci.* 2016, 33 (9), 615-649.

[36] Li, Z.; Zhang, P.; Shao, T.; Wang, J.; Jin, L.; Li, X. Different Nanostructured In_2O_3 for Photocatalytic Decomposition of Perfluorooctanoic Acid (PFOA). *J. Hazard. Mater.* 2013, 260, 40-46.

[37] Li, X.; Zhang, P.; Jin, L.; Shao, T.; Li, Z.; Cao, J. Efficient Photocatalytic Decomposition of Perfluorooctanoic Acid by Indium Oxide and Its Mechanism. *Environ. Sci. Technol.* 2012, 46 (10), 5528-5534.

[38] Mahapatra, C. T.; Damayanti, N. P.; Guffey, S. C.; Serafin, J. S.; Irudayaraj, J.; Sepúlveda, M. S. Comparative in Vitro Toxicity Assessment of Perfluorinated Carboxylic Acids. *J. Appl. Toxicol.* 2017, 37 (6), 699-708.

[39] Yang, L.; He, L.; Xue, J.; Ma, Y.; Xie, Z.; Wu, L.; Huang, M.; Zhang, Z. Persulfate-Based Degradation of Perfluorooctanoic Acid (PFOA) and Perfluorooctane Sulfonate (PFOS) in Aqueous Solution: Review on Influences, Mechanisms and Prospective. *J. Hazard. Mater.* 2020, 393, 122405.

[40] Wu, Y.; Li, Y.; Fang, C.; Li, C. Highly Efficient Degradation of Perfluorooctanoic Acid over a MnOx-Modified Oxygen-Vacancy-Rich In_2O_3 Photocatalyst. *ChemCatChem* 2019, 11 (9), 2297-2303.

[41] Xu, B.; Ahmed, M. B.; Zhou, J. L.; Altaee, A. Visible and UV Photocatalysis of Aqueous Perfluorooctanoic Acid by TiO_2 and Peroxymonosulfate: Process Kinetics and Mechanistic Insights. *Chemosphere* 2020, 243, 125366.

[42] Estrellan, C. R.; Salim, C.; Hinode, H. Photocatalytic Decomposition of Perfluorooctanoic Acid by Iron and Niobium co-Doped Titanium Dioxide. *J. Hazard. Mater.* 2010, 179 (1), 79-83.

[43] Li, S.; Wang, X.; Liu, L.; Guo, Y.; Mu, Q.; Mellouki, A. Enhanced Degradation of Perfluorooctanoic Acid Using Dielectric Barrier Discharge with La/Ce-Doped TiO_2. *Environ. Sci. Pollut. Res.* 2017, 24 (18), 15794-15803.

[44] Chen, M.-J.; Lo, S.-L.; Lee, Y.-C.; Huang, C.-C. Photocatalytic Decomposition of Perfluorooctanoic Acid by Transition-Metal Modified Titanium Dioxide. *J. Hazard. Mater.* 2015, 288, 168-175.

[45] Li, M.; Yu, Z.; Liu, Q.; Sun, L.; Huang, W. Photocatalytic Decomposition of Perfluorooctanoic Acid by Noble Metallic Nanoparticles Modified TiO_2. *Chem. Eng. J.* 2016, 286, 232-238.

[46] Fu, X.; Long, J.; Wang, X.; Leung, D. Y. C.; Ding, Z.; Wu, L.; Zhang, Z.; Li, Z.; Fu, X. Photocatalytic Reforming of Biomass: A Systematic Study of Hydrogen Evolution from Glucose Solution. *Int. J. Hydrog. Energy* 2008, 33 (22), 6484-6491.

[47] Javed, H.; Metz, J.; Eraslan, T. C.; Mathieu, J.; Wang, B.; Wu, G.; Tsai, A.-L.; Wong, M. S.; Alvarez, P. J. J. Discerning the Relevance of Superoxide in PFOA Degradation. *Environ. Sci. Technol. Lett.* 2020, 7 (9), 653-658.

[48] Wang, K.; Huang, D.; Wang, W.; Ji, Y.; Niu, J. Enhanced Perfluorooctanoic Acid Degradation by Electrochemical Activation of Peroxymonosulfate in Aqueous Solution. *Environ. Int.* 2020, 137, 105562.

[49] Huang, J.; Wang, X.; Pan, Z.; Li, X.; Ling, Y.; Li, L. Efficient Degradation of Perfluorooctanoic Acid (PFOA) by Photocatalytic Ozonation. *Chem. Eng. J.* 2016, 296, 329-334.

[50] Wu, D.; Li, X.; Tang, Y.; Lu, P.; Chen, W.; Xu, X.; Li, L. Mechanism Insight of PFOA Degradation by ZnO Assisted-Photocatalytic Ozonation: Efficiency and Intermediates. *Chemosphere* 2017, 180, 247-252.

[51] Kandeva, M.; Vencl, A.; Karastoyanov, D. *Advanced Tribological Coatings for Heavy-Duty Applications: Case Studies*, 2016.

[52] Navidpour, A. H.; Kalantari, Y.; Salehi, M.; Salimijazi, H. R.; Amirnasr, M.; Rismanchian, M.; Azarpour Siahkali, M. Plasma-Sprayed Photocatalytic Zinc Oxide Coatings. *J. Therm. Spray Technol.* 2017, 26 (4), 717-727.

[53] Dörr, T. S.; Deilmann, L.; Haselmann, G.; Cherevan, A.; Zhang, P.; Blaha, P.; de Oliveira, P. W.; Kraus, T.; Eder, D. Ordered Mesoporous TiO_2 Gyroids: Effects of Pore Architecture and Nb-Doping on Photocatalytic Hydrogen Evolution under UV and Visible Irradiation. *Adv. Energy Mater.* 2018, 8 (36), 1802566.

[54] García-Benjume, M. L.; Espitia-Cabrera, M. I.; Contreras-García, M. E. Enhanced Photocatalytic Activity of Hierarchical Macro-Mesoporous Anatase by ZrO_2 Incorporation. *Int. J. Photoenergy* 2012, 2012, 1-10.

[55] Liu, H.; Zhang, Y.; Yang, H.; Xiao, W.; Sun, L. Study on Synthesis and Photocatalytic Activity of Porous Titania Nanotubes. *Adv. Mater. Sci. Eng.* 2016, 2016, 1-10.

[56] Yu, J.; Zhao, X.; Zhao, Q. Effect of Film Thickness on the Grain Size and Photocatalytic Activity of the Sol–Gel Derived Nanometer TiO_2 Thin Films. *J. Mater. Sci. Lett.* 2000, 19, 1015-1017.

[57] Chen, Y.-H.; Tu, K.-J. Thickness Dependent on Photocatalytic Activity of Hematite Thin Films. *Int. J. Photoenergy* 2012, 2012, 980595.

[58] Xianyu, W. X.; Park, M. K.; Lee, W. I. Thickness Effect in the Photocatalytic Activity of TiO_2 Thin Films Derived from Sol-Gel Process. *Korean J. Chem. Eng.* 2001, 18 (6), 903-907.

[59] Heikkilä, M.; Puukilainen, E.; Ritala, M.; Leskelä, M. Effect of Thickness of ALD Grown TiO_2 Films on Photoelectrocatalysis. *J. Photochem. Photobiol. A* 2009, 204 (2), 200-208.

[60] Roy, P.; Berger, S.; Schmuki, P. TiO_2 Nanotubes: Synthesis and Applications. *Angew. Chem. Int. Ed. Engl.* 2011, 50 (13), 2904-2939.

[61] Karuppusamy, I.; Ningshenb, S.; Mudali, K.; Nallaiyan, R. Effect of Anodization Parameters on the Structural Morphology of Titanium in Fluoride Containing Electrolytes. *Mater. Charact.* 2012, 71, 58-65.

[62] Fu, Y.; Mo, A. A Review on the Electrochemically Self-organized Titania Nanotube Arrays: Synthesis, Modifications, and Biomedical Applications. *Nanoscale Res. Lett.* 2018, 13 (1), 187.

[63] Sreekantan, S.; Saharudin, K. A.; Wei, L. C. Formation of TiO_2 Nanotubes via Anodization and Potential Applications for Photocatalysts, Biomedical Materials, and Photoelectrochemical Cell. *IOP Conf. Ser. Mater. Sci. Eng.* 2011, 21, 012002.

[64] Mura, F.; Masci, A.; Pasquali, M.; Pozio, A. Effect of a Galvanostatic Treatment on the Preparation of Highly Ordered TiO_2 Nanotubes. *Electrochim. Acta* 2009, 54 (14), 3794-3798.

[65] Indira, K.; Mudali, U. K.; Nishimura, T.; Rajendran, N. A Review on TiO_2 Nanotubes: Influence of Anodization Parameters, Formation Mechanism, Properties, Corrosion Behavior, and Biomedical Applications. *J. Bio Tribocorros.* 2015, 1 (4), 28.

[66] Likodimos, V.; Stergiopoulos, T.; Falaras, P.; Kunze, J.; Schmuki, P. Phase Composition, Size, Orientation, and Antenna Effects of Self-Assembled Anodized Titania Nanotube Arrays: A Polarized Micro-Raman Investigation. *J. Phys. Chem. C* 2008, 112 (51), 20574.

[67] Gupta, B. K.; Kedawat, G.; Agrawal, Y.; Kumar, P.; Dwivedi, J.; Dhawan, S. K. A Novel Strategy to Enhance Ultraviolet Light Driven Photocatalysis from Graphene Quantum Dots Infilled TiO_2 Nanotube Arrays. *RSC Adv.* 2015, 5 (14), 10623-10631.

[68] Li, S.; Zhang, G.; Guo, D.; Yu, L.; Zhang, W. Anodization Fabrication of Highly Ordered TiO_2 Nanotubes. *J. Phys. Chem. C* 2009, 113 (29), 12759-12765.

[69] Song, J.; Zheng, M.; Zhang, B.; Li, Q.; Wang, F.; Ma, L.; Li, Y.; Zhu, C.; Ma, L.; Shen, W. Fast Growth of Highly Ordered TiO_2 Nanotube Arrays on Si Substrate under High-Field Anodization. *Nano-Micro Lett.* 2016, 9 (2), 13.

[70] Ye, Y.; Bruning, H.; Li, X.; Yntema, D.; Rijnaarts, H. H. M. Significant Enhancement of Micropollutant Photocatalytic Degradation Using a TiO_2 Nanotube Array Photoanode Based Photocatalytic Fuel Cell. *Chem. Eng. J.* 2018, 354, 553-562.

[71] Adán, C.; Marugán, J.; Sánchez, E.; Pablos, C.; van Grieken, R. Understanding the Effect of Morphology on the Photocatalytic Activity of TiO_2 Nanotube Array Electrodes. *Electrochim. Acta* 2016, 191, 521-529.

[72] Liu, N.; Chen, X.; Zhang, J.; Schwank, J. W. A Review on TiO_2-Based Nanotubes Synthesized via Hydrothermal Method: Formation Mechanism, Structure Modification, and Photocatalytic Applications. *Catal. Today* 2014, 225, 34-51.

[73] Zhou, X.; Liu, N.; Schmuki, P. Photocatalysis with TiO_2 Nanotubes: "Colorful" Reactivity and Designing Site-Specific Photocatalytic Centers into TiO_2 Nanotubes. *ACS Catal.* 2017, 7 (5), 3210-3235.

[74] Meriam Suhaimy, S. H.; Lai, C. W.; Tajuddin, H. A.; Samsudin, E. M.; Johan, M. R. Impact of TiO_2 Nanotubes' Morphology on the Photocatalytic Degradation of Simazine Pollutant. *Materials* 2018, 11 (11), 2066.

[75] Liang, H. C.; Li, X. Z.; Nowotny, J. Photocatalytical Properties of TiO_2 Nanotubes. *Solid State Phenom.* 2010, 162, 295-328.

[76] Mor, G. K.; Varghese, O. K.; Paulose, M.; Shankar, K.; Grimes, C. A. A Review on Highly Ordered, Vertically Oriented TiO_2 Nanotube Arrays: Fabrication, Material Properties, and Solar Energy Applications. *Sol. Energy Mater. Sol. Cells* 2006, 90 (14), 2011-2075.

[77] Jenkins, S. B. *Nanoporous Materials: Types, Properties and Uses*. 2010; p 1-366.

[78] Sulka, G. D.; Kapusta-Kołodziej, J.; Brzózka, A.; Jaskuła, M. Fabrication of Nanoporous TiO_2 by Electrochemical Anodization. *Electrochim. Acta* 2010, 55 (14), 4359-4367.

[79] Macak, J. M.; Albu, S. P.; Schmuki, P. Towards Ideal Hexagonal Self-Ordering of TiO_2 Nanotubes. *Phys. Status Solidi Rapid Res. Lett.* 2007, 1 (5), 181-183.

[80] Mahdi, N.; Kumar, P.; Goswami, A.; Perdicakis, B.; Shankar, K.; Sadrzadeh, M. Robust Polymer Nanocomposite Membranes Incorporating Discrete TiO_2 Nanotubes for Water Treatment. *Nanomaterials* 2019, 9 (9), 1186.

[81] Jing-zhong, Z.; Yang, B.; Kun, Z.; Ye, L.; Lu, K. Preparation of Separated and Open End TiO_2 Nanotubes. *Ceram. Int.* 2015, 41 (6), 7235-7240.

[82] Liao, J.; Lin, S.; Pan, N.; Li, D.; Li, S.; Li, J. Free-Standing Open-Ended TiO_2 Nanotube Membranes and Their Promising Through-Hole Applications. *Chem. Eng. J.* 2012, 211-212, 343-352.

[83] Pasikhani, J. V.; Gilani, N.; Pirbazari, A. E. The Effect of the Anodization Voltage on the Geometrical Characteristics and Photocatalytic Activity of TiO_2 Nanotube Arrays. *Nano-Struct. Nano-Objects* 2016, 8, 7-14.

[84] Zhang, G.; Huang, H.; Zhang, Y.; Chan, H. L. W.; Zhou, L. Highly Ordered Nanoporous TiO_2 and Its Photocatalytic Properties. *Electrochem. Commun.* 2007, 9 (12), 2854-2858.

[85] Dikici, T.; Yildirim, S.; Yurddaskal, M.; Erol, M.; Yigit, R.; Toparli, M.; Celik, E. A Comparative Study on the Photocatalytic Activities of Microporous and Nanoporous TiO_2 Layers Prepared by Electrochemical Anodization. *Surf. Coat. Technol.* 2015, 263, 1-7.

[86] Heydari, G.; Hollman, J.; Achari, G.; Langford, H. C. Comparative Study of Four TiO_2-Based Photocatalysts to Degrade 2,4-D in a Semi-Passive System. *Water* 2019, 11 (3), 621.

[87] Sornalingam, K.; McDonagh, A.; Zhou, J. L. Photodegradation of Estrogenic Endocrine Disrupting Steroidal Hormones in Aqueous Systems: Progress and Future Challenges. *Sci. Total Environ.* 2016, 550, 209-224.

[88] Macak, J. M.; Zlamal, M.; Krysa, J.; Schmuki, P. Self-Organized TiO_2 Nanotube Layers as Highly Efficient Photocatalysts. *Small* 2007, 3 (2), 300-304.

[89] Park, K.; Ali, I.; Kim, J.-O. Photodegradation of Perfluorooctanoic Acid by Graphene Oxide-Deposited TiO_2 Nanotube Arrays in Aqueous Phase. *J. Environ. Manage.* 2018, 218, 333-339.

[90] Rajeshwar, K.; Osugi, M. E.; Chanmanee, W.; Chenthamarakshan, C. R.; Zanoni, M. V. B.; Kajitvichyanukul, P.; Krishnan-Ayer, R. Heterogeneous Photocatalytic Treatment of Organic Dyes in Air and Aqueous Media. *J. Photochem. Photobiol. C* 2008, 9 (4), 171-192.

[91] Huang, J.; Tan, X.; Yu, T.; Zhao, L.; Liu, H. Enhanced Photovoltaic and Photoelectrocatalytic Properties by Free-Standing TiO_2 Nanotubes via Anodization. *J. Solid State Electrochem.* 2015, 19 (4), 1151-1160.

[92] Liu, Y.; Su, D.; Zhang, Y.; Wang, L.; Yang, G.; Shen, F.; Deng, S.; Zhang, X.; Zhang, S. Anodized TiO_2 Nanotubes Coated with Pt Nanoparticles for Enhanced Photoelectrocatalytic Activity. *J. Mater. Res.* 2017, 32, 1-9.

[93] Li, X.; Yu, J.; Jaroniec, M. Hierarchical Photocatalysts. *Chem. Soc. Rev.* 2016, 45 (9), 2603-2636.

[94] Li, M.; Liu, Y.; Dong, L.; Shen, C.; Li, F.; Huang, M.; Ma, C.; Yang, B.; An, X.; Sand, W. Recent Advances on Photocatalytic Fuel Cell for Environmental Applications-The Marriage of Photocatalysis and Fuel Cells. *Sci. Total Environ.* 2019, 668, 966-978.

[95] Kaneko, M.; Gokan, N.; Katakura, N.; Takei, Y.; Hoshino, M. Artificial Photochemical Nitrogen Cycle to Produce Nitrogen and Hydrogen from Ammonia by Platinized TiO_2 and Its Application to a Photofuel Cell. *Chem. Commun.* 2005, (12), 1625-1627.

[96] Sfaelou, S.; Lianos, P. Photoactivated Fuel Cells (PhotoFuelCells). An Alternative Source of Renewable Energy with Environmental Benefits. *AIMS Mater. Sci.* 2016, 3, 270-288.

[97] Zhu, A.; Zhao, Q.; Li, X.; Shi, Y. $BiFeO_3/TiO_2$ Nanotube Arrays Composite Electrode: Construction, Characterization, and Enhanced Photoelectrochemical Properties. *ACS Appl. Mater. Interfaces* 2014, 6 (1), 671-679.

[98] Zhai, C.; Zhu, M.; Bin, D.; Wang, H.; Du, Y.; Wang, C.; Yang, P. Visible-Light-Assisted Electrocatalytic Oxidation of Methanol Using Reduced Graphene Oxide Modified Pt Nanoflowers-TiO_2 Nanotube Arrays. *ACS Appl. Mater. Interfaces* 2014, 6 (20), 17753-17761.

[99] Liu, D.; Tian, R.; Wang, J.; Nie, E.; Piao, X.; Li, X.; Sun, Z. Photoelectrocatalytic Degradation of Methylene Blue Using F Doped TiO_2 Photoelectrode Under Visible Light Irradiation. *Chemosphere* 2017, 185, 574-581.

[100] Huang, J.-R.; Tan, X.; Yu, T.; Zhao, L.; Hu, W.-L. Enhanced Photoelectrocatalytic and Photoelectrochemical Properties by High-Reactive $TiO_2/SrTiO_3$ Hetero-Structured Nanotubes with dominant {001} Facet of Anatase TiO_2. *Electrochim. Acta* 2014, 146, 278-287.

[101] Cardoso, J. C.; Bessegato, G. G.; Boldrin Zanoni, M. V. Efficiency Comparison of Ozonation, Photolysis, Photocatalysis and Photoelectrocatalysis Methods in Real Textile Wastewater Decolorization. *Water Res.* 2016, 98, 39-46.

[102] Li, L.; Feng, H.; Wei, X.; Jiang, K.; Xue, S.; Chu, P. K. Ag as Cocatalyst and Electron-Hole Medium in CeO_2 QDs/Ag/Ag_2Se Z-scheme Heterojunction Enhanced the Photo-Electrocatalytic Properties of the Photoelectrode. *Nanomaterials* 2020, 10 (2), 253.

[103] Wang, M.; Sun, L.; Lin, Z.; Cai, J.; Xie, K.; Lin, C. p–n Heterojunction Photoelectrodes Composed of Cu_2O-Loaded TiO_2 Nanotube Arrays with Enhanced Photoelectrochemical and Photoelectrocatalytic Activities. *Energy Environ. Sci.* 2013, 6 (4), 1211-1220.

[104] Zhang, Q.; Zhu, J.; Wang, Y.; Feng, J.; Yan, W.; Xu, H. Electrochemical Assisted Photocatalytic Degradation of Salicylic Acid with Highly Ordered TiO_2 Nanotube Electrodes. *Appl. Surf. Sci.* 2014, 308, 161-169.

[105] Zhou, Q.; Xing, A.; Li, J.; Zhao, D.; Zhao, K.; Lei, M. Synergistic Enhancement in Photoelectrocatalytic Degradation of Bisphenol A by CeO_2 and Reduced Graphene Oxide co-Modified TiO_2 Nanotube Arrays in Combination with Fenton Oxidation. *Electrochim. Acta* 2016, 209, 379-388.

[106] Zhou, Q.; Xing, A.; Zhao, D.; Zhao, K. Tetrabromobisphenol A Photoelectrocatalytic Degradation Using Reduced Graphene Oxide and Cerium Dioxide Comodified TiO_2 Nanotube Arrays as Electrode under Visible Light. *Chemosphere* 2016, 165, 268-276.

[107] Ojani, R.; Raoof, J. B.; Zarei, E. Electrochemical Monitoring of Photoelectrocatalytic Degradation of Rhodamine B Using TiO_2 Thin Film Modified Graphite Electrode. *J. Solid State Electrochem.* 2012, 16, 2143–2149.

[108] He, S.; Yan, C.; Chen, X.-Z.; Wang, Z.; Ouyang, T.; Guo, M.-L.; Liu, Z.-Q. Construction of Core-Shell Heterojunction Regulating α-Fe_2O_3 Layer on CeO_2 Nanotube Arrays Enables Highly Efficient Z-Scheme Photoelectrocatalysis. *Appl. Catal. B* 2020, 276, 119138.

[109] Hou, W.-M.; Ku, Y. Photoelectrocatalytic Decomposition of Gaseous Isopropanol in a Polymer Electrolyte Photoreactor. *J. Solid State Electrochem.* 2012, 17, 737-741.

[110] Yu, Y.; Yu, X.; Yang, S. Preparation and Characterization of CeO_2 Decorated TiO_2 Nanotube Arrays Photoelectrode and Its Enhanced Photoelectrocatalytic Efficiency for Degradation of Methyl Orange. *J. Mater. Sci.: Mater. Electron.* 2015, 26 (8), 5715-5723.

[111] Wang, Y.; Hu, B.; Hu, C.; Zhou, X. Fabrication of a Novel Ti/SnO_2–Sb–CeO_2@TiO_2–SnO_2 Electrode and Photoelectrocatalytic Application in Wastewater Treatment. *Mater. Sci. Semicond. Process.* 2015, 40, 744-751.

[112] Peng, Y. P.; Chen, H.; Huang, C. P. The Synergistic Effect of Photoelectrochemical (PEC) Reactions Exemplified by Concurrent Perfluorooctanoic acid (PFOA) Degradation and Hydrogen Generation over Carbon and Nitrogen codoped TiO_2 Nanotube Arrays (C-N-TNTAs) Photoelectrode. *Appl. Catal. B* 2017, 209, 437-446.

[113] Liu, C.-F.; Lu, Y.-J.; Hu, C.-C. Effects of Anions and pH on the Stability of ZnO Nanorods for Photoelectrochemical Water Splitting. *ACS Omega* 2018, 3 (3), 3429-3439.

[114] He, S.; Zheng, M.; Yao, L.; Yuan, X.; Li, M.; Ma, L.; Shen, W. Preparation and Properties of ZnO Nanostructures by Electrochemical Anodization Method. *Appl. Surf. Sci.* 2010, 256 (8), 2557-2562.

[115] Farrukh, M. A.; Thong, C.-K.; Adnan, R.; Kamarulzaman, M. A. Preparation and Characterization of Zinc Oxide Nanoflakes Using Anodization Method and Their Photodegradation Activity on Methylene Blue. *Russ. J. Phys. Chem. A* 2012, 86 (13), 2041-2048.

[116] Ramirez-Canon, A.; Miles, D. O.; Cameron, P. J.; Mattia, D. Zinc Oxide Nanostructured Films Produced via Anodization: A Rational Design Approach. *RSC Adv.* 2013, 3 (47), 25323-25330.

[117] Basu, P. K.; Saha, N.; Maji, S.; Saha, H.; Basu, S. Nanoporous ZnO Thin Films Deposited by Electrochemical Anodization: Effect of UV Light. *J. Mater. Sci.: Mater. Electron.* 2008, 19 (6), 493-499.

[118] Su, Z.; Zhang, L.; Jiang, F.; Hong, M. Formation of Crystalline TiO_2 by Anodic Oxidation of Titanium. *Prog. Nat. Sci.* 2013, 23 (3), 294–301.

[119] Gibran, K.; Ibadurrahman, M.; Slamet. Effect of Electrolyte Type on the Morphology and Crystallinity of TiO_2 Nanotubes from Ti-6Al-4V Anodization. *IOP Conf. Ser. Earth Environ. Sci.* 2018, 105, 012038.

[120] Wang, X.; Zhang, D.; Xiang, Q.; Zhong, Z.; Liao, Y. Review of Water-Assisted Crystallization for TiO_2 Nanotubes. *Nano-Micro Lett.* 2018, 10 (4), 77.

[121] Hoseinzadeh, T.; Ghorannevis, Z.; Ghoranneviss, M.; Sari, A. H.; Salem, M. K. Effects of Various Applied Voltages on Physical Properties of TiO_2 Nanotubes by Anodization Method. *J. Theor. Appl. Phys.* 2017, 11 (3), 243-248.

[122] Kim, G. E.; Champagne, V. K.; Trexler, M.; Sohn, Y. 20 - Processing Nanostructured Metal and Metal-Matrix Coatings by Thermal and Cold spraying. In *Nanostructured Metals and Alloys*, Whang, S. H., Ed. Woodhead Publishing: 2011; pp 615-662.

[123] Li, C. J. 7 - Thermal Spraying of Light Alloys. In *Surface Engineering of Light Alloys*, Dong, H., Ed. Woodhead Publishing: 2010; pp 184-241.

[124] Boccaccini, A. R.; Keim, S.; Ma, R.; Li, Y.; Zhitomirsky, I. Electrophoretic Deposition of Biomaterials. *J. R. Soc. Interface* 2010, 7, S581-S613.

[125] Bai, M.; Khammas, R.; Guan, L.; Murray, J. W.; Hussain, T. Suspension High Velocity Oxy-Fuel Spraying of a Rutile TiO_2 Feedstock: Microstructure, Phase Evolution and Photocatalytic Behaviour. *Ceram. Int.* 2017, 43 (17), 15288-15295.

[126] Pala, Z.; Shaw, E.; Murray, J. W.; Senin, N.; Hussain, T. Suspension High Velocity Oxy-Fuel Spraying of TiO_2: A Quantitative Approach to Phase Composition. *J. Eur. Ceram. Soc.* 2017, 37 (2), 801-810.

[127] Moore, B.; Asadi, E.; Lewis, G. Deposition Methods for Microstructured and Nanostructured Coatings on Metallic Bone Implants: A Review. *Adv. Mater. Sci. Eng.* 2017, 2017, 5812907.

[128] Ang, A. S. M.; Berndt, C. C. A Review of Testing Methods for Thermal Spray Coatings. *Int. Mater. Rev.* 2014, 59 (4), 179-223.

[129] Oksa, M.; Turunen, E.; Suhonen, T.; Varis, T.; Hannula, S.-P. Optimization and Characterization of High Velocity Oxy-fuel Sprayed Coatings: Techniques, Materials, and Applications. *Coatings* 2011, 1 (1), 17-52.

[130] Ang, A. S. M.; Sanpo, N.; Sesso, M. L.; Kim, S. Y.; Berndt, C. C. Thermal Spray Maps: Material Genomics of Processing Technologies. *J. Therm. Spray Technol.* 2013, 22 (7), 1170-1183.

[131] Chagnon, P.; Fauchais, P. Thermal Spraying of Ceramics. *Ceram. Int.* 1984, 10 (4), 119-131.

[132] Joshi, S.; Nylen, P. Advanced Coatings by Thermal Spray Processes. *Technologies* 2019, 7 (4), 79.

[133] Vuoristo, P. 4.10 - Thermal Spray Coating Processes. In *Comprehensive Materials Processing*, Hashmi, S.; Batalha, G. F.; Van Tyne, C. J.; Yilbas, B., Eds. Elsevier: Oxford, 2014; pp 229-276.

[134] Mahade, S.; Narayan, K.; Govindarajan, S.; Björklund, S.; Curry, N.; Joshi, S. Exploiting Suspension Plasma Spraying to Deposit Wear-Resistant Carbide Coatings. *Materials* 2019, 12 (15), 2344.

[135] Mauer, G.; Guignard, A.; Vaßen, R. Plasma Spraying of Efficient Photoactive TiO_2 Coatings. *Surf. Coat. Technol.* 2013, 220, 40-43.

[136] Pawlowski, L. Suspension and Solution Thermal Spray Coatings. *Surf. Coat. Technol.* 2009, 203 (19), 2807-2829.

[137] Davis, J. R. *Surface Engineering for Corrosion and Wear Resistance*; ASM International: 2001.

[138] Dorfman, M. R.; Sharma, A. Challenges and Strategies for Growth of Thermal Spray Markets: The Six-Pillar Plan. *J. Therm. Spray Technol.* 2013, 22 (5), 559-563.

[139] Korobov, Y.; Shalimov, M. *Energy Production and Management in the 21st Century*; WIT Press: 2014; p 455-466.

[140] Medricky, J.; Musalek, R.; Janata, M.; Chraska, T.; Lukac, F. Cost-effective plasma spraying for large-scale applications. In *ITSC 2018*, Proceedings of the International Thermal Spray Conference, USA, May 7-10, 2018; Azarmi, F.; Balani, K.; Eden, T.; Hussain, T., Lau, Y.-C.; Li, H.; Shinoda, K.; Toma, F.-L.; Veilleux, J., Eds., ASM international, 2018, 683-689.

[141] Tejero-Martin, D.; Rezvani Rad, M.; McDonald, A.; Hussain, T. Beyond Traditional Coatings: A Review on Thermal-Sprayed Functional and Smart Coatings. *J. Therm. Spray Technol.* 2019, 28 (4), 598-644.

[142] Vardelle, A.; Moreau, C.; Akedo, J.; Ashrafizadeh, H.; Berndt, C. C.; Berghaus, J. O.; Boulos, M.; Brogan, J.; Bourtsalas, A. C.; Dolatabadi, A.; et al. The 2016 Thermal Spray Roadmap. *J. Therm. Spray Technol.* 2016, 25 (8), 1376-1440.

[143] Ctibor, P.; Stengl, V.; Pala, Z. Structural and Photocatalytic Characteristics of TiO_2 Coatings Produced by Various Thermal Spray Techniques. *J. Adv. Ceram.* 2013, 2, 218-226.

[144] Bozorgtabar, M.; Rahimipour, M.; Salehi, M. Novel Photocatalytic TiO_2 Coatings Produced by HVOF Thermal Spraying Process. *Mater. Lett.* 2010, 64 (10), 1173-1175.

[145] Bozorgtabar, M.; Rahimipour, M.; Salehi, M.; Jafarpour, M. Structure and Photocatalytic Activity of TiO_2 Coatings Deposited by Atmospheric Plasma Spraying. *Surf. Coat. Technol.* 2011, 205, S229-S231.

[146] Bozorgtabar, M.; Rahimipour, M.; Salehi, M. Effect of Thermal Spray Processes on Anatase–Rutile Phase Transformation in Nano-structured TiO_2 Photo-Catalyst Coatings. *Surf. Eng.* 2010, 26 (6), 422-427.

[147] Berger, L.-M. *Titanium Oxide – New Opportunities for an Established Coating Material*, 2004.

[148] Bordes, M. C.; Vicent, M.; Moreno, A.; Moreno, R.; Borrell, A.; Salvador, M. D.; Sánchez, E. Microstructure and Photocatalytic Activity of APS Coatings Obtained from Different TiO_2 Nanopowders. *Surf. Coat. Technol.* 2013, 220, 179-186.

[149] Toma, F. L.; Berger, L. M.; Jacquet, D.; Wicky, D.; Villaluenga, I.; de Miguel, Y. R.; Lindeløv, J. S. Comparative Study on the Photocatalytic Behaviour of Titanium Oxide Thermal Sprayed Coatings from Powders and Suspensions. *Surf. Coat. Technol.* 2009, 203 (15), 2150-2156.

[150] Wierzbicka, E.; Domaschke, M.; Denisov, N.; Fehn, D.; Hwang, I.; Kaufmann, M.; Kunstmann, B.; Schmidt, J.; Meyer, K.; Peukert, W.; et al. Magnéli Phases Doped with Pt for Photocatalytic Hydrogen Evolution. *ACS Appl. Energy Mater.* 2019, 2 (12), 8399-8404.

[151] Toma, F.-L.; Bertrand, G.; Klein, D.; Meunier, C.; Begin, S. Development of Photocatalytic Active TiO_2 Surfaces by Thermal Spraying of Nanopowders. *J. Nanomater.* 2008, 2008, 1-8.

[152] Fauchais, P.; Vardelle, M.; Vardelle, A.; Goutier, S. What Do We Know, What Are the Current Limitations of Suspension Plasma Spraying? *J. Therm. Spray Technol.* 2015, 24 (7), 1120-1129.

[153] Bannier, E.; Darut, G.; Sánchez, E.; Denoirjean, A.; Bordes, M. C.; Salvador, M. D.; Rayón, E.; Ageorges, H. Microstructure and Photocatalytic Activity of Suspension Plasma Sprayed TiO_2 Coatings on Steel and Glass Substrates. *Surf. Coat. Technol.* 2011, 206 (2), 378-386.

[154] Rampon, R.; Marchand, O.; Filiatre, C.; Bertrand, G. Influence of Suspension Characteristics on Coatings Microstructure Obtained by Suspension Plasma Spraying. *Surf. Coat. Technol.* 2008, 202 (18), 4337-4342.

[155] Curry, N.; VanEvery, K.; Snyder, T.; Susnjar, J.; Bjorklund, S. Performance Testing of Suspension Plasma Sprayed Thermal Barrier Coatings Produced with Varied Suspension Parameters. *Coatings* 2015, 5 (3), 338-356.

[156] Toma, F.-L.; Bertrand, G.; Begin, S.; Meunier, C.; Barres, O.; Klein, D.; Coddet, C. Microstructure and Environmental Functionalities of TiO_2-Supported Photocatalysts Obtained by Suspension Plasma Spraying. *Appl. Catal. B* 2006, 68 (1), 74-84.

[157] Kozerski, S.; Toma, F.-L.; Pawlowski, L.; Leupolt, B.; Latka, L.; Berger, L.-M. Suspension Plasma Sprayed TiO_2 Coatings Using Different Injectors and Their Photocatalytic Properties. *Surf. Coat. Technol.* 2010, 205 (4), 980-986.

[158] Bernard, B.; Quet, A.; Bianchi, L.; Joulia, A.; Malié, A.; Schick, V.; Rémy, B. Thermal Insulation Properties of YSZ Coatings: Suspension Plasma Spraying (SPS) versus Electron Beam Physical Vapor Deposition (EB-PVD) and Atmospheric Plasma Spraying (APS). *Surf. Coat. Technol.* 2017, 318, 122-128.

[159] Aranke, O.; Gupta, M.; Markocsan, N.; Li, X.-H.; Kjellman, B. Microstructural Evolution and Sintering of Suspension Plasma-Sprayed Columnar Thermal Barrier Coatings. *J. Therm. Spray Technol.* 2019, 28 (1), 198-211.

[160] Yamada, M.; Isago, H.; Nakano, H.; Fukumoto, M. Cold Spraying of TiO_2 Photocatalyst Coating With Nitrogen Process Gas. *J. Therm. Spray Technol.* 2010, 19 (6), 1218-1223.

[161] Toibah, A. R.; Sato, M.; Yamada, M.; Fukumoto, M. Cold-Sprayed TiO_2 Coatings from Nanostructured Ceramic Agglomerated Powders. *Mater. Manuf. Process.* 2016, 31 (11), 1527-1534.

[162] Freitag, J.; Bahnemann, D. W. Evaluation of the Photocatalytic (Visible-Light) Activity of Cold Gas sprayed TiO_2 Layers on Metal Sheets. *Phys. Status Solidi Rapid Res. Lett.* 2014, 8 (6), 596-599.

[163] Yamada, M.; Kandori, Y.; Sato, K.; Fukumoto, M. Fabrication of Titanium Dioxide Photocatalyst Coatings by Cold Spray. *J. Solid Mech. Mater. Eng.* 2009, 3 (2), 210-216.

[164] Gardon, M.; Fernández-Rodríguez, C.; Garzón Sousa, D.; Doña-Rodríguez, J. M.; Dosta, S.; Cano, I. G.; Guilemany, J. M. Photocatalytic Activity of Nanostructured Anatase Coatings Obtained by Cold Gas Spray. *J. Therm. Spray Technol.* 2014, 23 (7), 1135-1141.

[165] Salim, N. T.; Yamada, M.; Nakano, H.; Fukumoto, M. The Synthesis of Titanium Dioxide (TiO_2) Powder for Cold Spray Process. *IOP Conf. Ser. Mater. Sci. Eng.* 2011, 18 (3), 032019.

[166] Assadi, H.; Gärtner, F.; Stoltenhoff, T.; Kreye, H. Bonding Mechanism in Cold Gas Spraying. *Acta Mater.* 2003, 51 (15), 4379-4394.

[167] Vlcek, J.; Gimeno, L.; Huber, H.; Lugscheider, E. A Systematic Approach to Material Eligibility for the Cold-Spray Process. *J. Therm. Spray Technol.* 2005, 14 (1), 125-133.

[168] Yang, G.-J.; Li, C.-J.; Han, F.; Li, W.-Y.; Ohmori, A. Low Temperature Deposition and Characterization of TiO_2 Photocatalytic Film Through Cold Spray. *Appl. Surf. Sci.* 2008, 254 (13), 3979-3982.

[169] Wolfe, D.; Eden, T. 14 - Cold Spray Particle Deposition for Improved Wear Resistance. In *The Cold Spray Materials Deposition Process*, Champagne, V. K., Ed. Woodhead Publishing: 2007; pp 264-301.

[170] Shen, Y.; Gyansah, L.; Song, W.; Feng, B.; Wang, J.; Cui, X.; Tao, Y.; Xiong, T. Cold Spray (P, N, Mo)-TiO_2 Photocatalytic Coatings: Synthesis, Microstructural Characterization and Photocatalytic Properties. *Mater. Res. Express* 2019, 6 (9), 096599.

[171] Ameta, R.; Ameta, S. C. *Photocatalysis: Principles and Applications*; CRC Press: 2016.

[172] Tang, J.; Zhao, Z.; Cui, X.; Wang, J.; Xiong, T. Microstructure and Bioactivity of a Cold Sprayed Rough/Porous Ta Coating on Ti6Al4V Substrate. *Sci. China Technol. Sci.* 2020, 63 (5), 731-739.

[173] Yang, G. J.; Suo, X. *Advanced Nanomaterials and Coatings by Thermal Spray: Multi-Dimensional Design of Micro-Nano Thermal Spray Coatings*. Elsevier Science: 2019.

[174] Tang, J.; Zhao, Z.; Li, N.; Qiu, X.; Shen, Y.; Cui, X.; Du, H.; Wang, J.; Xiong, T. Influence of Feedstock Powder on Microstructure and Mechanical Properties of Ta Cold Spray Depositions. *Surf. Coat. Technol.* 2019, 377, 124903.

[175] Cañas, E.; Orts, M. J.; Boccaccini, A. R.; Sánchez, E. Solution Precursor Plasma Spraying (SPPS): A Novel and Simple Process to Obtain Bioactive Glass Coatings. *Mater. Lett.* 2018, 223, 198-202.

[176] Chen, D.; Jordan, E. H.; Gell, M. Porous TiO_2 Coating Using the Solution Precursor Plasma Spray Process. *Surf. Coat. Technol.* 2008, 202 (24), 6113-6119.

[177] Unabia, R.; Candidato, R.; Pawłowski, L. Current Progress in Solution Precursor Plasma Spraying of Cermets: A Review. *Metals* 2018, 8 (6), 420.

[178] Chen, D.; Jordan, E. H.; Gell, M. Effect of Solution Concentration on Splat Formation and Coating Microstructure Using the Solution Precursor Plasma Spray Process. *Surf. Coat. Technol.* 2008, 202 (10), 2132-2138.

[179] Chen, D.; Jordan, E. H.; Gell, M.; Ma, X. Dense TiO_2 Coating Using the Solution Precursor Plasma Spray Process. *J. Am. Ceram. Soc.* 2008, 91 (3), 865-872.

[180] Joulia, A.; Bolelli, G.; Gualtieri, E.; Lusvarghi, L.; Valeri, S.; Vardelle, M.; Rossignol, S.; Vardelle, A. Comparing the Deposition Mechanisms in Suspension Plasma Spray (SPS) and Solution Precursor Plasma Spray (SPPS) Deposition of Yttria-Stabilised Zirconia (YSZ). *J. Eur. Ceram. Soc.* 2014, 34 (15), 3925-3940.

[181] Yu, Z.; Moussa, H.; Liu, M.; Schneider, R.; Moliere, M.; Liao, H. Solution Precursor Plasma Spray Process as an Alternative Rapid One-Step Route for the Development of Hierarchical ZnO Films for Improved Photocatalytic Degradation. *Ceram. Int.* 2018, 44 (2), 2085-2092.

[182] Tejero-Martin, D.; Pala, Z.; Rushworth, S.; Hussain, T. Splat Formation and Microstructure of Solution Precursor Thermal Sprayed Nb-Doped Titanium Oxide Coatings. *Ceram. Int.* 2020, 46 (4), 5098-5108.

[183] Su, C. Y.; Lu, C. T.; Hsiao, W. T.; Liu, W. H.; Shieu, F. S. Evaluation of the Microstructural and Photocatalytic Properties of Aluminum-Doped Zinc Oxide Coatings Deposited by Plasma Spraying. *Thin Solid Films* 2013, 544, 170-174.

[184] Tului, M.; Arezzo, F.; Pawlowski, L. Optical Properties of Plasma Sprayed ZnO+Al_2O_3 Coatings. *Surf. Coat. Technol.* 2004, 179 (1), 47-55.

[185] Drouilly, C.; Krafft, J.-M.; Averseng, F.; Casale, S.; Bazer-Bachi, D.; Chizallet, C.; Lecocq, V.; Vezin, H.; Lauron-Pernot, H.; Costentin, G. ZnO Oxygen Vacancies Formation and Filling Followed by in Situ Photoluminescence and in Situ EPR. *J. Phys. Chem. C* 2012, 116 (40), 21297-21307.

[186] Wallenhorst, L.; Gurău, L.; Gellerich, A.; Militz, H.; Ohms, G.; Viöl, W. UV-Blocking Properties of Zn/ZnO Coatings on Wood Deposited by Cold Plasma Spraying at Atmospheric Pressure. *Appl. Surf. Sci.* 2018, 434, 1183-1192.

[187] Chen, K.; Liu, Y.; Fu, Y.; Huang, J.; Feng, X.; Wang, J.; Zhai, M.; Lupoi, R.; Yin, S.; Li, H. Loading of Zn/ZnO Particles in the Precursor Feedstock Affects the Characteristics of Liquid Plasma Sprayed Nano-ZnO Coatings for Photocatalytic Applications. *Nanotechnology* 2020, 31 (18), 185301.

[188] Yu, Z.; Moussa, H.; Ma, Y.; Liu, M.; Chouchene, B.; Schneider, R.; Moliere, M.; Liao, H. Oxygen-Defective ZnO Films with Various Nanostructures Prepared via a Rapid One-Step Process and Corresponding Photocatalytic Degradation Applications. *J. Colloid Interface Sci.* 2019, 534, 637-648.

[189] Zhang, C.; Geng, X.; Liao, H.; Li, C.-J.; Debliquy, M. Room-Temperature Nitrogen-Dioxide Sensors Based on ZnO_{1-x} Coatings Deposited by Solution Precursor Plasma Spray. *Sens. Actuators B Chem.* 2017, 242, 102-111.

[190] Shimamura, K.; Kirihara, S.; Akedo, J.; Ohji, T.; Naito, M.; Singh, M.; Michaelis, A. *Additive Manufacturing and Strategic Technologies in Advanced Ceramics*. Wiley, 2016.

[191] Yu, Z.; Moussa, H.; Liu, M.; Schneider, R.; Wang, W.; Moliere, M.; Liao, H. Development of Photocatalytically Active Heterostructured MnO/ZnO and CuO/ZnO Films via Solution Precursor Plasma Spray Process. *Surf. Coat. Technol.* 2019, 371, 107-116.

[192] Cai, Y.; Coyle, T. W.; Azimi, G.; Mostaghimi, J. Superhydrophobic Ceramic Coatings by Solution Precursor Plasma Spray. *Sci. Rep.* 2016, 6 (1), 24670.

[193] Yu, Z. X.; Ma, Y. Z.; Zhao, Y. L.; Huang, J. B.; Wang, W. Z.; Moliere, M.; Liao, H. L. Effect of Precursor Solutions on ZnO Film via Solution Precursor Plasma Spray and Corresponding Gas Sensing Performances. *Appl. Surf. Sci.* 2017, 412, 683-689.

[194] Fauchais, P.; Vardelle, A. Solution and Suspension Plasma Spraying of Nanostructure Coatings. In *Advanced Plasma Spray Applications*; InTech: 2012.

[195] Jordan, E. H.; Jiang, C.; Gell, M. The Solution Precursor Plasma Spray (SPPS) Process: A Review with Energy Considerations. *J. Therm. Spray Technol.* 2015, 24 (7), 1153-1165.

[196] Tesar, T.; Musalek, R.; Lukac, F.; Medricky, J.; Cizek, J.; Csaki, S.; Panak, O.; Drzkova, M. Solution Precursor Plasma Spraying of Cr-Doped Al_2O_3 Thermochromic Coatings. *J. Therm. Spray Technol.* 2020, 29 (1), 199-211.

[197] Yu, Z.; Moussa, H.; Liu, M.; Chouchene, B.; Schneider, R.; Wang, W.; Moliere, M.; Liao, H. Tunable Morphologies of ZnO Films via the Solution Precursor Plasma Spray Process for Improved Photocatalytic Degradation Performance. *Appl. Surf. Sci.* 2018, 455, 970-979.

[198] Omar, N. I.; Selvami, S.; Kaisho, M.; Yamada, M.; Yasui, T.; Fukumoto, M. Deposition of Titanium Dioxide Coating by the Cold-Spray Process on Annealed Stainless Steel Substrate. *Coatings* 2020, 10 (10), 991.

[199] Prasad, N. E.; Wanhill, R. J. H. *Aerospace Materials and Material Technologies: Volume 1: Aerospace Materials*. Springer Singapore, 2016.

[200] Park, Y.-K.; Kim, B.-J.; Jeong, S.; Jeon, K.-J.; Chung, K.-H.; Jung, S.-C. Characteristics of Hydrogen Production by Photocatalytic Water Splitting Using Liquid Phase Plasma over Ag-Doped TiO_2 Photocatalysts. *Environ. Res.* 2020, 188, 109630.

[201] Zafar, Z.; Kim, J.O. Optimization of Hydrothermal Synthesis of Fe–TiO_2 Nanotube Arrays for Enhancement in Visible Light Using an Experimental Design Methodology. *Environ. Res.* 2020, 189, 109908.

Figure captions

Fig. 1. (a) Exposure pathways of PFAS. Reproduced with permission from [33]. Copyright © 2012 Fardin Oliaei et al., Springer Nature. (b) chemical structures of PFOA and PFOS (C: gray, F: blue, O: red, S: yellow, and H: white). Reproduced with permission from [32]. Copyright © 2017 Shana Wang et al., Elsevier. (c) recent methods used for degradation of PFOA and PFOS. Reproduced with permission from [32]. Copyright © 2017 Shana Wang et al., Elsevier.

Fig. 2. Schematic common pathway for photo-oxidation of PFOA. Reproduced with permission from [40]. Copyright © 2019 Yaoyao Wu et al., John Wiley and Sons.

Fig. 3. (a-f) FE-SEM elemental mapping and TEM images of TiO_2 nanoparticle modified by Pt, Pd, and Ag nanoparticles, (g) UV-vis DRS spectrum of TiO_2 modified by Pt, Pd, and Ag nanoparticles; and (h) effect of initial concentration of PFOA on the efficiency of degradation. Reproduced with permission from [45]. Copyright © 2016 Mingjie Li et al., Elsevier.

Fig. 4. (a) Schematic illustration of the anodization setup and the structure of resultant titania nanotubes. Reproduced with permission from [80]. Copyright © 2019 Najia Mahdi et al., MDPI. (b) ideal structure of porous anodic TiO_2 (ATO). Reproduced with permission from [78]. Copyright © 2010 Grzegorz D. Sulka et al., Elsevier. (c) cross section of the anodized layer with structural features of anodic TiO_2. Reproduced with permission from [78]. Copyright © 2010 Grzegorz D. Sulka et al., Elsevier. SEM micrographs of ordered TiO_2 nanotubes grown on pure Ti (99.6%) after 1st (d) and 2nd anodization (e); (f) and (g) show micrographs for TiO_2 nanotubes grown on Ti with 99.99% purity, with insets showing magnifications. Reproduced with permission from [79]. Copyright © 2007 Jan M. Macak et al., John Wiley and Sons.

Fig. 5. (a) C-N co-doped TiO_2 photoanode, (b) surface topography of C-N co-doped TiO_2 nanotubes, (c) surface morphology of C-N co-doped TiO_2 nanotubes, (d) comparison of direct pyrolysis (P), electrocatalysis (EC), photocatalysis (PC), and photoelectrocatalysis (PEC) for

degradation of PFOA, (e) Time dependency of short-chain intermediates (PFCAs) in PEC, and (f) main mechanism for degradation of PFOA in PEC. Reproduced with permission from [112]. Copyright © 2017 Yen-Ping Peng et al., Elsevier.

Fig. 6. Comparison of typical thicknesses of major immobilization processes. Reproduced with permission from [127]. Copyright © 2017 Bailey Moore et al., Hindawi.

Fig. 7. (a) Schematic illustration of thermal spraying process. Reproduced with permission from [128]. Copyright © 2014 Andrew Siao Ming Ang et al., Taylor & Francis. (b) flame temperature against particle velocity for some general thermal spraying processes. Reproduced with permission from [129]. Copyright © 2011 Maria Oksa et al., MDPI.

Fig. 8. (a) Schematic comparison of microstructure and feedstock relationship in SPS and APS films. Reproduced with permission from [134]. Copyright © 2019 Satyapal Mahade et al., MDPI. (b) schematic of the formation of droplets in SPS. Reproduced with permission from [136]. Copyright © 2009 Lech Pawlowski, Elsevier.

Fig. 9. Comparison of (a) typical pore size, and (b) relative cost of some major deposition processes. Reproduced with permission from [127]. Copyright © 2017 Bailey Moore et al., Hindawi.

Fig. 10. (a) Dependency of photocatalytic activity on anatase content of TiO_2 films deposited by HVOF, suspension HVOF and SPS. Reproduced with permission from [149]. Copyright © 2009 F.-L. Toma et al., Elsevier. (b) schematic of effect of average particle size on the microstructure of coatings fabricated by SPS. Reproduced with permission from [155]. Copyright © 2015 F.-L. Nicholas Curry et al., MDPI. (c) schematic of phonon scattering for coatings fabricated by SPS, APS and EB-PVD. Reproduced with permission from [158]. Copyright © 2017 Benjamin Bernard et al., Elsevier.

Fig. 11. (a-h) Surface topographies of ZnO coatings deposited by SPPS. Reproduced with permission from [188]. Copyright © 2019 Zexin Yu et al., Elsevier. (i) surface topography of TiO_2 film deposited by APS. Reproduced with permission from [151]. Copyright © 2008

Filofteia-Laura Toma et al., Hindawi. (j) surface morphology of TiO_2 film deposited by SPPS. Reproduced with permission from [179]. Copyright © 2008 Dianying Chen et al., John Wiley and Sons. (k) surface morphology of TiO_2 film deposited by HVOF. Reproduced with permission from [151]. Copyright © 2008 Filofteia-Laura Toma et al., Hindawi. (l) surface morphology of TiO_2 film deposited by CS. Reproduced with permission from [198]. Copyright © 2020 Noor Irinah Omar et al., MDPI.

Table captions

Table 1. Application of photoelectrocatalysis in degradation of various organic pollutants and comparison of its efficiency with photocatalysis.

Table 2. Anatase phase content and its crystallite average size created by different methods of APS, SPS, FS, and HVOF (SPS-W: SPS using aqueous suspension, SPS-A: SPS using alcoholic suspension).

Supplementary

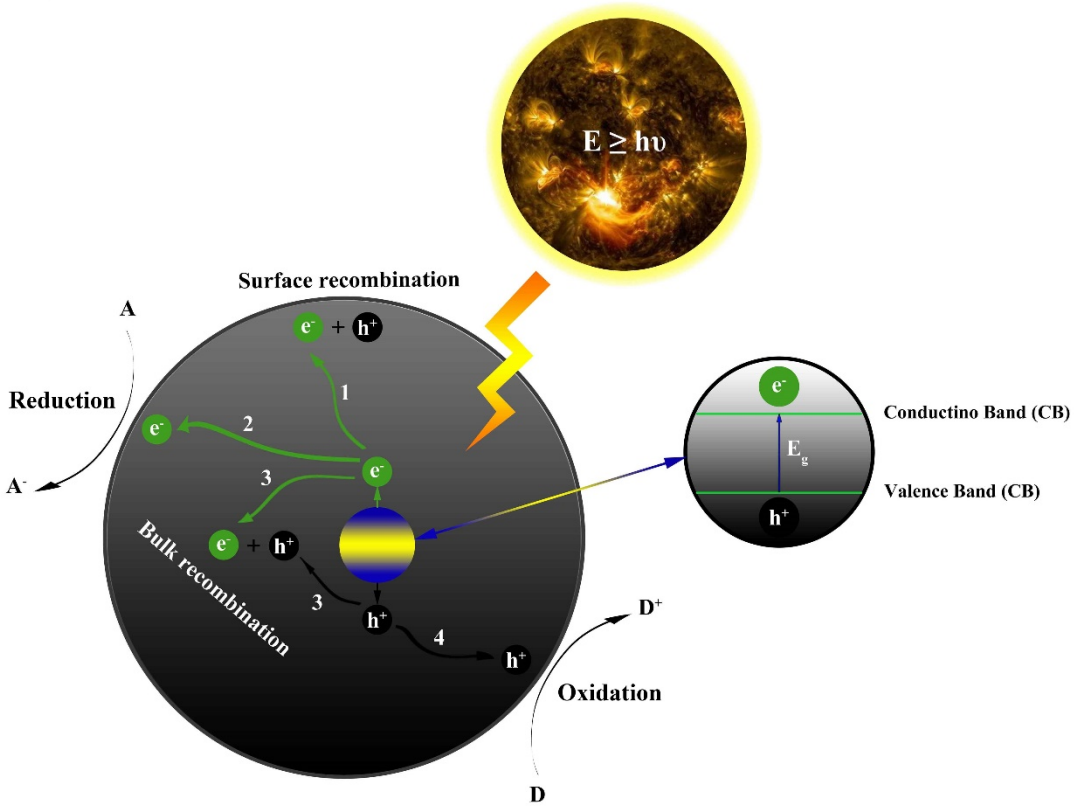

Fig. S1. The events during a custom photocatalytic process. Adapted with permission from [1].

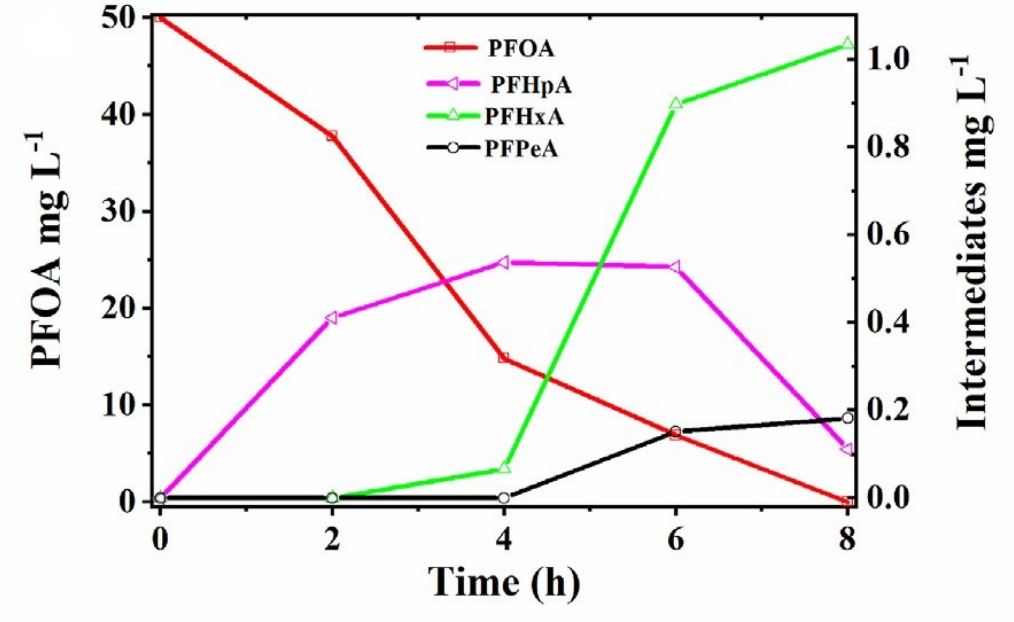

Fig. S2. Time-dependence of PFOA and its intermediates during photocatalysis using TiO_2 as the catalyst. Reproduced with permission from [2]. Copyright © 2020 Bentuo Xu et al., Elsevier.

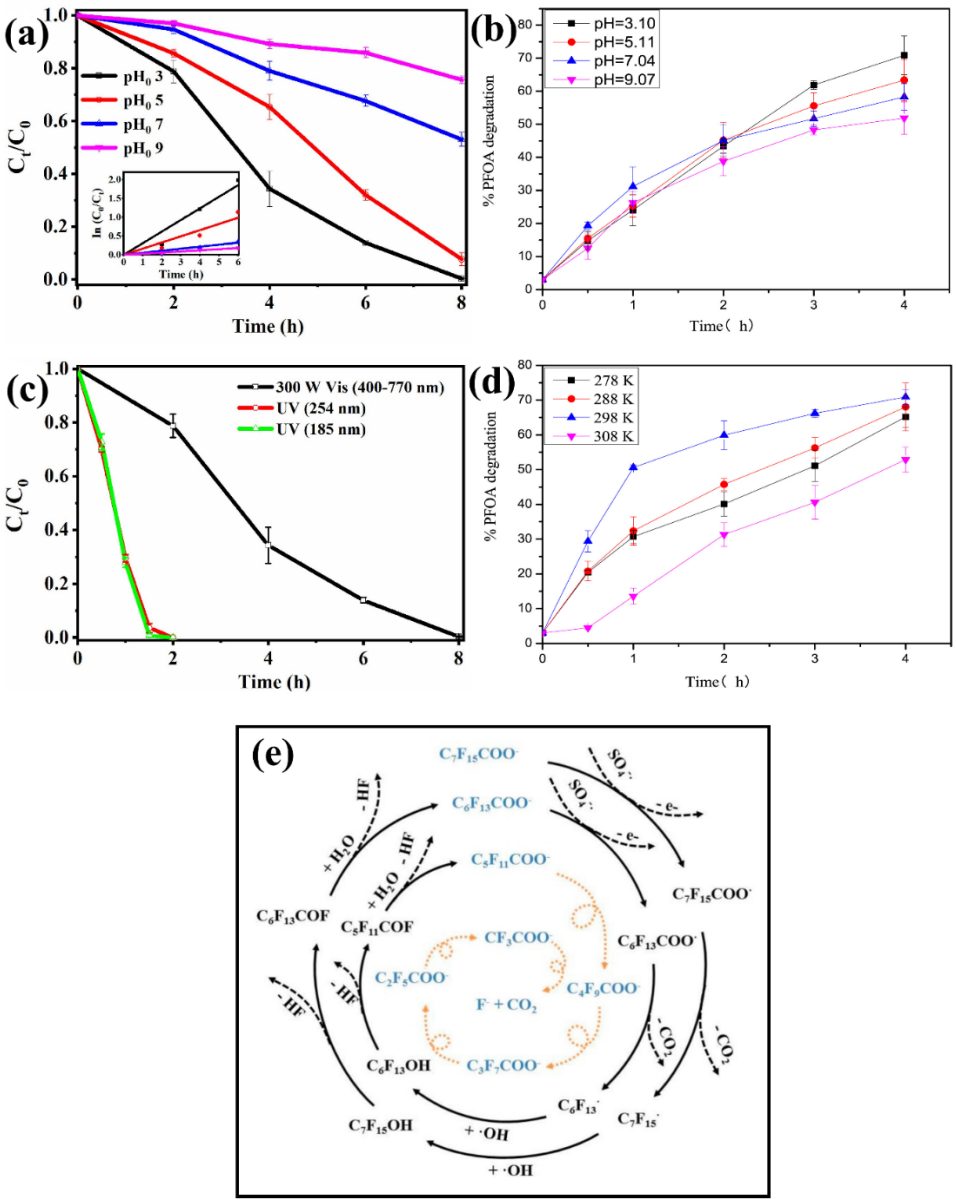

Fig. S3. (a) Effect of *pH* on the photodegradation of PFOA using TiO_2. Reproduced with permission from [2]. Copyright © 2020 Bentuo Xu et al., Elsevier. (b) effect of *pH* on the photodegradation of PFOA using ZnO. Reproduced with permission from [3]. Copyright © 2017 Dan Wu et al., Elsevier. (c) effect of wavelength of light source on the photodegradation of PFOA using TiO_2. Reproduced with permission from [2]. Copyright © 2020 Bentuo Xu et al., Elsevier. (d) effect of temperature on the photodegradation of PFOA using ZnO. Reproduced with permission from [3]. Copyright © 2017 Dan Wu et al., Elsevier. (e) schematic mechanism of photodegradation of PFOA using PMS. Reproduced with permission from [4]. Copyright © 2016 Penghua Yin et al., MDPI.

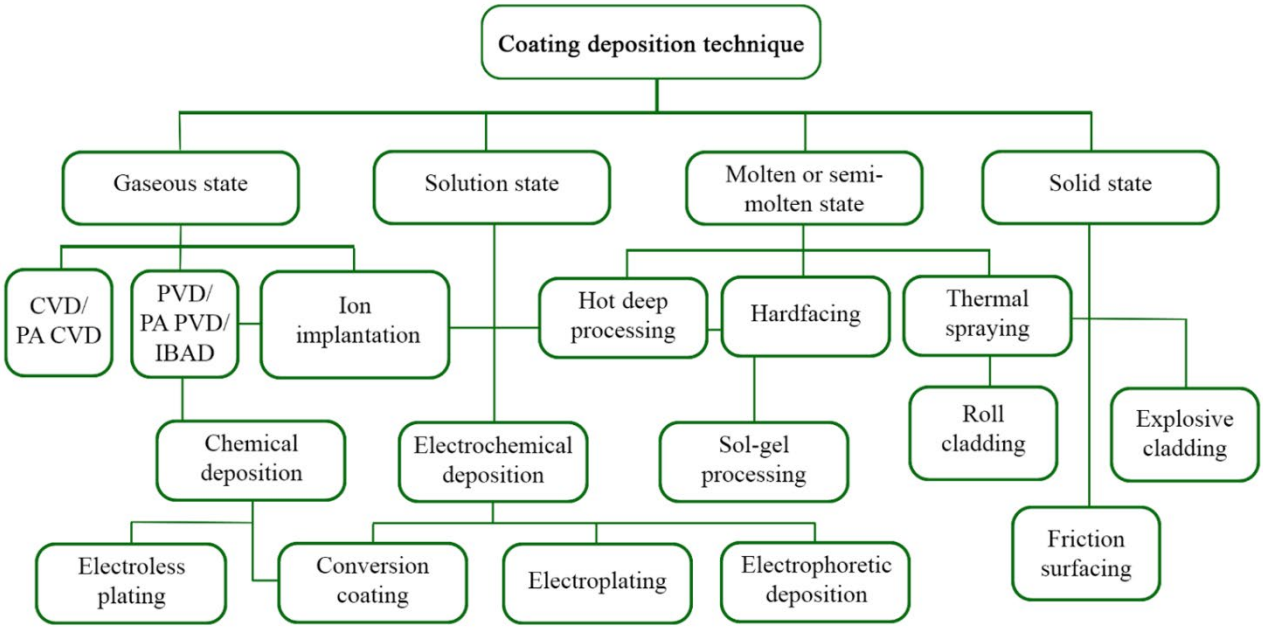

Fig. S4. Major methods of deposition of semiconductors for photocatalytic applications.

Adapted with permission from [5]. Copyright © 2019 Bogdan Sovilj et al., EDP Sciences.

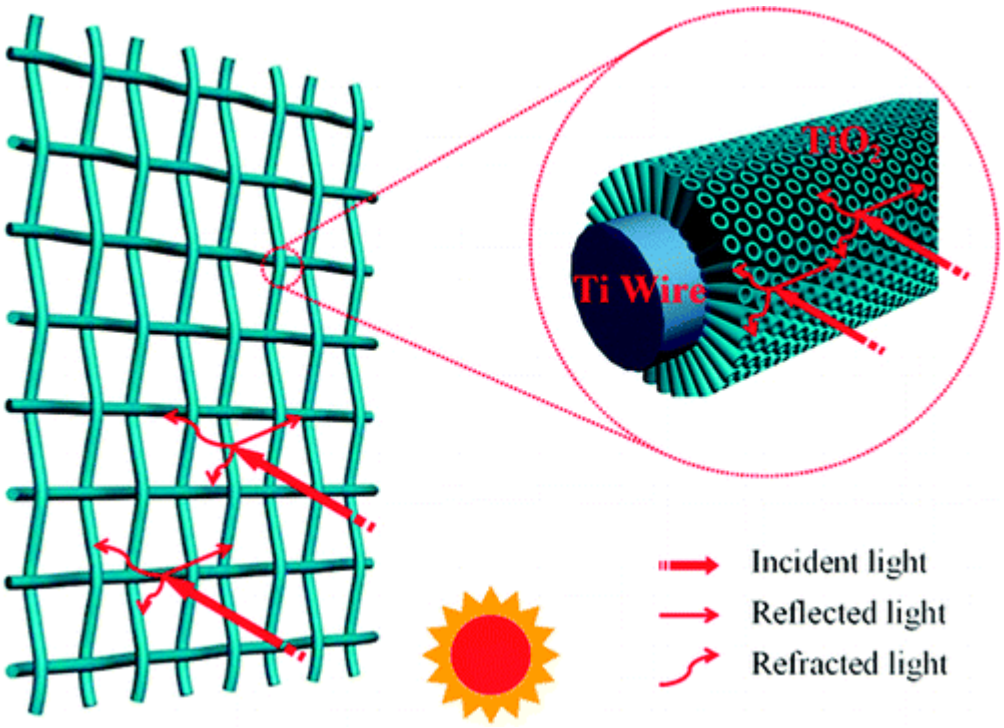

Fig. S5. Schematic representation of the improvement in the photoactivity of TiO_2 nanotubes formed on Ti mesh because of the ability to absorb reflected and refracted light. Reproduced with permission from [6]. Copyright © 2012 Jianjun Liao et al., American Chemical Society.

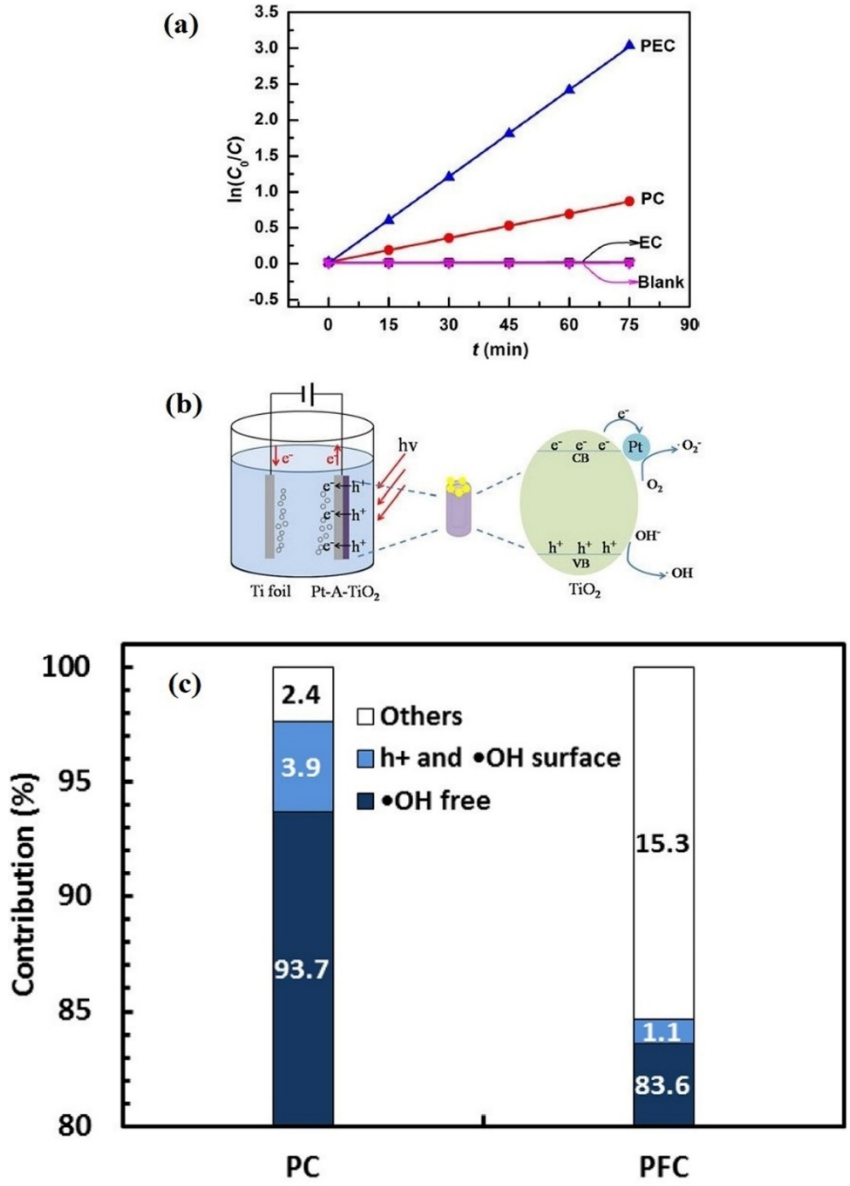

Fig. S6. (a) PEC, PC (photocatalytic) and EC (electrocatalytic) activities of TiO_2 composite nanotubes during the degradation of methylene blue. Reproduced with permission from [7]. Copyright © 2015 Juanru Huang et al., Springer Nature. (b) schematic illustration of the proposed mechanism for the improvement of PEC activity of anodized TiO_2 by deposition of Pt nanoparticles. Reproduced with permission from [8]. Copyright © 2017 Yan Liu et al., Springer Nature. (c) contributions of different oxidants on MCPA degradation by PC and PFC (photocatalytic fuel cells) methods. Conditions: $[MCPA]_0 = 1.0$ mg/L, $pH_0 = 3$, $[Na_2SO_4] = 0.1$ M. Reproduced with permission from [9]. Copyright © 2018 Yin Ye et al., Elsevier.

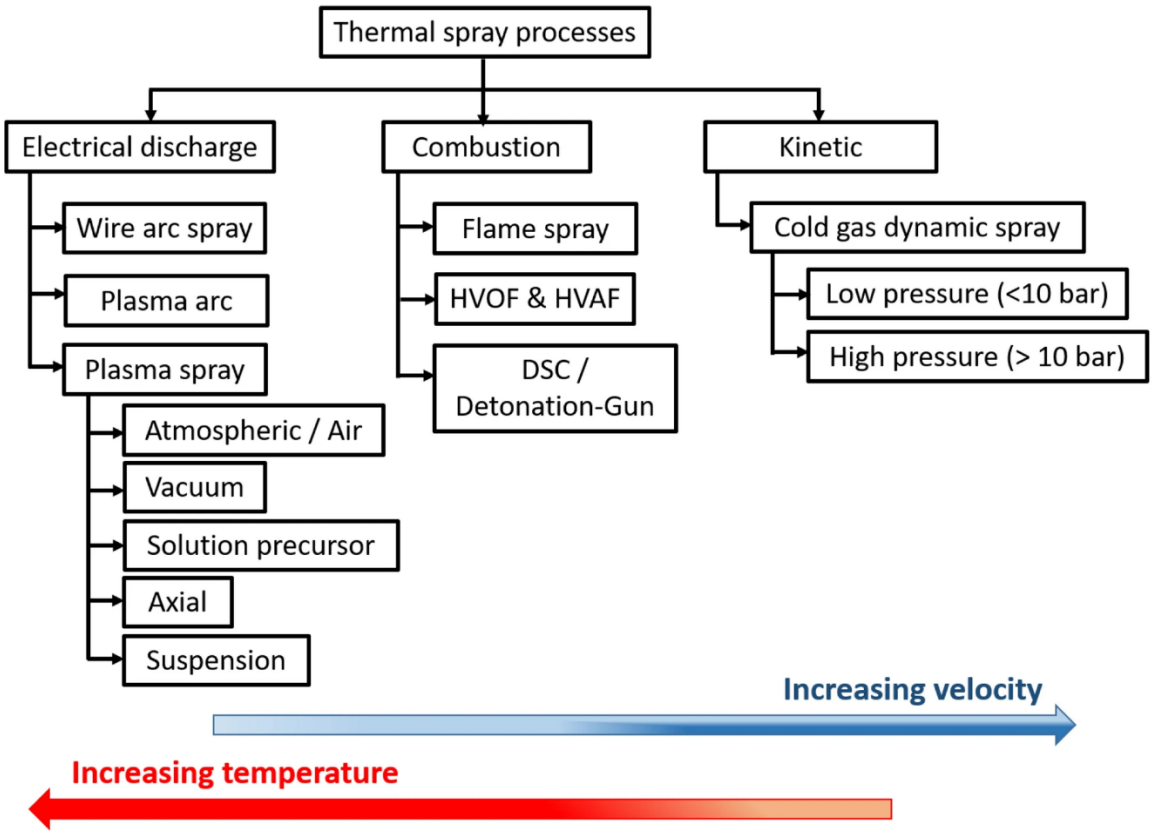

Fig. S7. General sources of energy and classification of thermal spray processes. Reproduced with permission from [10]. Copyright © 2020 P. Suresh Babu et al., Springer Nature.

Table S1. Comparison of the photocatalytic activity of ZnO and TiO_2.

Pollutant	**$m_{catalyst}$**	**TiO_2 efficiency**	**ZnO efficiency**	**Reference**
Cibarcon Yellow-FN 2R	600 mg/L	41.7% (240 min)	69.8% (180 min)	[11]
Crystal violet	400 mg/L	$k_{app}(min^{-1}) = 0.026$	$k_{app}(min^{-1}) = 0.079$	[12]
Methyl red	400 mg/L	$k_{app}(min^{-1}) = 0.014$	$k_{app}(min^{-1}) = 0.008$	
Tetrazine	0.28 (mg/cm^2)	$k_{app}(min^{-1}) = 0.023$	$k_{app}(min^{-1}) = 0.040$	[13]
	0.56 (mg/cm^2)	$k_{app}(min^{-1}) = 0.030$	$k_{app}(min^{-1}) = 0.050$	
	0.84 (mg/cm^2)	$k_{app}(min^{-1}) = 0.029$	$k_{app}(min^{-1}) = 0.049$	
Methyl orange	-	~26% (160 min)	~40% (160 min)	[14]

Table S2. Chemical and physical properties of PFOA and PFOS. Adapted with permission from [15]. Copyright © 2017 P. Henrik Viberg et al., Elsevier.

	PFOS	**PFOA**
Molecular formula	$C_8HF_{17}O_3S$	$C_8HF_{15}O_2$
Molar mass	500.13 g/mol	414.07 g/mol
Density	1.25 g/cm^3	1.8 g/cm^3
Melting point	90 °C	40–50 °C
Boiling point	258–260 °C	189–192 °C
Solubility in water	519 mg/L at 20 °C	9.5 g/L
Solubility in other solvents	polar organic solvents	polar organic solvents

Table S3. Concentrations of PFOA and PFOS in drinking water from different countries. Adapted with permission from [16]. Copyright © 2020 Georgia M. Sinclair et al., Elsevier.

Country	PFOS (ng/L)	PFOA (ng/L)	Original source
Germany	<10	<10 - 68	[17]
Australia	0-16	0-9.7	[18]
USA	<1 - 57	<5 - 30	[19]
Brazil	0.58–6.7	0.81–2.8	[20]
India	<0.03–8.4	<0.005–2	[21]
Japan	<0.1–6.9	2.3–84	[22]
China	<0.1–14.8	<0.1–45.9	[23]

Table S4. Mean concentration and range of some individual PFAS in landfill leachate. Adapted with permission from [24]. Copyright © 2020 Abunada et al., MDPI.

Header	Eggen et al. [25] (ng/L)	Busch et al. [26] (ng/L)	Robey et al. [27] (ng/L)	Gallen et al. [28] (ng/L)	Garg et al. [29] (ng/L)	Herzke et al. [30] (ng/L)	Fuertes et al. [31] (ng/L)	Yin et al. [32] (ng/L)	Benskin et al. [33] (ng/L)	Huset et al. [34] (ng/L)
Type of PFAS	PFCs analysis (untreated leachate Water)	Compounds in landfill leachates	Foam produced by bubble aeration of landfill leachate	landfill (>50% SW)	Manufacturing and disposing electronic products	Teflon waste, Coated textiles, papers, fire-fighting foam, and furniture	Treated Leachate in MSW landfill	Leachate from CW outlet system (Max. level)	Municipal landfill leachate	Leachates from six landfill
PFOA	767	926	951	510	118.3	9500	520	3457	1500	380–1100
PFPeA	-	-	-	-	-	-	325	-	-	-
PFHxA	757	2509	2178	1300	76	-	77	868	2500	270–2200
PFHxS	281	178	2058	940	133,330	-	870	308	190	120–700
PFDS	-	-	ND	-	-	-		0.72	63	0–16
PFDA	70	51	87	22	8	-	-	27	1100	0.3–64
PFBS	<5	1350	-	-	-	NA	-	1916	190	280–2300
PFAA	-	NA	-	NA	-	-	-	55	-	-

PFNA	539	80	64	29	8	-	-	100	450	19–140
PFOS	2920	235	104	300	128,670	570	NA	439	4400	56–160
PFHpA	277	280	454	360	9	-	-	486	690	100–2800

Note 1: PFOA (Perfluorooctanoic acid), PFPeA (Perfluoropentanoic Acid), PFHxA (Perfluorohexanoic acid), PFHxS (Perfluorohexane sulfonate), PFDS (Perfluorodecane sulfonic acid), PFDA (perfluorodecanoic acid), PFBS (perfluorobutane sulfonic acid), PFAA (perfluoroalkyl acid), PFNA (perfluorononanoic acid), PFOS (Perfluorooctane sulfonate), PFHpA (perfluoroheptanoic acid)

Note 2: ND*: not detected, NA*: not analysed.

Table S5. Photocatalytic degradation of PFOA using TiO_2 and ZnO.

Catalyst	Dosage of catalyst	Initial concentration of PFOA	Source of light	pH	Degradation efficiency	Reference
TiO_2 (P25)	0.5 g L^{-1}	24 µmol L^{-1}	UVC-254 nm (23 W)	NA	10.5% (t = 3 h)	[35]
TiO_2	0.66 g L^{-1}	4 mmol L^{-1}	315-400 nm (500 W)	NA	~ 40% (t = 4 h)	[36]
TiO_2	0.25 g L^{-1}	50 mg L^{-1}	400-770 nm (300 W)	3	20% (t = 8 h)	[2]
TiO_2	0.1 g L^{-1}	0.24 mmol L^{-1}	UV	3.8	24% (t = 12 h)	[37]
TiO_2	0.1 g L^{-1}	30 mg L^{-1}	UVB (36 W)	NA	9% (t = 3 h)	[38]
TiO_2	0.2 g L^{-1}	30 mg L^{-1}	UVB (36 W)	NA	6% (t = 3 h)	[38]
TiO_2	0.5 g L^{-1}	30 mg L^{-1}	UVB (36 W)	NA	18% (t = 3 h)	[38]
TiO_2	1.0 g L^{-1}	30 mg L^{-1}	UVB (36 W)	NA	23% (t = 3 h)	[38]
TiO_2 (P25), anatase:rutile (84:16)	0.5 g L^{-1}	0.1 mmol L^{-1}	200-600 nm (150 W)	4.3	~ 1% (t = 3 h)	[39]
TiO_2 (synthetic), anatase:rutile (90:10)	0.5 g L^{-1}	0.1 mmol L^{-1}	200-600 nm (150 W)	4.3	~ 8% (t = 3 h)	[39]
Fe:Nb doped TiO_2, 100% anatase	0.5 g L^{-1}	0.1 mmol L^{-1}	200-600 nm (150 W)	4.3	~ 14% (t = 3 h)	[39]
TiO_2	0.5 g L^{-1}	50 mg L^{-1}	UVC-254 nm (400 W)	5	14% (t = 12 h)	[40]
Fe-loaded TiO_2	0.5 g L^{-1}	50 mg L^{-1}	UVC-254 nm (400 W)	5	69% (t = 12 h)	[40]
Cu-loaded TiO_2	0.5 g L^{-1}	50 mg L^{-1}	UVC-254 nm (400 W)	5	91% (t = 12 h)	[40]

Pt-loaded TiO_2	0.5 g L^{-1}	60 mg L^{-1}	365 nm (125 W)	3	100% (t = 5h)	[41]
Pd-loaded TiO_2	0.5 g L^{-1}	60 mg L^{-1}	365 nm (125 W)	3	94.2% (t = 7h)	[41]
Ag-loaded TiO_2	0.5 g L^{-1}	60 mg L^{-1}	365 nm (125 W)	3	57.7% (t = 7h)	[41]
ZnO	1.0 g L^{-1}	19.9 µmol L^{-1}	365 nm (4 W)	5	< 1% (t = 72h)	[42]
ZnO	0.2 g L^{-1}	10 mg L^{-1}	254 nm (28 W)	4.5	58.2% (t = 4h)	[3]
ZnO	0.2 g L^{-1}	10 mg L^{-1}	254 nm (28 W)	NA	~ 65% (t = 4h)	[43]

Table S6. Photocatalytic degradation of PFOA using TiO_2 nanotubes.

Catalyst	**Volume of solution**	**Initial concentration of PFOA**	**Source of light**	**pH**	**Degradation efficiency**	**Reference**
TiO_2 nanotubes	150 mL	30 mg L^{-1}	UVC-254 nm (23 W)	5	41% (t = 8 h)	[44]
Ag-loaded/TiO_2 nanotubes	NA	50 mg L^{-1}	UVC-254 nm (23 W)	5	43% (t = 8 h)	[45]
Graphene oxide-deposited TiO_2 nanotubes	1.4 L	0.121 µmol L^{-1}	UV (8 W)	3	~ 60% (t = 4 h)	[46]
Graphene oxide-deposited TiO_2 nanotubes	1.4 L	0.121 µmol L^{-1}	UV (8 W)	5	~ 40% (t = 4 h)	[46]
Graphene oxide-deposited TiO_2 nanotubes	1.4 L	0.121 µmol L^{-1}	UV (8 W)	7	~ 25% (t = 4 h)	[46]
Graphene oxide-deposited TiO_2 nanotubes	1.4 L	0.121 µmol L^{-1}	UV (8 W)	9	~ 20% (t = 4 h)	[46]
Graphene oxide-deposited TiO_2 nanotubes	1.4 L	0.121 µmol L^{-1}	UV (8 W)	11	~ 10% (t = 4 h)	[46]
C and N co-doped TiO_2 nanotubes	NA	40 mg L^{-1}	Hg lamp (100 W)	4	18.1% (t = 3 h)	[47]

Table S7. Comparison of process variables for typical thermal spraying processes. Adapted with permission from [48]. Copyright © 2014 P. Vuoristo, Elsevier.

Spray method	**Temperature of heat source (°C)**	**Particle velocity (m s^{-1})**	**Adhesion (MPa)**	**Oxide content in metal deposits (%)**	**Porosity (%)**	**Relative cost**	**Coating thickness (mm)**
Flame	3000	40	8	10–15	10–15	1 (lowest)	0.1–15
Electric arc	4000	100	12	10–20	10	2	0.1–15
HVOF	3000	600–800	~ 70	1–5	1–2	3	0.1–2
HVAF	2000–3000	600–1200	~ 70	L*	0–0.2	2	0.1–12
D-gun	4000	800–1200	~ 70	1–5	1–2	4	0.05–0.3
APS	12000	200–400	10–70	1–3	1–5	4	0.1–1
LPPS/VPS	12000	400–600	~ 70	0	~ 0.5	5 (highest)	0.1–1
LPCS	200–650	300–500	5–30	0	~ 0.5	1 (lowest)	0.2–2
HPCS	500–1000	400–800	10–40	0	~ 0.5	4	0.3–4

L*: ~ 1.5–2 times the oxide content of the feedstock powder

Table S8. Some characteristic properties of TiO_2 coatings deposited by methods of WSP, GSP, HVOF, and flame spraying. Adapted with permission from [49]. Copyright © 2013 Pavel Ctibor et al., Springer Nature.

Parameter	**WSP**	**GSP**	**HVOF**	**Flame**
Surface roughness R_a (µm)	13.4 ± 0.5	4.3 ± 0.14	5.7 ± 0.2	5.9 ± 1.4
Surface roughness R_y (µm)	97.7 ± 6.4	35.2 ± 3.8	50.6 ± 4.7	48.8 ± 2.4
Porosity (%)	8.5	3.4	4.4	8.3
Mean pore size	13.6	12.9	7.8	13.9

Table S9. Main advantages and disadvantages of thermal spraying processes for deposition of photocatalytic TiO_2 and ZnO coatings.

Process	Advantage	Disadvantage	Reference
Thermal spraying	• Possibility of on-site repairs • High deposition rate • No significant heat input to the substrates • Deposition of materials over a wide thickness range from tens to hundreds of microns • Low cost • Control of microstructure (columnar, dense, or porous) and phase composition using suspension plasma spraying and cold spraying processes	• Large pore size[1] • High volume porosity (2-15%)[1] • Coarse microstructural texture[1] • A line of sight method • Occurrence of phase transformation (in the case of TiO_2) • Creation of some amorphous content[2]	[48,50-55]

1: This might be considered as an advantage for photocatalytic applications

2: This might be observed in the case of TiO_2 and ZnO films deposited by solution precursor-based methods [56]

Table S10. Comparing general aspects of some surface engineering methods for deposition of various kinds of materials.

Properties/Processes	Dip coating	Spin coating	Spray pyrolysis	PVD	Anodizing	EPD	Thermal spraying
Typical thickness	Thin to thick film[57]	Thin film[57]	Thin to thick film[58,59]	1-10 μm[60]	20 nm[61] to hundreds of μm[62]	Submicron to above 100 μm[60]	10-1000 μm[60]
Surface roughness (in some case studies)	4.6 – 19.8 nm[63]	1.6 – 7.8 nm[64]	0.8 - 1.2 nm[65]	35 – 102 nm[66]	139 – 236 nm[67]	1.64 – 500 nm[68-71]	4300 – 16000 nm[72-75]
Possibility of depositing large areas/large scale production	Yes[57]	No[57]	Yes[76,77]	Yes[78]	Yes[79]	Yes[80]	Yes[81]
Necessity of post annealing treatment (after deposition)	Generally yes[82]	Generally yes[83]	Not in all cases[84]	Generally yes[85-87]	Generally yes[88-90]	Generally yes[91]	Generally no

*: In limited processes such as SPPS

**: Generally lower than other methods

References

[1] Al-Madanat, O.; AlSalka, Y.; Ramadan, W.; Bahnemann, D. W. TiO_2 Photocatalysis for the Transformation of Aromatic Water Pollutants into Fuels. *Catalysts* 2021, 11 (3), 317.

[2] Xu, B.; Ahmed, M. B.; Zhou, J. L.; Altaee, A. Visible and UV Photocatalysis of Aqueous Perfluorooctanoic Acid by TiO_2 and Peroxymonosulfate: Process Kinetics and Mechanistic Insights. *Chemosphere* 2020, 243, 125366.

[3] Wu, D.; Li, X.; Tang, Y.; Lu, P.; Chen, W.; Xu, X.; Li, L. Mechanism Insight of PFOA Degradation by ZnO Assisted-Photocatalytic Ozonation: Efficiency and Intermediates. *Chemosphere* 2017, 180, 247-252.

[4] Yin, P.; Hu, Z.; Song, X.; Liu, J.; Lin, N. Activated Persulfate Oxidation of Perfluorooctanoic Acid (PFOA) in Groundwater under Acidic Conditions. *Int. J. Environ. Res. Public Health* 2016, 13 (6), 602.

[5] Sovilj, B.; Sovilj-Nikić, S.; Javorova, J. Tribological Researches of Triboelements Topography of Hob Milling Process of Cylindrical Gear Serration. *MATEC Web of Conferences* 2019, 287, 05003.

[6] Liao, J.; Lin, S.; Zhang, L.; Pan, N.; Cao, X.; Li, J. Photocatalytic Degradation of Methyl Orange Using a TiO_2/Ti Mesh Electrode with 3D Nanotube Arrays. *ACS Appl. Mater. Interfaces* 2012, 4 (1), 171-177.

[7] Huang, J.; Tan, X.; Yu, T.; Zhao, L.; Liu, H., Enhanced Photovoltaic and Photoelectrocatalytic Properties by Free-Standing TiO_2 Nanotubes via Anodization. *J. Solid State Electrochem.* 2015, 19 (4), 1151-1160.

[8] Liu, Y.; Su, D.; Zhang, Y.; Wang, L.; Yang, G.; Shen, F.; Deng, S.; Zhang, X.; Zhang, S. Anodized TiO_2 Nanotubes Coated with Pt Nanoparticles for Enhanced Photoelectrocatalytic Activity. *J. Mater. Res.* 2017, 32, 1-9.

[9] Ye, Y.; Bruning, H.; Li, X.; Yntema, D.; Rijnaarts, H. H. M. Significant Enhancement of Micropollutant Photocatalytic Degradation Using a TiO_2 Nanotube Array Photoanode Based Photocatalytic Fuel Cell. *Chem. Eng. J.* 2018, 354, 553-562.

[10] Babu, P. S.; Madhavi, Y.; Krishna, L. R.; Sivakumar, G.; Rao, D. S.; Padmanabham, G. Thermal Spray Coatings for Erosion–Corrosion Resistant Applications. *Trans. Indian Inst. Met.* 2020, 73 (9), 2141-2159.

[11] Cataño, F. A.; Valencia, S.; Hincapié, E. A.; Restrepo, G.; Marín, J. M. A Comparative Study between TiO_2 and ZnO Photocatalysis: Photocatalytic Degradation of Cibacron Yellow FN-2R Dye. *Lat. Am. Appl. Res.* 2012, 42, 33-38.

[12] Shinde, D.; Tambade, P.; Chaskar, M.; Gadave, K. Photocatalytic Degradation of Dyes in Water by Analytical Reagent Grades ZnO, TiO_2. and SnO_2 : A Comparative Study. *Drink. Water Eng. Sci.* 2017, 10, 109-117.

[13] Djilali, T.; Lebouachera, S. E. I.; Dechir, S.; Chekir, N.; Benhabiles, O.; Bentahar, F. Comparison between TiO_2 and ZnO Photocatalytic Efficiency for the Degradation of Tartrazine Contaminant in Water. *Int. J. Environ. Sci. Technol.* 2016, 1, 357-360.

[14] Raliya, R.; Avery, C.; Chakrabarti, S.; Biswas, P. Photocatalytic Degradation of Methyl Orange Dye by Pristine Titanium Dioxide, Zinc Oxide, and Graphene Oxide Nanostructures and Their Composites under Visible Light Irradiation. *Appl. Nanosci.* 2017, 7 (5), 253-259.

[15] Viberg, H.; Eriksson, P. Chapter 43 - Perfluorooctane Sulfonate and Perfluorooctanoic Acid. In *Reproductive and Developmental Toxicology (Second Edition)*, Gupta, R. C., Ed. Academic Press: 2017; pp 811-827.

[16] Sinclair, G. M.; Long, S. M.; Jones, O. A. H. What Are the Effects of PFAS Exposure at Environmentally Relevant Concentrations? *Chemosphere* 2020, 258, 127340.

[17] Wilhelm, M.; Bergmann, S.; Dieter, H. H. Occurrence of Perfluorinated Compounds (PFCs) in Drinking Water of North Rhine-Westphalia, Germany and New Approach to Assess

Drinking Water Contamination by Shorter-Chained C4–C7 PFCs. *Int. J. Hyg. Environ. Health* 2010, 213 (3), 224-232.

[18] Thompson, J.; Eaglesham, G.; Mueller, J. Concentrations of PFOS, PFOA and Other Perfluorinated Alkyl Acids in Australian Drinking Water. *Chemosphere* 2011, 83 (10), 1320-1325.

[19] Quiñones, O.; Snyder, S. A. Occurrence of Perfluoroalkyl Carboxylates and Sulfonates in Drinking Water Utilities and Related Waters from the United States. *Environ. Sci. Technol.* 2009, 43 (24), 9089-9095.

[20] Quinete, N.; Wu, Q.; Zhang, T.; Yun, S. H.; Moreira, I.; Kannan, K. Specific Profiles of Perfluorinated Compounds in Surface and Drinking Waters and Accumulation in Mussels, Fish, and Dolphins from Southeastern Brazil. *Chemosphere* 2009, 77 (6), 863-869.

[21] Mak, Y. L.; Taniyasu, S.; Yeung, L. W. Y.; Lu, G.; Jin, L.; Yang, Y.; Lam, P. K. S.; Kannan, K.; Yamashita, N. Perfluorinated Compounds in Tap Water from China and Several Other Countries. *Environ. Sci. Technol.* 2009, 43 (13), 4824-4829.

[22] Takagi, S.; Adachi, F.; Miyano, K.; Koizumi, Y.; Tanaka, H.; Mimura, M.; Watanabe, I.; Tanabe, S.; Kannan, K. Perfluorooctanesulfonate and Perfluorooctanoate in Raw and Treated Tap Water from Osaka, Japan. *Chemosphere* 2008, 72 (10), 1409-1412.

[23] Jin, Y. H.; Liu, W.; Sato, I.; Nakayama, S. F.; Sasaki, K.; Saito, N.; Tsuda, S. PFOS and PFOA in Environmental and Tap Water in China. *Chemosphere* 2009, 77 (5), 605-611.

[24] Abunada, Z.; Alazaiza, M. Y. D.; Bashir, M. J. K. An Overview of Per- and Polyfluoroalkyl Substances (PFAS) in the Environment: Source, Fate, Risk and Regulations. *Water* 2020, 12 (12).

[25] Eggen, T.; Moeder, M.; Arukwe, A. Municipal Landfill Leachates: A Significant Source for New and Emerging Pollutants. *Sci. Total Environ.* 2010, 408 (21), 5147-5157.

[26] Busch, J.; Ahrens, L.; Sturm, R.; Ebinghaus, R. Polyfluoroalkyl Compounds in Landfill Leachates. *Environ. Pollut.* 2010, 158 (5), 1467-1471.

[27] Robey, N. M.; da Silva, B. F.; Annable, M. D.; Townsend, T. G.; Bowden, J. A. Concentrating Per- and Polyfluoroalkyl Substances (PFAS) in Municipal Solid Waste Landfill Leachate Using Foam Separation. *Environ. Sci. Technol.* 2020, 54 (19), 12550-12559.

[28] Gallen, C.; Drage, D.; Eaglesham, G.; Grant, S.; Bowman, M.; Mueller, J. F. Australia-Wide Assessment of Perfluoroalkyl Substances (PFASs) in Landfill Leachates. *J. Hazard. Mater.* 2017, 331, 132-141.

[29] Garg, S.; Kumar, P.; Mishra, V.; Guijt, R.; Singh, P.; Dumée, L. F.; Sharma, R. S. A Review on the Sources, Occurrence and Health Risks of Per-/Poly-Fluoroalkyl Substances (PFAS) Arising from the Manufacture and Disposal of Electric and Electronic Products. *J. Water Process Eng.* 2020, 38, 101683.

[30] Herzke, D.; Olsson, E.; Posner, S. Perfluoroalkyl and Polyfluoroalkyl Substances (PFASs) in Consumer Products in Norway – A Pilot Study. *Chemosphere* 2012, 88 (8), 980-987.

[31] Fuertes, I.; Gómez-Lavín, S.; Elizalde, M. P.; Urtiaga, A. Perfluorinated Alkyl Substances (PFASs) in Northern Spain Municipal Solid Waste Landfill Leachates. *Chemosphere* 2017, 168, 399-407.

[32] Yin, T.; Chen, H.; Reinhard, M.; Yi, X.; He, Y.; Gin, K. Y.-H. Perfluoroalkyl and Polyfluoroalkyl Substances Removal in a Full-Scale Tropical Constructed Wetland System Treating Landfill Leachate. *Water Res.* 2017, 125, 418-426.

[33] Benskin, J. P.; Li, B.; Ikonomou, M. G.; Grace, J. R.; Li, L. Y. Per- and Polyfluoroalkyl Substances in Landfill Leachate: Patterns, Time Trends, and Sources. *Environ. Sci. Technol.* 2012, 46 (21), 11532-11540.

[34] Huset, C. A.; Barlaz, M. A.; Barofsky, D. F.; Field, J. A. Quantitative Determination of Fluorochemicals in Municipal Landfill Leachates. *Chemosphere* 2011, 82 (10), 1380-1386.

[35] Wang, Y.; Zhang, P. Photocatalytic Decomposition of Perfluorooctanoic Acid (PFOA) by TiO_2 in the Presence of Oxalic Acid. *J. Hazard. Mater.* 2011, 192 (3), 1869-1875.

[36] Gatto, S.; Sansotera, M.; Persico, F.; Gola, M.; Pirola, C.; Panzeri, W.; Navarrini, W.; Bianchi, C. L. Surface Fluorination on TiO_2 Catalyst Induced by Photodegradation of Perfluorooctanoic Acid. *Catal. Today* 2015, 241, 8-14.

[37] Gomez-Ruiz, B.; Ribao, P.; Diban, N.; Rivero, M. J.; Ortiz, I.; Urtiaga, A. Photocatalytic Degradation and Mineralization of Perfluorooctanoic Acid (PFOA) Using a Composite TiO_2 −RGO Catalyst. *J. Hazard. Mater.* 2018, 344, 950-957.

[38] Lopes da Silva, F.; Laitinen, T.; Pirilä, M.; Keiski, R. L.; Ojala, S. Photocatalytic Degradation of Perfluorooctanoic Acid (PFOA) From Wastewaters by TiO_2, In_2O_3 and Ga_2O_3 Catalysts. *Top. Catal.* 2017, 60 (17), 1345-1358.

[39] Estrellan, C. R.; Salim, C.; Hinode, H. Photocatalytic Decomposition of Perfluorooctanoic Acid by Iron and Niobium co-Doped Titanium Dioxide. *J. Hazard. Mater.* 2010, 179 (1), 79-83.

[40] Chen, M.-J.; Lo, S.-L.; Lee, Y.-C.; Huang, C.-C. Photocatalytic Decomposition of Perfluorooctanoic Acid by Transition-Metal Modified Titanium Dioxide. *J. Hazard. Mater.* 2015, 288, 168-175.

[41] Li, M.; Yu, Z.; Liu, Q.; Sun, L.; Huang, W. Photocatalytic Decomposition of Perfluorooctanoic Acid by Noble Metallic Nanoparticles Modified TiO_2. *Chem. Eng. J.* 2016, 286, 232-238.

[42] Abada, B.; Alivio, T. E. G.; Shao, Y.; O'Loughlin, T. E.; Klemashevich, C.; Banerjee, S.; Jayaraman, A.; Chu, K.-H. Photodegradation of Fluorotelomer Carboxylic 5:3 Acid and Perfluorooctanoic Acid Using Zinc Oxide. *Environ. Pollut.* 2018, 243, 637-644.

[43] Wu, D.; Li, X.; Zhang, J.; Chen, W.; Lu, P.; Tang, Y.; Li, L. Efficient PFOA Degradation by Persulfate-Assisted Photocatalytic Ozonation. *Sep. Purif. Technol.* 2018, 207, 255-261.

[44] Wu, Y.; Li, Y.; Tian, A.; Mao, K.; Liu, J. Selective Removal of Perfluorooctanoic Acid Using Molecularly Imprinted Polymer-Modified TiO_2 Nanotube Arrays. *Int. J. Photoenergy* 2016, 2016, 7368795.

[45] Tian, A.; Wu, Y.; Mao, K. Enhanced Performance of Surface Modified TiO_2 Nanotubes for the Decomposition of Perfluorooctanoic Acid. *AIP Conf. Proc.* 2017, 1794 (1), 020029.

[46] Park, K.; Ali, I.; Kim, J.-O. Photodegradation of Perfluorooctanoic Acid by Graphene Oxide-Deposited TiO_2 Nanotube Arrays in Aqueous Phase. *J. Environ. Manage.* 2018, 218, 333-339.

[47] Peng, Y.-P.; Chen, H.; Huang, C. P. The Synergistic Effect of Photoelectrochemical (PEC) Reactions Exemplified by Concurrent Perfluorooctanoic Acid (PFOA) Degradation and Hydrogen Generation over Carbon and Nitrogen codoped TiO_2 Nanotube Arrays (C-N-TNTAs) Photoelectrode. *Appl. Catal. B* 2017, 209, 437-446.

[48] Vuoristo, P. 4.10 - Thermal Spray Coating Processes. In *Comprehensive Materials Processing*, Hashmi, S.; Batalha, G. F.; Van Tyne, C. J.; Yilbas, B., Eds. Elsevier: Oxford, 2014; pp 229-276.

[49] Ctibor, P.; Stengl, V.; Pala, Z. Structural and Photocatalytic Characteristics of TiO_2 Coatings Produced by Various Thermal Spray Techniques. *J. Adv. Ceram.* 2013, 2, 218-226.

[50] Li, C. J. 7 - Thermal Spraying of Light Alloys. In *Surface Engineering of Light Alloys*, Dong, H., Ed. Woodhead Publishing: 2010; pp 184-241.

[51] Kim, G. E.; Champagne, V. K.; Trexler, M.; Sohn, Y. 20 - Processing Nanostructured Metal and Metal-Matrix Coatings by Thermal and Cold Spraying. In *Nanostructured Metals and Alloys*, Whang, S. H., Ed. Woodhead Publishing: 2011; pp 615-662.

[52] Joshi, S.; Nylen, P. Advanced Coatings by Thermal Spray Processes. *Technologies* 2019, 7 (4), 79.

[53] Taylor, S. R. Coatings for Corrosion Protection: Inorganic. In *Encyclopedia of Materials: Science and Technology*, Buschow, K. H. J.; Cahn, R. W.; Flemings, M. C.; Ilschner, B.; Kramer, E. J.; Mahajan, S.; Veyssière, P., Eds. Elsevier: Oxford, 2001; pp 1263-1269.

[54] Crawmer, D. E. Plasma Spray Coatings. In *Encyclopedia of Materials: Science and Technology*, Buschow, K. H. J.; Cahn, R. W.; Flemings, M. C.; Ilschner, B.; Kramer, E. J.; Mahajan, S.; Veyssière, P., Eds. Elsevier: Oxford, 2001; pp 7035-7040.

[55] BellWall Colmonoy Ltd, G. R. Thermal Spraying for Cost Reduction and Efficiency. *Mater. Des.* 1983, 4 (3), 783-790.

[56] Tejero-Martin, D.; Pala, Z.; Rushworth, S.; Hussain, T. Splat Formation and Microstructure of Solution Precursor Thermal Sprayed Nb-Doped Titanium Oxide Coatings. *Ceram. Int.* 2020, 46 (4), 5098-5108.

[57] Wright, J. D.; Sommerdijk, N. A. J. M. *Sol-Gel Materials: Chemistry and Applications*. CRC Press, 2018.

[58] Weber, S. B.; Grande, T.; Scherer, G. W.; Einarsrud, M.-A. Crack Engineering in Thick Coatings Prepared by Spray Pyrolysis Deposition. *J. Am. Ceram. Soc.* 2013, 96 (2), 420-428.

[59] Weber, S. B.; Lein, H. L.; Grande, T.; Einarsrud, M.-A. Deposition Mechanisms of Thick Lanthanum Zirconate Coatings by Spray Pyrolysis. *J. Am. Ceram. Soc.* 2011, 94 (12), 4256-4262.

[60] Boccaccini, A. R.; Keim, S.; Ma, R.; Li, Y.; Zhitomirsky, I. Electrophoretic Deposition of Biomaterials. *J. R. Soc. Interface* 2010, 7, S581-S613.

[61] Sunija, A. J. 8 - Biomaterials and Biotechnological Schemes Utilizing TiO_2 Nanotube Arrays-A Review. In *Fundamental Biomaterials: Metals*, Balakrishnan, P.; M S, S.; Thomas, S., Eds. Woodhead Publishing: 2018; pp 175-195.

[62] Chu, P. K.; Wu, G. S. 3 - Surface Design of Biodegradable Magnesium Alloys for Biomedical Applications. In *Surface Modification of Magnesium and its Alloys for Biomedical Applications*, Narayanan, T. S. N. S.; Park, I.-S.; Lee, M.-H., Eds. Woodhead Publishing: Oxford, 2015; pp 89-119.

[63] Bharti, B.; Kumar, S.; Kumar, R. Superhydrophilic TiO_2 Thin Film by Nanometer Scale Surface Roughness and Dangling Bonds. *Appl. Surf. Sci.* 2016, 364, 51-60.

[64] Zulkefle, M. A.; Abdul Rahman, R.; Yusof, K. A.; Abdullah, W. F. H.; Rusop, M.; Herman, S. H. Spin Speed and Duration Dependence of TiO_2 Thin Films pH Sensing Behavior. *J. Sens.* 2016, 2016, 9746156.

[65] Dundar, I.; Krichevskaya, M.; Katerski, A.; Acik, I. O. TiO_2 Thin Films by Ultrasonic Spray Pyrolysis as Photocatalytic Material for Air Purification. *R. Soc. Open Sci.* 2019, 6 (2), 181578.

[66] Ballo, A. M.; Bjöörn, D.; Åstrand, M.; Palmquist, A.; Lausmaa, J.; Thomsen, P. Bone Response to Physical-Vapour-Deposited Titanium Dioxide Coatings on Titanium Implants. *Clin. Oral Implants Res.* 2013, 24 (9), 1009-1017.

[67] Qadir, M.; Lin, J.; Biesiekierski, A.; Li, Y.; Wen, C. Effect of Anodized TiO_2–Nb_2O_5–ZrO_2 Nanotubes with Different Nanoscale Dimensions on the Biocompatibility of a $Ti_{35}Zr_{28}Nb$ Alloy. *ACS Appl. Mater. Interfaces* 2020, 12 (5), 6776-6787.

[68] Bartmański, M.; Pawłowski, Ł.; Zieliński, A.; Mielewczyk-Gryń, A.; Strugała, G.; Cieślik, B. Electrophoretic Deposition and Characteristics of Chitosan–Nanosilver Composite Coatings on a Nanotubular TiO_2 Layer. *Coatings* 2020, 10 (3), 245.

[69] Joung, Y. S.; Buie, C. R. Electrophoretic Deposition of Unstable Colloidal Suspensions for Superhydrophobic Surfaces. *Langmuir* 2011, 27 (7), 4156-4163.

[70] Toh, A. G. G.; Cai, R.; Butler, D. L. The Influence of Surface Topography on the Photocatalytic Activity of Electrophoretically Deposited Titanium Dioxide Thin Films. *Wear* 2009, 266 (5), 585-588.

[71] Chava, R. K.; Raj, S.; Yu, Y.-T. Synthesis and Electrophoretic Deposition of Hollow-TiO_2 Nanoparticles for Dye Sensitized Solar Cell Applications. *J. Alloys Compd.* 2016, 672, 212-222.

[72] Kaur, S.; Bala, N.; Khosla, C. Characterization of Thermal-Sprayed HAP and HAP/TiO_2 Coatings for Biomedical Applications. *J. Therm. Spray Technol.* 2018, 27 (8), 1356-1370.

[73] Navidpour, A. H.; Salehi, M.; Salimijazi, H. R.; Kalantari, Y.; Azarpour Siahkali, M. Photocatalytic Activity of Flame-Sprayed Coating of Zinc Ferrite Powder. *J. Therm. Spray Technol.* 2017, 26 (8), 2030-2039.

[74] Navidpour, A. H.; Salehi, M.; Amirnasr, M.; Salimijazi, H. R.; Azarpour Siahkali, M.; Kalantari, Y.; Mohammadnezhad, M. Photocatalytic Iron Oxide Coatings Produced by Thermal Spraying Process. *J. Therm. Spray Technol.* 2015, 24 (8), 1487-1497.

[75] Navidpour, A. H.; Kalantari, Y.; Salehi, M.; Salimijazi, H. R.; Amirnasr, M.; Rismanchian, M.; Azarpour Siahkali, M. Plasma-Sprayed Photocatalytic Zinc Oxide Coatings. *J. Therm. Spray Technol.* 2017, 26 (4), 717-727.

[76] Bube, R. H. Cadmium Sulfide and Telluride. In *Encyclopedia of Materials: Science and Technology*, Buschow, K. H. J.; Cahn, R. W.; Flemings, M. C.; Ilschner, B.; Kramer, E. J.; Mahajan, S.; Veyssière, P., Eds. Elsevier: Oxford, 2001; pp 873-879.

[77] Falcony, C.; Aguilar-Frutis, M.; García-Hipólito, M. Spray Pyrolysis Technique; High-K Dielectric Films and Luminescent Materials: A Review. *Micromachines* 2018, 9 (8), 414.

[78] Schiller, S.; Kirchhoff, V.; Schiller, N.; Morgner, H. PVD Coating of Plastic Webs and Sheets with High Rates on Large Areas. *Surf. Coat. Technol.* 2000, 125 (1), 354-360.

[79] Jain, V. K.; Verma, A. *Physics of Semiconductor Devices: 17th International Workshop on the Physics of Semiconductor Devices 2013*. Springer International Publishing, 2013.

[80] Lee, V.; Whittaker, L.; Jaye, C.; Baroudi, K. M.; Fischer, D. A.; Banerjee, S. Large-Area Chemically Modified Graphene Films: Electrophoretic Deposition and Characterization by Soft X-Ray Absorption Spectroscopy. *Chem. Mater.* 2009, 21 (16), 3905-3916.

[81] Vardelle, A.; Moreau, C.; Akedo, J.; Ashrafizadeh, H.; Berndt, C. C.; Berghaus, J. O.; Boulos, M.; Brogan, J.; Bourtsalas, A. C.; Dolatabadi, A.; et al. The 2016 Thermal Spray Roadmap. *J. Therm. Spray Technol.* 2016, 25 (8), 1376-1440.

[82] Sakka, S. Preparation and Properties of Sol-Gel Coating Films. *J. Sol-Gel Sci. Technol.* 1994, 2, 451-455.

[83] Nguyen, N.-T. Chapter 4 - Fabrication Technologies. In *Micromixers (Second Edition)*, Nguyen, N.-T., Ed. William Andrew Publishing: Oxford, 2012; pp 113-161.

[84] Krunks, K.; Bijakina, O.; Mikli, V.; Varema, T.; Mellikov, E. Zinc Oxide Thin Films by Spray Pyrolysis Method. *Phys. Scr.* 1999, T79 (1), 209.

[85] Taherniya, A.; Raoufi, D. The Annealing Temperature Dependence of Anatase TiO_2 Thin Films Prepared by the Electron-Beam Evaporation Method. *Semicond. Sci. Technol.* 2016, 31 (12), 125012.

[86] Yao, J. K.; Huang, H. L.; Ma, J. Y.; Jin, Y. X.; Zhao, Y. A.; Shao, J. D.; He, H. B.; Yi, K.; Fan, Z. X.; Zhang, F.; et al. High Refractive Index TiO_2 Film Deposited by Electron Beam Evaporation. *Surf. Eng.* 2013, 25 (3), 257-260.

[87] Scheffel, B.; Modes, T.; Metzner, C. Reactive High-Rate Deposition of Titanium Oxide Coatings Using Electron Beam Evaporation, Spotless Arc and Dual Crucible. *Surf. Coat. Technol.* 2016, 287, 138-144.

[88] Mercado, C. C.; Lubrin, M. E. L.; Hernandez, H. A. J.; Carubio, R. A. Comparison of Photoelectrochemical Current in Amorphous and Crystalline Anodized TiO_2 Nanotube Electrodes. *Int. J. Photoenergy* 2019, 2019, 8.

[89] Liao, Y.; Que, W.; Zhong, P.; Zhang, J.; He, Y. A Facile Method to Crystallize Amorphous Anodized TiO_2 Nanotubes at Low Temperature. *ACS Appl. Mater. Interfaces* 2011, 3, 2800-2804.

[90] Indira, K.; Mudali, U. K.; Nishimura, T.; Rajendran, N. A Review on TiO_2 Nanotubes: Influence of Anodization Parameters, Formation Mechanism, Properties, Corrosion Behavior, and Biomedical Applications. *J. Bio Tribocorros.* 2015, 1 (4), 28.

[91] Dhiflaoui, H.; Jaber, N. B.; Lazar, F. S.; Faure, J.; Larbi, A. B. C.; Benhayoune, H. Effect of Annealing Temperature on the Structural and Mechanical Properties of Coatings Prepared by Electrophoretic Deposition of TiO_2 Nanoparticles. *Thin Solid Films* 2017, 638, 201-212.

Highlights

- Nanotubular structure is the best TiO_2 and ZnO morphology for photocatalytic applications.
- Photoelectrocatalysis is more efficient than photocatalysis for degradation of organic pollutants.
- In-situ formation of oxygen vacancies is a highlight for TiO_2 and ZnO coatings from thermal spraying processes.
- SPPS provides the most promising method for deposition of ZnO for photocatalytic purposes.
- HVOF and SPS yield TiO_2 coatings with higher anatase phase content than feedstock.